VIBRATIONAL AND ELECTRONIC SPECTROSCOPY OF MASS-SELECTED ORGANIC CATIONS AND CLUSTERS

by

DANIEL TODD MAUNEY

(Under the Direction of Michael A. Duncan)

ABSTRACT

The structures and properties of organic cations and clusters are an area of intense research. We readily produce these species in a pulsed electrical discharge. Size-selected ions are probed using infrared laser photodissociation spectroscopy. Theoretical calculations of molecular geometries and frequencies are used to augment the assignment of the obtained spectra. The spectra of $[C,H_2,O]^+$ exhibits different features based on the conditions used to produce the ions. Infrared spectra for protonated acetylacetone/water complexes indicate possible tautomerization of the acetylacetone molecule upon addition of a single water molecule. Calculations of the electronic states of some small organic cations indicate that it may be possible to guide future investigations into carriers of the diffuse interstellar bands using theoretical predictions.

INDEX WORDS: Infrared Ion Spectroscopy, Carbocations, Electronic States, Vibrational Spectroscopy

VIBRATIONAL AND ELECTRONIC SPECTROSCOPY OF MASS-SELECTED ORGANIC CATIONS AND CLUSTERS

by

DANIEL TODD MAUNEY

B.S., Elon University, 2009

M.S., University of North Carolina at Greensboro, 2012

A Dissertation Submitted to the Graduate Faculty of the University of Georgia in Partial Fulfillment of the Requirements for the Degree

DOCTOR OF PHILOSOPHY

ATHENS, GEORGIA

2017

VIBRATIONAL AND ELECTRONIC SPECTROSCOPY OF MASS-SELECTED ORGANIC CATIONS AND CLUSTERS

by

DANIEL TODD MAUNEY

Major Professor: Michael A. Duncan

Committee: Gary E. Douberly
Henning Meyer

Electronic Version Approved:

Suzanne Barbour
Dean of the Graduate School
The University of Georgia
August 2017

DEDICATION

To my wife, Karen.

TABLE OF CONTENTS

Page

CHAPTER

CHAPTER 1

INTRODUCTION

Carbon based cations have been the subject of research in numerous fields in the past. They are commonly found as fragmentation products in mass spectrometry,[1-2] as intermediates in organic chemistry reactions,[3-5] and as important mediating species in reactions leading to larger molecules in the interstellar medium.[6-9] In all of these situations, knowing the structure of these cations helps our fundamental understanding of the underlying mechanisms involved in such processes. Using spectroscopy can provide direct structural information, whereas techniques such as ion reactivity and collisional dynamics can only indicate the presence of multiple isomers and does not give structural evidence.[1-5] However, ion spectroscopy is difficult due to low densities and high temperatures depending on the production method.[5] Recent advances in ion production and laser technology now allow us to collect spectra of mass-selected ions using laser photodissociation.[10-13] This work focuses on three different avenues of research that directly involve organic cations: determining the structure of astrophysically relevant species, studying the effect of water solvation on the structure of produced cations, and calculating electronic excitations of cations that could be present in the interstellar medium for possible future laboratory measurements.

Astrophysically Relevant Species

Determining the presence of organic cations in space requires the comparison of observed astronomical spectra to known spectra. One of the first organic cations seen in space was CH^+, which was only discovered based on its well-known electronic spectrum.[14] For this reason, only a handful of organic cations have been seen in space but many more are expected to be found.[15-17] Detection of new species in space requires the collection of new laboratory spectra. However, this can be difficult. Typical interstellar detection revolves around rotational spectroscopy, but low signal levels, low ion densities produced in the laboratory, and the necessity of a permanent dipole make obtaining clean spectra of a variety of different cations difficult. For this reason, only a few ions have been detected this way.[18-20] Vibrational spectroscopy on the other hand is widely applicable to almost any type of cationic species regardless of whether the molecule possesses a permanent dipole moment.

Laboratory measurements of vibrational spectra for organic cations can be traced back to the 1950s where the ions were produced in "superacid" matrices.[21-24] These measurements suffered from the inability to fully distinguish effects of solvent and counterions. The complications encountered in a solution phase environment can be counteracted by moving to the gas phase. The first measurements in the gas phase came from the Oka group where direct absorption measurements were done in discharges.[25-28] Because of the high temperatures and complex mixtures in these environments, the spectra produced had broad absorption bands. During this same time period, the group of Y.T. Lee began mass-selected photodissociation experiments on carbocations.[10-11] Outside of the discharge environment, the density of ions is too

low to measure direct absorption. For this reason, the Lee group developed the use of rare gas "spectator" atoms that could be eliminated using photodissociation.[10]

The spectator photodissociation technique that Lee described has been used extensively by the groups of Maier and Dopfer,[29-33] Johnson,[34] and others.[35-38] The Duncan group has also used this technique to study a number of organic cations including: $C_3H_3^+$ (cyclopropenyl and propargyl),[43] $C_3H_5^+$ (allyl and 2-propenyl),[39] t-butyl cation,[42] protonated toluene,[40] protonated benzene, protonated naphthalene, protonated formaldehyde,[44] glyoxal,[46] and methanol.[45] This technique is used in the experiments herein to determine the structure of the formaldehyde cation (CH_2O^+) which is predicted to be in space but has not yet been observed. Its isomer, hydroxymethylene ($CHOH^+$), lies only 6 kcal/mol higher in energy, and could also be in space but its spectrum has never been measured in the laboratory until this work.

Protonation and Solvation of Organic Ions

Proton transfer is a key process in many different areas throughout chemistry and biology including photosynthesis, acid-base chemistry, and electrochemistry.[47-54] It is the main mechanism behind chemical ionization mass spectrometry[55-56] and has been implicated in astro and atmospheric chemistries.[57-59] Solvent assisted proton transfer has also been suggested in a number of mechanisms across chemistry and biology.[60-61] For this reason, the study of solvation and protonation is an area of great interest. A number of studies have been performed to understand the role of protonation and solvation in hydrogen bonded systems using size-selected infrared spectroscopy along with theoretical methods.[62-94] The structures in these systems have characteristic vibrational frequencies stemming from the motion of shared protons. The

relationship of these frequencies to the difference in proton affinities for the species involved was demonstrated by the Johnson group.[90]

In the current work, the effect of protonation is investigated for the acetylacetone molecule (Hacac). This molecule, a β-diketone, is known to have two tautomeric forms whose stability is dictated by the solvent.[95-96] By studying this system in the gas phase, it is possible to perform a stepwise solvation that could give definitive evidence for the effect of solvent molecules on the equilibrium between the two forms. Herein, it is shown that the introduction of a single water molecule causes a shift in the equilibrium of the tautomerization towards the lower stability form.

Electronically Excited States of Organic Cations

Due to the amount of visible and UV light produced by stars, it is relatively easy to collect spectra for these regions. The bands seen in these spectra are due to electronic absorption of molecules between the star and our telescopes. The most famous of these spectra are the diffuse interstellar bands (DIBs) which were first seen by Mary Lea Heger in 1922.[97] The DIBs, numbering well over 300, do not correspond to any known spectral lines of ions or molecules. Determining the carriers for these bands has been a high priority in molecular astrophysics for many years. The DIBs themselves have substructure, pointing to their attribution to molecules as opposed to atoms. With the majority of the bands in the visible region, the carriers for these bands are thought to be large carbon rich molecules like polycyclic aromatic hydrocarbons or long carbon chains.[98-99] Recently the Maier group has presented evidence for the attribution of

two of the lower frequency bands to C_{60}^{+}.[100] This is consistent with the earlier theories that DIB carriers are intermediates in the formation of larger polycyclic aromatic molecules.

However, due to the breadth of the UV/Vis region of the electromagnetic spectrum it is very difficult for laboratory spectroscopists to measure electronic spectra of proposed DIB carriers. To alleviate this difficulty, computations of electronic excitations can be performed to give a general area of where an absorption may occur. While ground state calculations can be performed with extreme levels of accuracy in the case of rotational constants and spectra, calculation of electronically excited states is quite difficult.[101] This difficulty can be attributed to greater sensitivity of electronic transition energies to the accuracy of the quantum mechanical model applied as well as coupling of electronic transitions to vibrational modes.[102-103] Efforts by a number of groups are ongoing to create more accurate models to properly describe the transitions of large numbers of proposed DIB carriers. In this work, time-dependent density functional theory (TD-DFT) is used to predict the electronic transitions for several organic cations that could possibly be present in the interstellar medium. TD-DFT is used for its low computational cost and reasonable accuracy.[102-103]

References

1. Baer, T.; Ng, C.-Y.; Powis, I., *The Structure, Energetics and Dynamics of Organic Ions*. John Wiley & Sons: Chichester, UK, 1996.

2. Holmes, J. L.; Aubrey, C.; Mayer, P. M., *Assigning Structures to Ions in Mass Spectrometry*. CRC Press: Boca Raton, FL, 2007.

3. Olah, G. A.; Prakash, G. K. S., *Carbocation Chemistry*. Hoboken, NJ, 2004.

4. Prakash, G. K. S.; Schleyer, P. v. R., *Stable Carbocation Chemistry*. John Wiley & Sons: New York, 1997.

5. Bowers, M. T.; *Gas Phase Ion Chemistry*. Academic Press: New York, 1984; Vol. I-III

6. Harquist, T. W.; Williams, D. A., *The Molecular Astrophysics of Stars and Galaxies*. Clarendon Press: Oxford, 1998.

7. Tielens, A. G. G. M., *The Physics and Chemistry of the Interstellar Medium*. Cambridge University Press: Cambridge, UK, 2005.

8. Kwok, S., *Physics and Chemistry of the Interstellar Medium*. University Science Books: Sausalito, CA, 2007.

9. Duley, W. W., Molecular cluster in interstellar clouds. *Astrophys. J* **1996**, *471*, L57-L60.

10. Boo, D. W.; Lee, Y. T., Vibrational spectroscopy and dynamics of ionic complexes of CH_5^+ and $CH_5^+(A)_x(B)_y$ (A, B = Ar, N_2, CH_4; x, y = 0-5). *Int. J. Mass. Spectrom. & Ion Process* **1996**, *159*, 209-229.

11. Yeh, L. I.; Price, J. M.; Lee, Y. T., Infrared spectroscopy of the pentacoordinated carbonium ion $C_2H_7^+$. *J. Am. Chem. Soc.* **1989,** *111*, 5597-5604.

12. Bieske, E. J.; Dopfer, O., High-resolution spectroscopy of cluster ions. *Chem. Rev.* **2000**, *100*, 3963-3998

13. Duncan, M. A., Frontiers in spectroscopy of mass-slected molecular ions. *Int. J. Mass Spectrom*. **2000**, *200*, 545-569

14. Douglas, A. E.; Herzberg, G., Band spectrum and structure of the CH^+ molecule; identification of three interstellar lines. *Can. J. Res*. **1942**, *20*, 71-82

15. Petrie, S.; Bohme, D. K., Ions in space. *Mass Spectrom. Rev*. **2007**, *26*, 258-280

16. Snow, T. P.; Bierbaum, V. M., Ion chemistry in the interstellar medium. *Annu. Rev. Anal. Chem*. **2008**, *1*, 229-259

17. Klemperer, W., Astronomical chemistry. *Annu. Rev. Phys. Chem*. **2011**, 62, 173-184.

18. Dixon, T. A.; Woods, R. C., Wicrowave absorption spectrum of the CO^+ ion. *Phys. Rev. Lett.* **1975**, *34*, 61-63.

19. Woods, R. C.; Dixon, T. C.; Saykally, R. J.; Szanto, P. G., Laboratory microwave spectrum of HCO^+. *Phys. Rev. Lett.* **1975**, *35*, 1269-1272.

20. Sandra, B.; Lars, K.; Alexander, S.; Oskar, A.; Stephan, S., Laboratory rotational spectrum of *l*-C_3H^+ and confirmation of its astronomical detection. *Astrophys. J. Lett.* **2014**, *783*, L4.

21. Fately, W. G.; Lippencott, E. R., Vibrational spectrum and structure of tropylium ion. *J. Chem. Phys.* **1957**, *26*, 1471-1481.

22. Perkampus, H. H.; Baumgarten, E., Proton-addition complexes of aromatic hydrocarbons. *Angew. Chem. Int. Ed.* **1964**, *3*, 776-783.

23. Olah, G. A.; Comisarow, M. B., Stable carbonium ions. XII. Direct observation of the allyl and 2-methylallyl cations. *J. Am. Chem. Soc.* **1964**, *86* ,5682-5683.

24. Olah, G. A.; Schlosberg, R. H.; Kelly, D. P.; Mateescu, G. D., Stable carbonium ions IC. The benzonium ion ($C_6H_7^+$) and its degenerate rearrangement. *J. Am. Chem. Soc.* **1970**, *92*, 2546-2548.

25. Crofton, M. W.; Jagod, M.-F.; Rehfuss, B. D.; Kreiner, W. A.; Oka, T., Infrared spectroscopy of carbo-ions III: n3 namd of methyl cation CH_3^+. *J. Chem. Phys.* **1988**, *88*, 666-678.

26. Crofton, M. W.; Jagod, M.-F.; Rehfuss, B. D.; Oka, T., Infrared spectroscopy of carbo-ions V: Classical vs nonclassical structure of protonated acetylene $C_2H_3^+$. *J. Chem. Phys.* **1989**, *91*, 5139-5153.

27. Rosslein, M.; Gabrys, C. M.; Jagod, M.-F.; Oka, T., Detection of infrared spectrum of CH_2^+. *J. Mol. Spec.* **1992**, *153*, 738-740.

28. Huang, X.; McCoy, A. B.; Bowman, J. M.; Johnson, L. M.; Savage, C.; Dong, F.; Nesbitt, D. J., Quantum deconstruction of the infrared spectrum of CH_5^+. *Science* **2006**, *284*, 135-137.

29. Olkhov, R. V.; Nizkorodov, S. A.; Dopfer, O., Infrared photodissociation spectra of CH_3^+–Ar_n complexes (n=1–8). *J. Chem. Phys.* **1998**, *108*, 10046-10060.

30. Dopfer, O.; Roth, D.; Maier, J. P., Infrared spectra of $C_3H_3^+$-N_2 dimers: Identification of proton-bound c-$C_3H_3^+$-N_2 and H_2CCCH^+-N2 isomers. *J. Am. Chem. Soc.* **2002**, *124*, 494-502.

31. Solcà, N.; Dopfer, O., Protonated benzene: IR spectrum and structure of $C_6H_7^+$. *Angew. Chem. Int. Ed.* **2002**, *41*, 3628-3631.

32. Nizkorodov, S. A.; Dopfer, O.; Ruchti, T.; Meuwly, M.; Maier, J. P.; Bieske, E. J., Size effects in cluster infrared spectra: The ν1 band of Ar_n-HCO^+ (n = 1-13). *J. Phys. Chem.* **1995**, *99*, 17118-17129.

33. Dopfer, O.; Olkhov, R. V.; Roth, D.; Maier, J. P., Intermolecular interaction in protonbound dimers.: Infrared photodissociation spectra of RG–$HOCO^+$ (RG=He, Ne, Ar) complexes. *Chem. Phys. Lett.* **1998**, *296*, 585-591.

34. Roscioli, J. R.; McCunn, L. R.; Johnson, M. A., Quantum structure of the intermolecular proton bond. *Science* **2007**, *316*, 249-254.

35. Jones, W.; Boissel, P.; Chiavarino, B.; Crestoni, M. E.; Fornarini, S.; Lemaire, J.; Maitre, P., Infrared fingerprint of protonated benzene in the gas phase. *Angew. Chem. Int. Ed.* **2003**, *42*, 2057-2059.

36. Polfer, N.; Sartakov, B. G.; Oomens, J., The infrared spectrum of the adamantyl cation. *Chem. Phys. Lett.* **2004**, *400*, 201-205.

37. Lorenz, U. J.; Solcà, N.; Lemaire, J.; Maître, P.; Dopfer, O., Infrared spectra of isolated protonated polycyclic aromatic hydrocarbons: Protonated naphthalene. *Angew. Chem. Int. Ed.* **2007**, *46*, 6714-6716.

38. Chiavarino, B.; Crestoni, M. E.; Fornarini, S.; Lemaire, J.; Mac Aleese, L.; Maître, P., Infrared absorption features of gaseous isopropyl carbocations. *ChemPhysChem* **2004**, *5*, 1679-1685.

39. Douberly, G. E.; Ricks, A. M.; Schleyer, P. v. R.; Duncan, M. A., Infrared spectroscopy of gas phase C_3H5^+: the allyl and 2-propenyl cations. *J. Chem. Phys.* **2008**, *128*, 021102.

40. Douberly, G. E.; Ricks, A. M.; Schleyer, P. v. R.; Duncan, M. A., Infrared spectroscopy of gas phase benzenium ions: Protonated benzene and protonated toluene from 750 to 3400 cm^{-1}. *J. Phys. Chem. A* **2008**, *112*, 4869-4874.

41. Douberly, G. E.; Ricks, A. M.; Ticknor, B. W.; McKee, W. C.; Schleyer, P. v. R.; Duncan, M. A., Infrared photodissociation spectroscopy of protonated acetylene and its clusters. *J. Phys. Chem. A* **2008**, *112*, 1897-1906.

42. Douberly, G. E.; Ricks, A. M.; Ticknor, B. W.; Schleyer, P. v. R.; Duncan, M. A., Infrared spectrocopy of the tert-butyl cation in the gas phase. *J. Am. Chem. Soc.* **2007**, *129*, 13782-13783.

43. Ricks, A. M.; Douberly, G. E.; Schleyer, P. v. R.; Duncan, M. A., Infrared spectroscopy of gas phase $C_3H_3^+$: The cyclopropenyl and propargyl cations. *J. Chem. Phys.* **2010**, *132*, 051101.

44. Mosley, J. D.; Cheng, T. C.; McCoy, A. B.; Duncan, M. A., Infrared spctroscopy of the mass 31 cation: protonated formaldehdye vs methoxy. *J. Phys. Chem. A* **2012**, *116*, 9287-9294.

45. Mosley, J. D. ; Young, J. W. ; Huang, M. ; McCoy, A. B. ; Duncan, M. A. Infrared spectroscopy of the methanol cation and its methylene-oxonium isomer. *J. Chem. Phys.* **2015**, *142*, 114301.

46. Leicht, D. ; Cheng, T. C. ; Duncan, M. A. Infrared spectroscopy of the glyoxal radical cation: The charge dependence of internal rotation. *Chem. Phys. Lett.* **2016**, *643*, 89 – 92.

47. Bell, R. P. *The Proton in Chemistry*; Chapman & Hall: London, 1973.

48. Caldin, E.; Gold, V.; eds. *Proton Transfer Reactions*; Chapman and Hall: London, 1975.

49. Hynes,J. T.; Klinman, J. P.; Limbach, H.-H.; Schowen, R. L.; eds. *Hydrogen Transfer Reactions*, Vols. 1–4; Wiley-VCH Publishers: Weinheim, 2006.

50. Bertini, I.; Gray, H. B.; Stiefel, E. I.; Valentine, J. S. *Biological Inorganic Chemistry*; University Science Books: Sausalito, CA, 2007.

51. Mohammed, O. F.; Pines, D.; Dreyer, J.; Pines, E.; Nibbering, E. T. J. Sequential Proton Transfer through Water Bridges in Acid-Base Reactions. *Science* **2005**, *310*, 83–86.

52. Wraight, C. A. Chance and Design - Proton Transfer in Water, Channels and Bioenergetic Proteins, *Biochimica et Biophysica Acta* **2006**, *1757*, 886–912.

53. Siwick, B. J.; Bakker, H. J. On the Role of Water in Intermolecular Proton-Transfer Reactions, *J. Am. Chem. Soc.* **2007**, *129*, 13412–13420.

54. Hammes-Schiffer, S.; Soudackov, A.V. Proton-Coupled Electron Transfer in Solution, Proteins, Electrochemistry, *J. Phys. Chem. B* **2008**, *112*, 14108–14123.

55. Harrison, A. G. *Chemical Ionization Mass Spectrometry*, 2nd edition; CRC Press: Boca Raton, FL, 1992.

56. Blake, R. S.; Monks, P. S.; Ellis, A. M. Proton-Transfer Reaction Mass Spectrometry, *Chem. Rev.* **2009**, *109*, 861–896.

57. Ferguson, E. E.; Fehsenfield, F. C.; Albritton, D. L. "Ion Chemistry of the Earth's Atmosphere," in Gas Phase Ion Chemistry, edited by M. T. Bowers, Vol. 1; Academic Press: New York, 1979, p. 45.

58. Duley, W. W. Molecular Clusters in Interstellar Clouds, *Astrophys. J.* **1996**, *471*, L57–L60.

59. Tielens, A. G. G. M. The Physics and Chemistry of the Interstellar Medium; Cambridge University Press: Cambridge, U.K., 2005

60. Peters, K. S. A Theory-Experiment Conundrum for Proton Transfer, *Acct. Chem. Res.* **2009**, *42*, 89-96.

61. Garczarek, F.; Gerwert, K. Functional Waters in Intraprotein Proton Transfer Monitored by FTIR Difference Spectroscopy. *Nature* **2006**, *439*, 109-112.

62. Yeh, L. I.; Okumura, M.; Myers, J. D.; Price, J. M.; Lee, Y. T. Vibrational Spectroscopy of the Hydrated Hydronium Cluster Ions $H_3O^+(H_2O)_n$ (n=1,2,3), *J. Chem. Phys.* **1989**, *91*, 7319-7330.

63. Yeh, L. I.; Lee, Y. T.; Hougen, J. T. Vibration-Rotation Spectroscopy of the Hydrated Hydronium Ions $H_5O_2^+$, $H_9O_4^+$, *J. Mol. Spec. 1994*, 164, 473-488.

64. Wang, Y.-S.; Jiang, J.-C.; Cheng, C.-L.; Lin, S. H.; Lee, Y. T.; Chang, H.-C. Indentifying 2-, 3-Coordinated H_2O in Protonated Ion-Water Clusters by Vibrational Pre-Dissociation Spectroscopy, Ab Initio Calculations, *J. Chem. Phys.* **1997**, *107*, 9695-9698.

65. Chang, H.-C.; Jiang, J.-C.; Hahndorf, I.; Lin, S. H.; Lee, Y. T.; Chang, H.-C. Migration of an Excess Proton upon Asymmetric Hydration: $H^+[(CH_3)_2O](H_2O)_n$ as a Model System, *J. Am. Chem. Soc.* **1999**, *121*, 4443-4450.

66. Jiang, J.-C.; Wang, Y.-S.; Chang, H.-C.; Lin, S. H.; Lee, Y. T.; Niedner-Schatteburg, G.; Chang, H.-C. Infrared Spectra of $H^+(H_2O)_{5-8}$ Clusters: Evidence for Symmetric Proton Hydration, *J. Am. Chem. Soc.* **2000**, *122*, 1398-1410.

67. Asmis, K. R.; Pivonka, N. L.; Santambrogio, G.; Brummer, M.; Kaposta, C.; Neumark, D.; Wöste, L. Gas-Phase Infrared Spectrum of the Protonated Water Dimer, *Science* **2003**, *299*, 1375−1377.

68. Fridgen, T. D.; McMahon, T. B.; MacAleese, L.; Lemaire, J.; Maitre, P. Infrared Spectrum of the Protonated Water Dimer in the Gas Phase, *J. Phys. Chem. A* **2004**, *108*, 9008−9010.

69. Headrick, J. M.; Bopp, J. C.; Johnson, M. A. Predissociation Spectroscopy of the Argon-Solvated $H_5O_2^+$ "Zundel" Cation in the 1000-1900 cm^{-1}. *J. Chem. Phys.* **2004**, *121*, 11523−11526.

70. Diken, E. G.; Headrick, J. M.; Roscioli, J. R.; Bopp, J. C.; Johnson, M. A.; McCoy, A. B. Fundamental Excitations of the Shared Proton in the $H_3O_2^-$ and $H_5O_2^+$ Complexes, *J. Phys. Chem. A* **2005**, *109*, 1487−1490.

71. Hammer, N. I.; Diken, E. G.; Roscioli, J. R.; Johnson, M. A.; Myshakin, E. M.; Jordan, K. D.; McCoy, A. B.; Huang, X.; Bowman, J. M.; Carter, S. The Vibrational Predissociation Spectra of the $H_5O_2^+RG_n$ (RG = Ar, Ne) Clusters: Correlation of the Solvent Perturbations in the Free OH and Shared Proton Transitions of the Zundel Ion, *J. Chem. Phys.* **2005**, *122*, 244301.

72. McCunn, L. R.; Roscioli, J. R.; Johnson, M. A.; McCoy, A. B. An H/D Isotopic Substitution Study of the $H_5O_2^+\cdot$Ar Vibrational Predissociation Spectra: Exploring the Putative Role of Fermi Resonances in the Bridging Proton Fundamentals, *J. Phys. Chem. B* **2008**, *112*, 321−327.

73. McCunn, L. R.; Roscioli, J. R.; Elliott, B. M.; Johnson, M. A.; McCoy, A. B. Why Does Argon Bind to Deuterium? Isotope Effects and Structures of $Ar\cdot H_5O_2^+$ Complexes, *J. Phys. Chem. A* **2008**, *112*, 6074−6078.

74. Olesen, S. G.; Guasco, T. L.; Roscioli, J. R.; Johnson, M. A. Tuning the Intermolecular Proton Bond in the $H_5O_2^+$ 'Zundel Ion' Scaffold, *Chem. Phys. Lett.* **2011**, *509*, 89−95.

75. Headrick, J. M.; Diken, E. G.; Walters, R. S.; Hammer, N. I.; Christie, R. A.; Cui, J.; Myshakin, E. M.; Duncan, M. A.; Johnson, M. A.; Jordan, K. D. Spectral Signatures of Hydrated Proton Vibrations in Water Clusters, *Science* **2005**, *308*, 1765−1769.

76. Chang, H.-C.; Wu, C.-C.; Kuo, J.-L. Recent Advances in Understanding the Structures of Medium-Sized Protonated Water Clusters, *Int. Rev. Phys. Chem.* **2005**, *24*, 553−578.

77. Douberly, G. E.; Walters, R. S.; Cai, J.; Jordan, K. D.; Duncan, M. A. Infrared Spectroscopy of Small Protonated Water Clusters, $H^+(H_2O)_n$ (n = 2−5): Isomers, Argon Tagging, and Deuteration, *J. Phys. Chem. A* **2010**, *114*, 4570−4579.

78. Mizuse, K.; Fujii, A. Infrared Photodissociation Spectroscopy of $H^+(H_2O)_6 \cdot M$ (M = Ne, Ar, Kr, Xe, H_2, N_2, and CH_4): Messenger-Dependent Balance Between H_3O^+ and $H_5O_2^+$ Core Isomers, *Phys. Chem. Chem. Phys.* **2011**, *13*, 7129-7135.

79. Shin, J.-W.; Hammer, N. I.; Diken, E. G.; Johnson, M. A.; Walters, R. S.; Jaeger, T. D.; Duncan, M. A.; Christie, R. A.; Jordan, K. D. Infrared Signature of Structures Associated with the $H^+(H_2O)_n$ (n = 6 to 27) Clusters, *Science* **2004**, *304*, 1137−1140.

80. Ebata, T.; Fujii, A.; Mikami, N. Vibrational Spectroscopy of Small-Sized Hydrogen-Bonded Clusters, Their Ions, *Intl. Rev. Phys. Chem.* **1998**, *17*, 331-361.

81. Miyazaki, M.; Fuji, A.; Ebata T.; Mikami, N. Infrared Spectroscopy of Hydrated Benzene Cluster Cations, $[C_6H_6\text{-}(H_2O)_n]^+$ (n = 1-6): Structural Changes upon Photoionization and Proton Transfer Reactions, *Phys. Chem. Chem. Phys.* **2003**, *5*, 1137-1148.

82. Miyazaki, M.; Asuka, F.; Ebata, T.; Mikami, N. Infrared Spectroscopic Evidence for Protonated Water Clusters Forming Nanoscale Cages, *Science* **2004**, *304*, 1134-1137.

83. Verdes, D.; Linnartz, H.; Maier, J. P.; Botschwina, P.; Oswald, R.; Rosmus, P.; Knowles, P.J. Spectroscopic, Theoretical Characterization of Linear Centrosymmetric NN---H^+---NN, *J. Chem. Phys.* **1999**, *111*, 8400-8403.

84. Bieske, E. J.; Dopfer, O. High-Resolution Spectroscopy of Cluster Ions, *Chem. Rev.* **2000**, *100*, 3963-3998.

85. Solca, N.; Dopfer, O. IR Spectrum of the Benzene-Water Cation: Direct Evidence for a Hydrogen-Bonded Charge-Dipole Complex, *Chem. Phys. Lett.* **2001**, *347*, 59-64.

86. Solca, N.; Dopfer, O. Interaction of the Benzenium Ion with Inert Ligands: IR Spectra of $C_6H_7^+$-L_n Cluster Cations (L=Ar, N_2, CH_4, H_2O), *Chem. Eur.* **2003**, *9*, 3154-3163.

87. Wu, C. -C.; Chaudhuri, C.; Jiang, J. C.; Lee, Y. T.; Chang, H. -C.; Hydration-Induced Conformational Changes in Protonated 2,4-Pentanedione in the Gas Phase. *Mol. Phys.* **2003**, *101*, 1285–1295.

88. Fridgen, T. D.; MacAleese, L.; McMahon, T. B.; Lemaire, J.; Maitre, P. Gas Phase Infrared Multiple-Photon Dissociation Spectra of Methanol, Ethanol, Propanol Proton-Bound Dimers, Protonated Propanol and the Propanol/Water Proton-Bound Dimer, *Phys. Chem. Chem. Phys.* **2006**, *8*, 955-966.

89. Roscioli, J. R.; McCunn, L. R.; Johnson, M. A. Quantum Structure of the Intermolecular Proton Bond, *Science* **2007**, *316*, 249-254.

90. Douberly, G. E.; Ricks, A. M.; Ticknor, B. W.; Duncan, M. A.; Infrared Spectroscopy of Protonated Acetone and its Dimer, *Phys. Chem. Chem. Phys.* **2008**, *10*, 77-79.

91. Douberly, G. E.; Ricks, A. M.; Ticknor, B. W.; McKee, W. C.; Schleyer, P. v. R.; Duncan, M. A.; Infrared Photodissociation Spectroscopy of Protonated Acetylene and its Clusters, *J. Phys. Chem. A* **2008**,*112*, 1897-1906.

92. Cheng, T. C.; Bandyopadhyay, B.; Mosley, J. D.; Duncan, M. A.; IR Spectroscopy of Protonation in Benzene–Water Nanoclusters: Hydronium, Zundel, and Eigen at a Hydrophobic Interface. *J. Am. Chem. Soc.* **2012**, *134*, 13046–13055.

93. DeBlase, A. F.; Bloom, S.; Lectka, T.; Jordan, K. D., McCoy, A. B.; Johnson, M. A.; Origin of the Diffuse Vibrational Signature of a Cyclic Intramolecular Proton Bond: Anharmonic Analysis of Protonated 1,8-Disubstituted Naphthalene. *J. Chem. Phys.* **2013**, *139*, 024301.

94. Leavitt, C. M.; DeBlase, A. F.; Johnson, C. J.; van Stipdonk, M.; McCoy, A. B.; Johnson, M. A.; Hiding in Plain Sight: Unmasking the Diffuse Spectral Signatures of the Protonated N-Terminus in Isolated Dipeptides Cooled in a Cryogenic Ion Trap. *J Phys. Chem. Lett.* **2013**, *3*, 3450–3457.

95. Howard, D. L.; Kjaergaard, H. G.; Huang, J.; Meuwly, M. Infrared and Near-Infrared Spectroscopy of Acetylacetone and Hexafluoroacetylacetone. *J. Phys. Chem. A* **2015**, *119*, 7980–7990.

96. Yoshida, Z.; Ogoshi, H.; Tokumitsu, T. Intramolecular Hydrogen Bond in Enol Form of 3-Substituted-2,4-Pentanedione. *Tetrahedron **1970**, 26*, 5691–5697.

97. Heger, M. L., Further study of the sodium lines in class B stars. *Lick Observatory Bulletin* **1922**, *10*, 337.

98. Herbig, G. H., The Diffuse Interstellar Bands. *Annu. Rev. Astron. Astrophys.* **1995**, *33*, 19-73.

99. Ehrenfreund, P., The Diffuse Interstellar Bands as evidence for polyatomic molecules in the diffuse interstellar medium. *Bull. Amer. Astronom. Soc.* **1999**, *31*, 880.

100. E. K. Campbell; M. Holz; Gerlich, D.; Maier, J. P., Laboratory confirmation of C_{60}^+ as the carrier of two diffuse interstellar bands. *Nature* **2015**, *523*, 322-323.

101. Yarkony, D. R., Conical intersections: Diabolical and often misunderstood. *Acc. Chem. Res.* **1998**, *31*, 511-518

102. Lee, T. J.; Scuseria, G. E., In Quantum Mechanical Electronic Structure Calculations with Chemical Accuracy (ed S. R. Langhoff), Kluwer Academic Publishers, Dordrecht, The Netherlands, **1995**, 47-108.

103. Helgaker, T.; Ruden, T.A.; Jorgensen, P.; Olsen, J.; Klopper, W., A priori calculation of molecular properties to chemical accuracy. *J. Phys. Org. Chem.* **2004**, *17*, 913-933.

CHAPTER 2

EXPERIMENTAL

Cations and clusters are produced via pulsed electrical discharge through a supersonic expansion using a needle type electrode design. Ions are produced using expansion gases consisting of mixtures of H_2 and Ar seeded with the vapor pressure of liquid precursor molecules. Backing pressure and pulse width duration are dependent on discharge conditions and the system studied. Typical backing pressures between 50 and 200 psig were used in these experiments. The gas is pulsed using a General Valve Series 9 nozzle, operated at a frequency of 10 Hz, with a pulse width ranging from 200 to 300 microseconds. The apparatus used in these experiments has been described previously.[1-5]

Figure 2.1 shows a diagram of the apparatus used to conduct these experiments. The ions are produced in the first chamber, known as the "source". This chamber has an operating pressure of 10^{-6} torr, which is maintained using a Varian VHS-10 diffusion pump (6600 l/s of He). An illustration of the needle type electrode design is shown in Figure 2.2. Two needles are mounted using a custom designed Teflon plate with copper mounting blocks so that a gap of 0.25 mm can be maintained between the tips of the needles. This gap is centered over the expansion hole and is positioned 8.7 mm downstream from the final expansion orifice. One needled is grounded, while the other is connected to the output of a Directed Energies (DEI) PVX-4140 high voltage pulser. The voltage is controlled by an external Bertan power supply

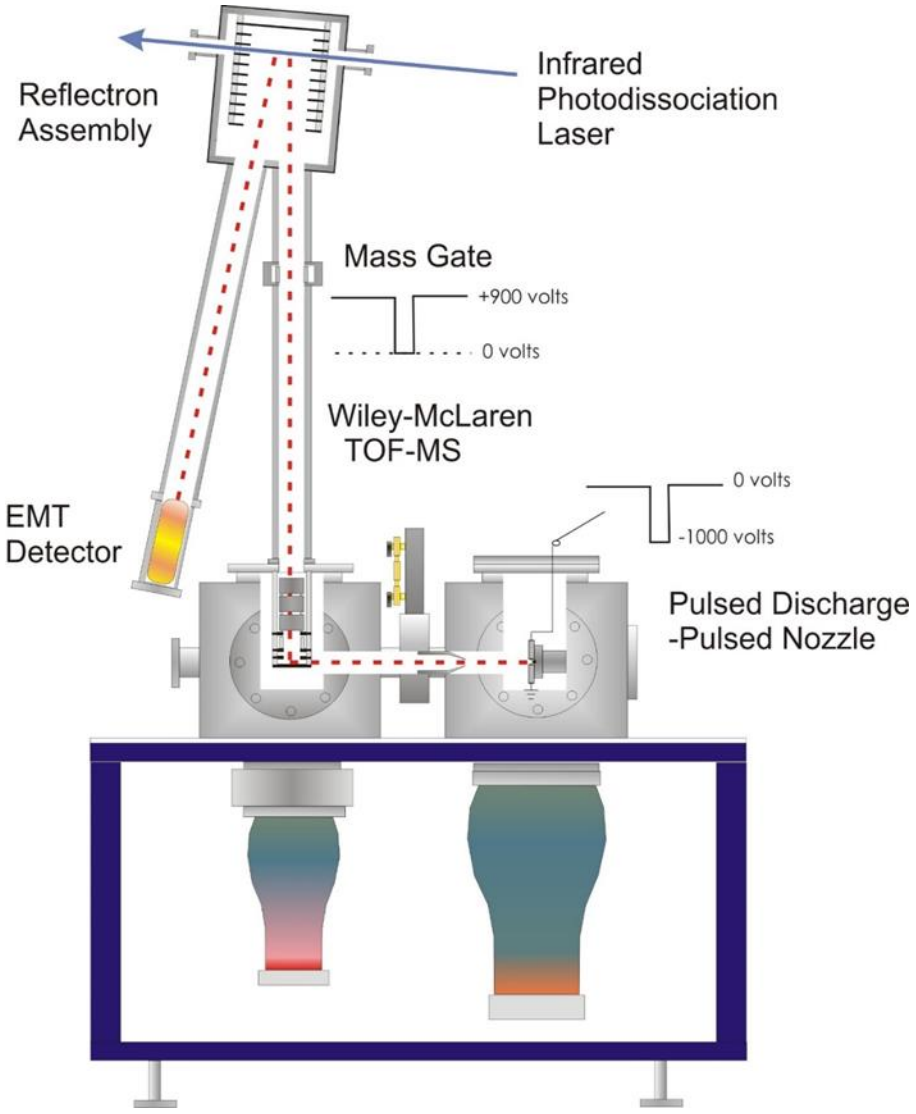

Figure 2.1. Schematic of the molecular beam apparatus

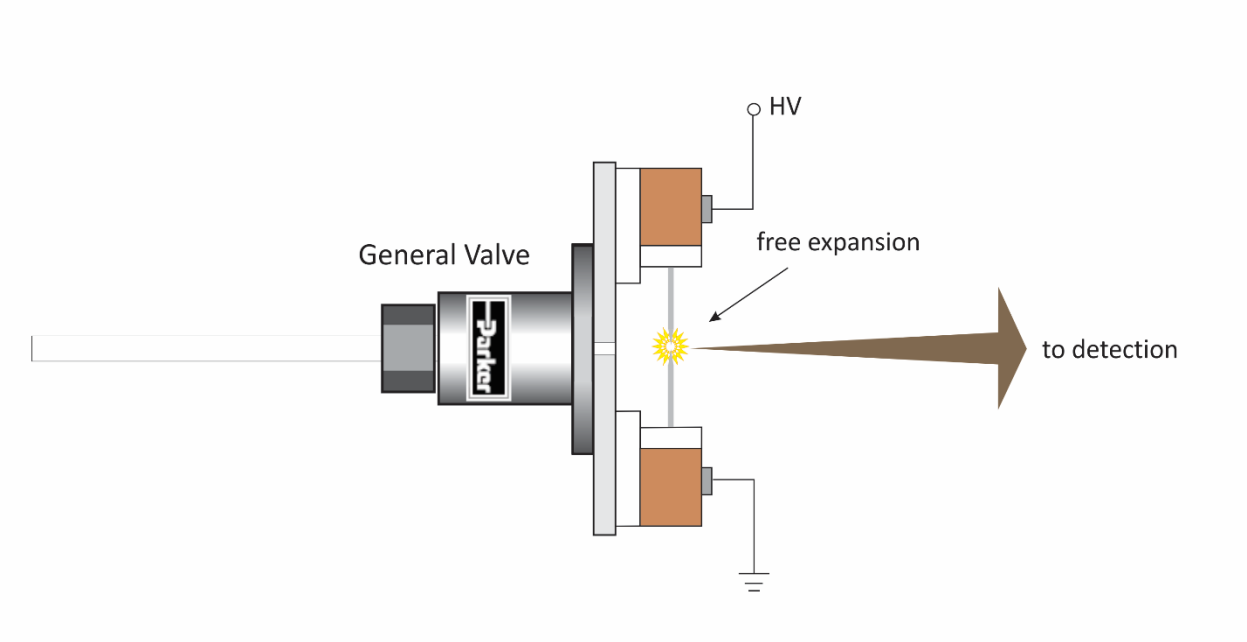

Figure 2.2. Illustration of needle type discharge design.

that operates from 0 to -3000V. The width and timing of the pulse is controlled by an externally generated 5V pulse (Stanford Research Systems) and is continuously variable over the nanosecond to millisecond range. Typical pulse widths are 5–20 microseconds. When the discharge is pulsed in the middle of the nozzle gas pulse, cooling inside the supersonic expansion is highly efficient. The plasma that results from the discharge contains a variety of neutrals, cations and anions.

Species produced in the discharge are entrained in the molecular beam and skimmed (Beam Dynamics) into a second, differentially pumped, mass spectrometer chamber. The mass spectrometer chamber is maintained at a pressure of 10^{-8} torr using a Varian VHS-6 diffusion pump (3000 l/s of He) to reduce collisions of the molecular beam with background gas. Ions in the beam are pulse extracted into the flight tube of a homemade, Wiley-McLaren type, time-of-flight mass spectrometer in the reflectron configuration.[3-4, 6] Because pulse extraction is performed perpendicular to the direction of the molecular beam, deflection plates (~40 V) are used to correct for any lateral motion of the extracted ions in the mass spectrometer flight tube. Ions are extracted between the repeller plate and "draw-out-grid" of the Wiley-McLaren stack, and the addition of a third grounded plate downstream, creates a two stage acceleration region. This configuration minimizes the spatial focusing caused by the finite width of the initial molecular beam and results in increased resolution of the resulting mass spectra. Voltages are supplied to the acceleration plates using fast high voltage switches (Behlke HTS-50) and timings are controlled by digital delay generators (Stanford Research Systems DG535). After extraction, ions pass through an einzel lens (~400V) to counteract space-charge effects in the beam and to

create a tightly focused ion packet. Following the einzel lens, ions enter a field-free region where they are separated by their flight time.

Because all ions are accelerated using the same kinetic energy (same voltage), the rate at which they fly through the field-free region is directly dependent on their mass, as shown in Equation 1:

$$Kinetic\ Energy = \frac{1}{2}mv^2 \quad (1)$$

where m represents the mass of the ion and v represents the velocity. This can be expressed alternatively as:

$$Kinetic\ Energy = \frac{1}{2}m(d/t)^2 \quad (2)$$

where d is the distance traveled and t represents the time taken to reach the destination. Based on these equations, lighter ions will travel through the mass spectrometer faster and reach the end of the flight tube in less time than the heavy ions. By using the onset of the extraction pulse as time zero, the time it takes ions to reach the detector can be measured using an oscilloscope. Solving Equation 2 for mass yields:

$$m = 2KE/(t/d)^2 \quad (3)$$

This demonstrates that knowing the distance travelled, flight time, and kinetic energy, it is possible to calculate the mass of any given ion. However doing this for every ion is not practical and the exact distance travelled can only be estimated. Using Equations 4 and 5, it is possible to assign the mass of any unknown ion, m_{unk}, using a reference mass, m_{ref}, and flight times, t_{unk} and t_{ref}.

$$m_{unk}v_{unk}^2 = m_{ref}v_{ref}^2 \quad (4)$$

$$m_{unk} = m_{ref}\left(t_{unk}/t_{ref}\right)^2 \quad (5)$$

Typically, the reference used for this apparatus under standard conditions is mass 19 which has a flight time of approximately 34 microseconds. This ion is H_3O^+ and is seen in almost all of our mass spectra.

At the end of the first field free region, the ions enter a reflectron field. This section consists of a series of plates with voltage adjusted by a voltage divider. As the ions enter the reflectron, their kinetic energy is converted rapidly into potential energy slowing them. This results in the ions having zero longitudinal velocity for a short period, 1-2 microseconds. Afterwards they are accelerated out with the same kinetic energy that they entered with. This mirroring effect is used to help with temporal focusing. If two ions of equal mass are extracted at different points within the acceleration plates, they will be given different kinetic energy and will arrive at the detector at different times causing broadening of peaks in the mass spectrum. This setup alleviates this because ions with different kinetic energies will penetrate the reflectron to differing degrees. Ions with greater energy will penetrate further into the reflectron, causing all ions of equal mass to exit at approximately the same time and reach the detector simultaneously.

Following the reflectron, the ions enter a post-accelerator, which is another field free region that is equipped with an interior tube that can be pulsed with a high positive voltage. As ions exit the tube, they are given an extra boost of kinetic energy before hitting the detector, causing an increase in signal level. Ions are detected using a Hamamatsu electron multiplier tube (Model R-595) whose signal is coupled to an oscilloscope through a Stanford Research Systems

SR445A pre-amplifier. The oscilloscope signal is sent to a computer using a GPIB interface. A typical mass spectrum produced by this apparatus is shown in the top frame of Figure 2.3.

In the first field free leg of the flight tube, we have the ability to select a single mass of ions using a mass gate. The mass gate consists of a pair of deflection plates that when positive voltage is applied, deflects ions out of the beam path preventing them from reaching the detector. These plate can be pulsed to ground with varying widths to allow the desired masses to pass through without perturbation. An example of a mass spectrum where the mass gate is used is shown in the second panel of Figure 2.3.

The ion densities produced in these experiments are too low for direct absorption measurements, so we must use a type of action spectroscopy to detect the absorption of a photon. We can accomplish this using photodissociation induced from absorption of tunable infrared light. Since the fragment ions are detected against a zero background, provides a highly sensitive way of measuring the spectrum of the ions of interest. To accomplish this, it is necessary for the molecule to possess a bond whose bond energy is less than that of an infrared photon (~0.5 eV). The energy of infrared photons is significantly less than that of typical bonds (4-5 eV), so the method of rare gas tagging is employed to enhance photodissociation yield. Using a rare gas atom, such as Ar, a weak bond is formed between the species under investigation and the rare gas atom (~0.1 eV). Due to the high polarizability of the Ar atom, charge-induced dipole interactions with the molecule form the interaction. Upon absorption of the infrared photon by the molecule, fast intramolecular vibrational relaxation (IVR) occurs providing enough energy to break the bond. The loss of the Ar atom is observed in the mass

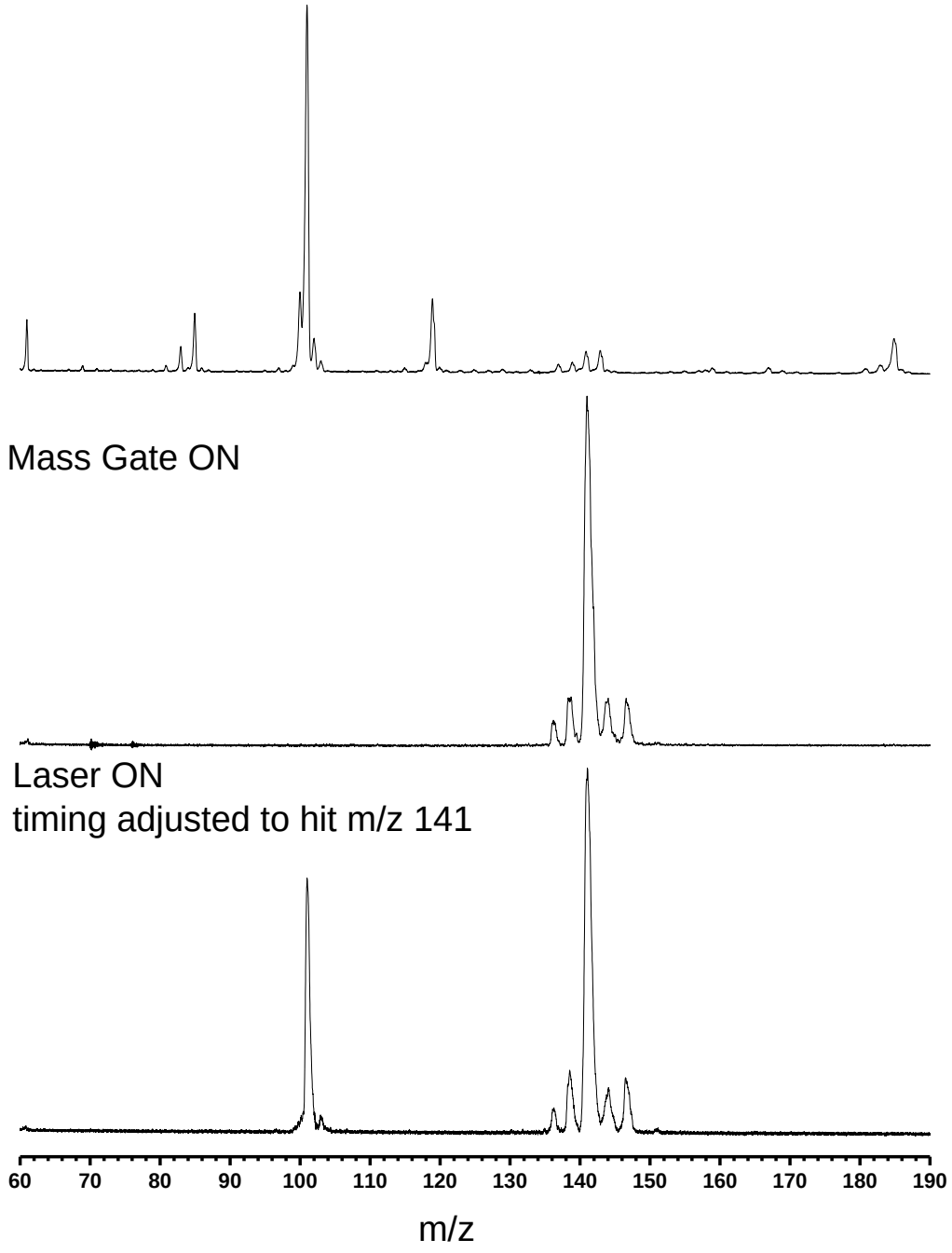

Fig 2.3. Top: Typical mass spectrum produced from the apparatus. Middle: Mass spectrum collected with the mass gate tuned to allow m/z 141 to pass. Bottom: Laser timing tuned to hit m/z 141 after the mass gate. The peak at m/z 101 represents loss of Ar.

spectrum as shown in the bottom panel of Figure 2.3. By integrating the fragment intensity as a function of wavelength, an infrared spectrum is obtained that is analogous to the absorption spectrum.

The tunable infrared light used in these experiments is produced using a LaserVision optical parametric oscillator/amplifier system. An illustration of this system can be seen in Figure 2.4. The OPO is pumped by the fundamental (1064 nm) output of a Spectra Physics Pro 230 Nd:YAG laser (430 mJ/pulse) operated at 10 Hz. The pump beam enters the OPO/OPA system and is split by a 70:30 beam splitter. The lower power beam is frequency double to 532 nm (~18800 cm^{-1}), while the 70% beam is sent to the amplifier stage via an optical delay line. A series of dichroic mirrors directs the 532 nm light onto a potassium titanyl phosphate (KTP) crystal in the OPO. This crystal splits the incident beam into two beams (signal and idler) whose energy is governed by the following equations:

$$\omega_{signal} \neq \omega_{idler} \tag{6}$$

$$\omega_{signal} > \omega_{idler} \tag{7}$$

$$\omega_{pump} = \omega_{signal} + \omega_{idler} \tag{8}$$

where ω is frequency in cm^{-1}. The signal beam, which is tunable from 710 – 880 nm (14085 – 11364 cm^{-1}) is dumped and the idler beam, which is tunable from 1340 – 2120 nm (4715 – 7436 cm^{-1}), is sent to the amplification stage. In the OPA, the idler is recombined with the 70% split of the 1064 nm (~9400 cm^{-1}) pump beam and directed through four potassium titanyl arsenate (KTA) crystals. Difference frequency mixing in these crystals generates tunable mid-IR light between 2000 and 4500 cm^{-1} with a linewidth of approximately 1 cm^{-1}. The transmitted idler

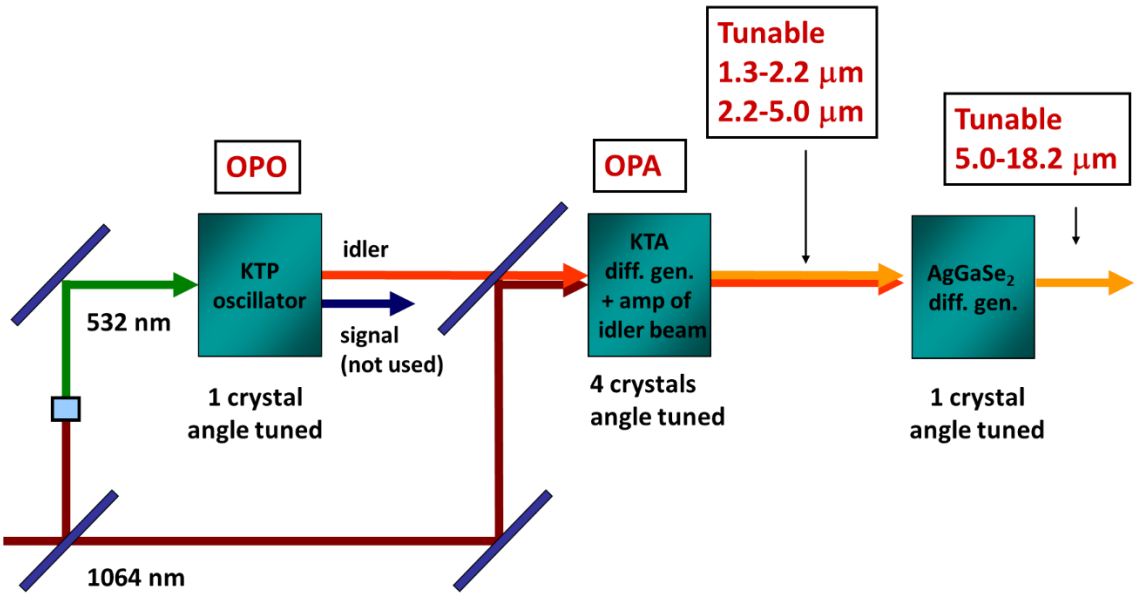

Figure 2.4. A schematic of the LaserVision OPO/OPA system.

and mid-IR beams are orthogonally polarized which allows for efficient separation using a polarizer. A second stage of difference frequency mixing can also be utilized using a silver gallium selenide ($AgGaSe_2$) crystal. This crystal mixes the idler and mid-IR beams through difference frequency generation to create light in the region between 600 and 2200 cm^{-1}. When combined with the mid-IR output of the OPO/OPA, this provides light which covers the majority of the infrared region, making it widely applicable for use in the vibrational spectroscopy of organic cations and clusters.

References

1. Dietz, T. G.; Duncan, M. A.; Powers, D. E.; Smalley, R. E., Laser production of supersonic metal cluster beams. *The Journal of Chemical Physics* **1981,** *74* (11), 6511-6512.
2. Powers, D. E.; Hansen, S. G.; Geusic, M. E.; Puiu, A. C.; Hopkins, J. B.; Dietz, T. G.; Duncan, M. A.; Langridge-Smith, P. R. R.; Smalley, R. E., Supersonic metal cluster beams: laser photoionization studies of copper cluster (Cu2). *The Journal of Physical Chemistry* **1982,** *86* (14), 2556-2560.
3. LaiHing, K.; Cheng, P. Y.; Taylor, T. G.; Willey, K. F.; Peschke, M.; Duncan, M. A., Photodissociation in a reflectron time-of-flight mass spectrometer: a novel mass spectrometry/mass spectrometry configuration for high-mass systems. *Analytical Chemistry* **1989,** *61* (13), 1458-1460.
4. Cornett, D. S.; Peschke, M.; LaiHing, K.; Cheng, P. Y.; Willey, K. F.; Duncan, M. A., Reflectron time-of-flight mass spectrometer for laser photodissociation. *Review of Scientific Instruments* **1992,** *63* (4), 2177-2186.
5. Duncan, M. A., Invited Review Article: Laser vaporization cluster sources. *Review of Scientific Instruments* **2012,** *83* (4), 041101.
6. Wiley, W. C.; McLaren, I. H., Time-of-Flight Mass Spectrometer with Improved Resolution. *Review of Scientific Instruments* **1955,** *26* (12), 1150-1157.

CHAPTER 3

INFRARED SPECTROSCOPY OF FORMALDEHYDE CATION AND ITS HYDROXYMETHYLENE ISOMER

Introduction

Determining the structures of ions has been a central focus of mass spectrometry for many years.[1-3] Small cationic structures are also of significant interest for interstellar chemistry.[4-8] For both of these, spectroscopy is needed to determine structures of ions and provide signatures for possible interstellar detection. This is difficult in practice due to harsh conditions and low ion densities in ion production.[9] Recent developments in ion spectroscopy have made it possible to produce higher densities of cold ions needed to obtain infrared spectra of mass-selected ions via resonance-enhanced photodissociation.[10-18] Our lab has used these methods to study a number of organic cations.[19-27] The present investigation provides the first infrared spectroscopy of formaldehyde cation and its hydroxymethylene structural isomer.

A number of small organic cations have been studied via infrared spectroscopy. The first experiments employed infrared laser absorption in discharges.[28-32] The next development came in the form of mass-selected photodissociation spectroscopy using the method of "tagging," which was demonstrated Lee and coworkers.[33-37] This type of experiment uses weakly bound messenger atoms or molecules that could easily be eliminated upon IR excitation. Several groups, other than our own, have utilized this method to study a number of different species.[38-44]

Our group has used infrared photodissociation to study various carbocations,[19-24] and recently small oxygen-containing species including CH_3OH^+, CH_2OH^+ , and $C_2H_3O^+$.[25-27]

$[C,H_2,O]^+$ radical cations have been extensively studied via mass spectrometry.[45-48] Theory predicts three stable isomers, the formaldehyde cation CH_2O^+, the hydroxymethylene cation $HCOH^+$, and the oxonium cation COH_2^+. CH_2O^+ and $HCOH^+$ are the lowest energy structures of this radical cation system, with CH_2O^+ being the lower energy isomer by about 5 kcal/mol.[49-51] By contrast, COH_2^+ lies ~60 kcal/mol higher in energy than CH_2O^+. The barrier for isomerization between CH_2O^+ and *trans*-$HCOH^+$ involving a 1,2 hydrogen shift has been determined to lie 45-50 kcal/mol above CH_2O^+. Only CH_2O^+ and $HCOH^+$ are thought to form experimentally.[2,48] Ionized formaldehyde has been studied before with photoelectron spectroscopy.[52-54] A recent study by Mishra and Symons showed the detection of CH2O+ using electron spin resonance.[55] Mass spectrometry suggests $HCOH^+$ is a stable isomer.[46-48] The thermodynamics of $[C,H_2,O]^+$ have been investigated thoroughly, revealing near-degenerate isomers, with ionized formaldehyde being slightly (~5 kcal/mol) lower in energy.[2] The present work provides spectroscopic evidence for CH_2O^+ and $HCOH^+$ with gas phase infrared spectroscopy.

Experimental

$[C,H_2,O]^+$ ions are produced in a pulsed discharge/supersonic expansion of 5-14 atm of argon seeded with the ambient vapor pressure of methanol (99.9%, Fisher Scientific) or formaldehyde solution (30%, J.T. Baker) at room temperature. The ions are mass-selected in a

reflectron time-of-flight mass spectrometer and observed with infrared photodissociation spectroscopy.[19-27] Since single-photon IR excitation cannot break the strong covalent bonds, we employ rare gas tagging.[10-18,33-37] In this method, $[C,H_2,O]^+$–Ar ions are produced, mass-selected, and IR absorption breaks the weak argon bond. The spectrum is recorded as the $[C,H_2,O]^+$ integrated ion intensity versus the frequency of the infrared laser. The laser system employed is an IR-optical parametric oscillator/amplifier (OPO/OPA) with $AgGaSe_2$ (LaserVision) that is pumped by an Nd:YAG laser (Spectra Physics Pro-230).

CCSD(T) calculations are carried out as implemented in the CFOUR programming package.[56] The atomic natural orbital (ANO) basis of Almlöf and Taylor is used for C, H and O atoms. The Roos augmented double ζ ANO basis is used for Ar atoms. Smaller and larger contractions of the Taylor ANO basis are designated by ANO0 and ANO1, respectively. Harmonic frequencies were scaled based on comparison of frequencies for neutral formaldehyde calculated at the same level versus the accepted values.[57]

Results and Discussion

Based on previous work done in our lab on both methanol cation[27] and protonated formaldehyde cation,[25] the expectation for the identity of the m/z = 30 cation produced from methanol was that of formaldehyde cation. Figure 1 shows an over/under comparison of the infrared spectrum of m/z = 30 cations produced from methanol measured via loss of argon versus the predicted frequencies for three isomers calculated at the CCSD(T)/ANO1 level of theory. The spectrum was measured between 1000 and 4000 cm^{-1}, but signal was only detected between 2600 and 3050 cm^{-1}. This region is typical of C-H and O-H fundamental stretching

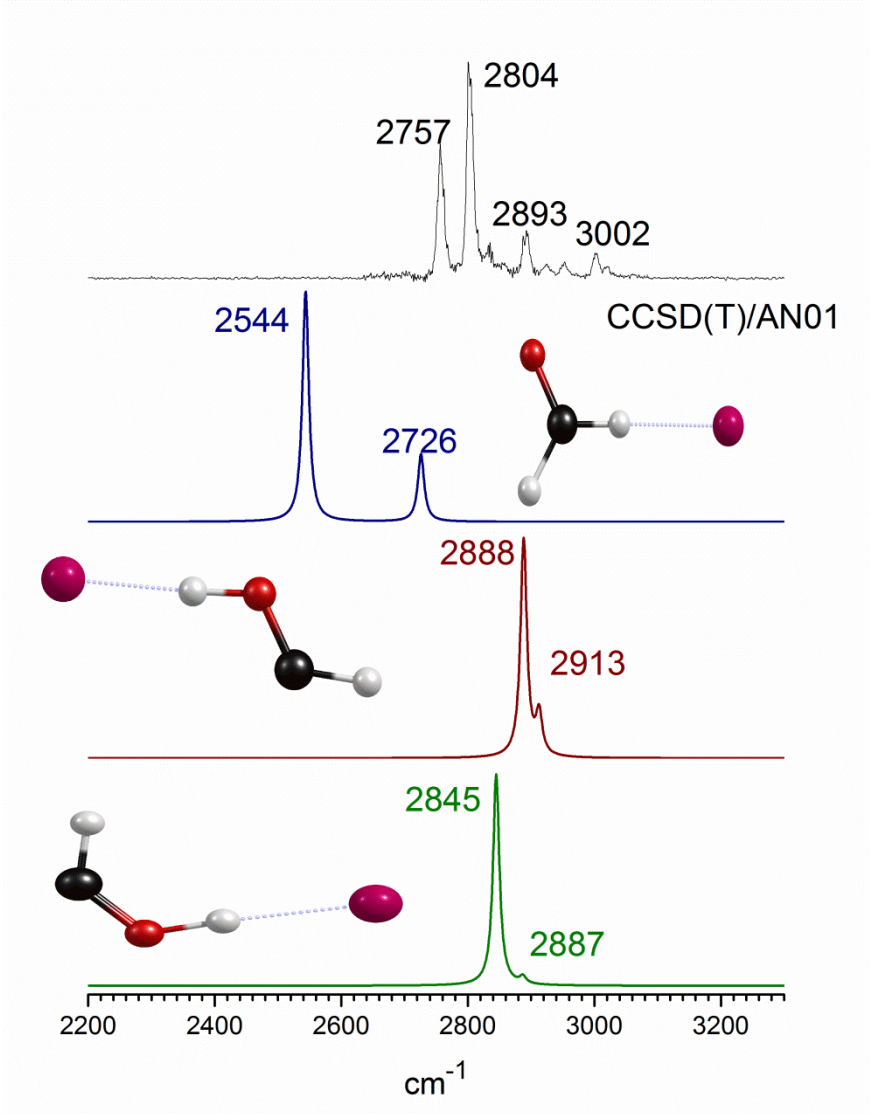

Figure 1. Experimental spectrum produced from the methanol precursor compared to theory calculated at the CCSD(T)/ANO1 level for formaldehyde (blue), trans (red) and cis-hydroxymethylene (green).

vibrations. Two intense peaks are observed at 2757 and 2804 cm^{-1} along with multiple smaller features, the biggest of which are observed at 2893 and 3002 cm^{-1}. The second trace (blue) is the predicted spectrum for the expected formaldehyde cation argon complex. It has two bands in this region at 2445 and 2720 cm^{-1} corresponding to the symmetric and asymmetric C-H stretches, respectively. On visual inspection, we conclude that the spectrum measured does not correspond to formaldehyde cation.

Hydroymethylene is a known isomer of neutral formaldehyde seen in its photochemistry. It has been predicted previously and is expected to be stable based on mass spectrometry experiments. Previous theoretical predictions place the *trans* form approximately 5 kcal/mol higher in energy than the global minimum formaldehyde structure.[50] However, although the cation has been seen is mass spectrometry, it has not been detected spectroscopically. The third (red) and fourth (green) traces of Figure 1 are predicted spectra for *cis* and *trans*-hydroxymethylene cation tagged with argon. Both *cis* and *trans* isomers are predicted to have two bands in the 2800-3000 cm-1 region with the bands belonging to *cis* being lower in frequency. As can be seen in Figure 1, the band positions for the hydroxymethylene isomers are more consistent with the experimental spectrum.

In order to better understand the differences between these isomers, we calculated the stationary points on the potential energy surface (PES) at the CCSD(T)/ANO1 level of theory, the results of which are shown in Table 1. All CCSD(T) structures are fully optimized with the ANO1 basis set (without tag), shown in Figure 2, and with the ANO1 basis for C, H, and O and

Table 1. The relative energies of stationary points on the potential energy surface of $[C,H_2,O]^{+\cdot}$ with and without the argon tag. Calculations were performed at the CCSD(T) level with the ANO1 basis set (without tag) and with the ANO1 basis set for C, H, and O and the Roos augmented double ζ basis set for Ar (with tag). Relative energies (kcal/mol) are corrected for zero-point vibrational energy.

Ion	ΔE [CCSD(T)]
CH_2O^+	0.0
trans $HCOH^+$	+6.1
cis $HCOH^+$	+9.6
COH_2^+	+57.8
T.S. 1	+43.0
T.S. 2	+23.5
T.S. 3	+88.2
CH_2O^+Ar (1) (Ar on H)	0.0
CH_2O^+Ar (2) (Ar above plane)	+0.4
trans $HCOH^+Ar$ (1)	+3.3
trans $HCOH^+Ar$ (2)	+6.8
cis $HCOH^+Ar$	+6.8
COH_2^+Ar	+54.5

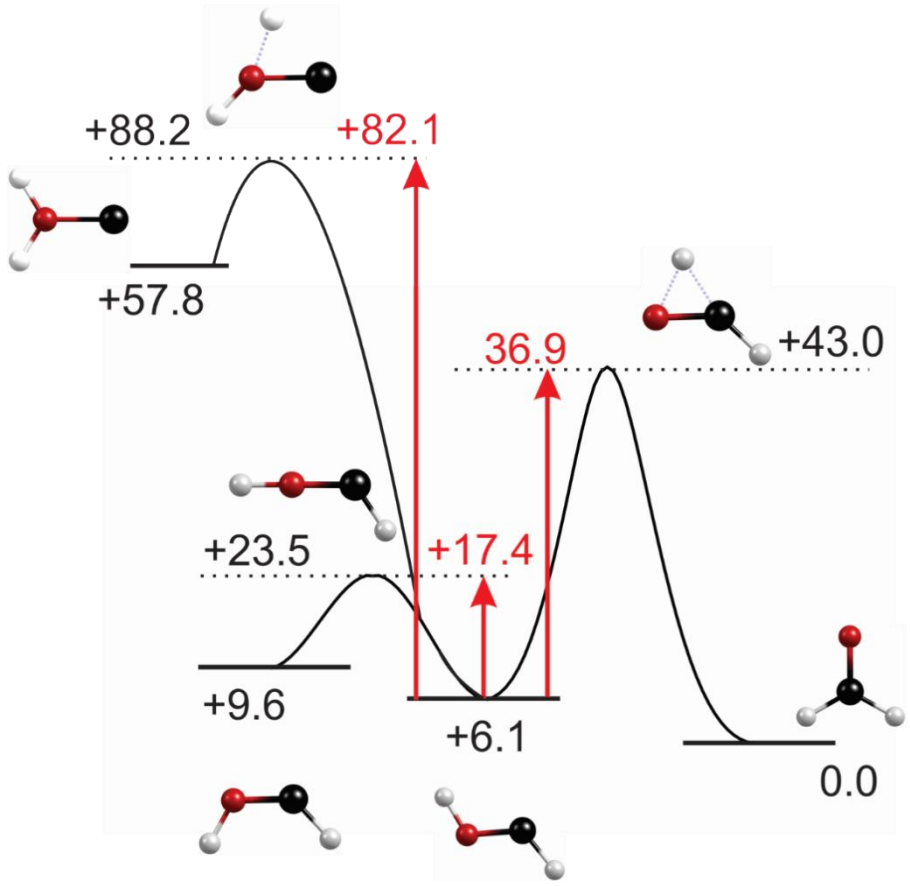

Figure 2. Schematic of the potential energy surface for $[C,H_2,O]^+$ cations including formaldehyde, cis- and trans-hydroxymethylene, and oxonium. Energies are in kcal/mol calculated at the CCSD(T)/ANO1 level of theory given relative to the formaldehyde cation in black. Barriers relative to trans-hydroxymethylene are in red.

the Roos ANO basis for Ar (with tag). We found four minima on the PES (without tag), whose relative energies are 0.0, +6.1, +9.6, and +57.8 kcal/mol for CH_2O^+, *trans*-$HCOH^+$, *cis*-$HCOH^+$, and COH_2^+, respectively. These results are fully consistent with previous theoretical results.[51,54] We also found three transition states: the first lying 43.0 kcal/mol higher than CH_2O^+ corresponds to a 1,2 hydrogen transfer reaction between *trans*-hydroxymethylene and formaldehyde cations, the second lying 17.4 kcal/mol higher than *trans*-hydroxymethylene corresponds to a *cis*/*trans* inversion, and the third lying +kcal/mol above *cis*-hydroxymethylene corresponds to another hydrogen transfer.

We also investigated the relative energetics of minima on the PES with argon (see Table I). Theory predicts two argon isomers for CH_2O^+−Ar. They correspond to argon attachment sites on the C−H(1) and above the C=O in plane(2). For *trans* $HCOH^+$−Ar, CCSD(T)/ANO1 predicts two argon isomers, corresponding to argon attachment sites on the O−H(1) and above the C=O out-of-plane(2). For *cis* $HCOH^+$−Ar , only one isomer is predicted corresponding to argon attachment on the O−H. The attachment of argon reduces the energy difference between formaldehyde and *trans*-hydroxymethylene to 3.3 kcal/mol, with formaldehyde remaining the lower energy isomer.

The goal of this project was to measure the infrared spectrum for the formaldehyde cation, so we remeasured the spectrum of the m/z=30 cation, this time produced using a commercial formaldehyde solution precursor. This spectrum is shown in Figure 3 versus the frequencies predicted for formaldehyde cation, *cis*, and *trans*-hydroxymethylene. Measureable signal was only seen between 2350 and 2850 cm^{-1} even though the spectrum was scanned from 1000-4000 cm^{-1}. The measured spectrum contained six peaks, the most intense of which are

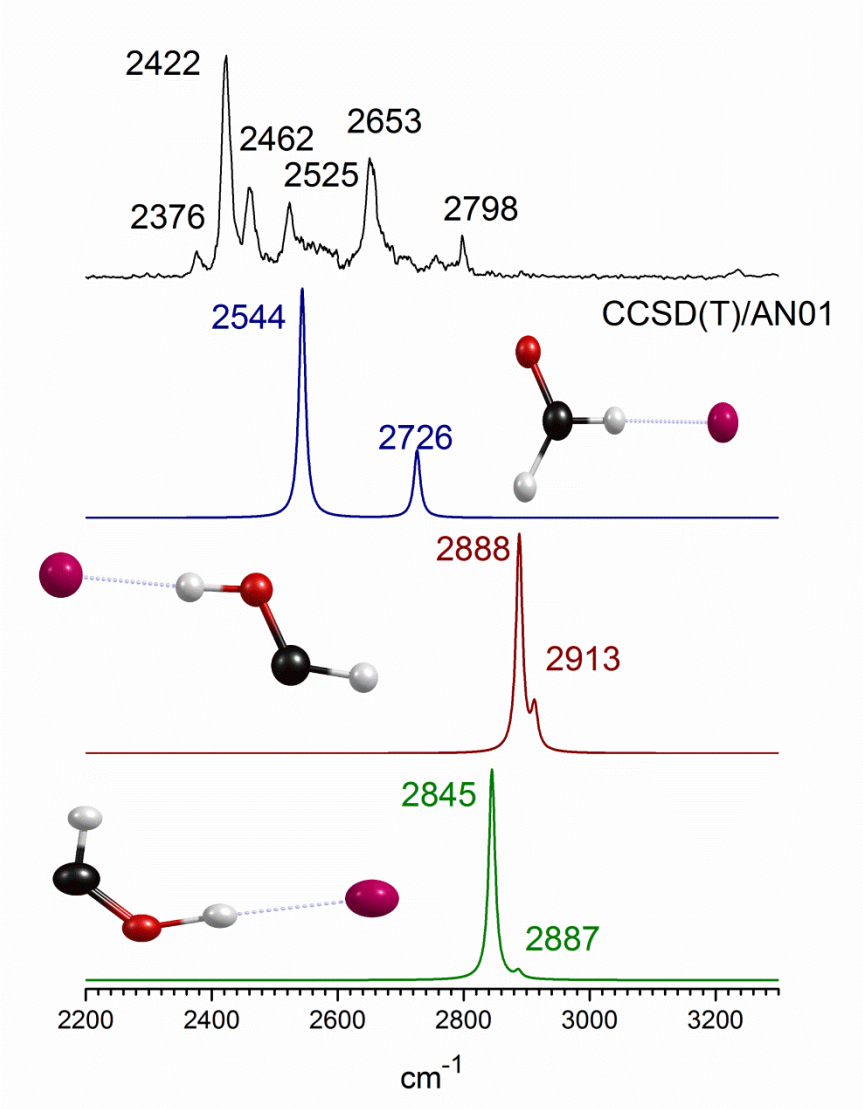

Figure 3. Experimental spectrum produced from the formaldehyde solution precursor compared to theory calculated at the CCSD(T)/ANO1 level for formaldehyde (blue), trans (red) and cis-hydroxymethylene (green).

observed at 2422 and 2653 cm^{-1}. Minor features were also observed at 2376, 2462, 2525, and 2798 cm^{-1}. For comparison, neutral formaldehyde has symmetric and antisymmetric C-H stretches at 2783 and 2843 cm^{-1}, respectively.[53] The C-O stretch and the HCH bend which were reported to occur at 1675 and 1210 cm^{-1} were not seen.[53] This could be due to lower IR intensities, lower laser power in the region, or the fact that the Ar binding energy (~1000 cm^{-1}) is close to the photon energy. The bands in the spectrum therefore occur at significantly lower frequencies than those of the neutral. The photoelectron spectrum of formaldehyde had a symmetric C-H stretch at 2580 cm^{-1} which would fall in the middle of the measured spectrum.[53] Note: the peak observed at 2798 cm^{-1} along with the minor feature to the left line up well with the peaks at 2757 and 2804 cm^{-1} in the methanol precursor spectrum. This is likely due to the presence of hydroxymethylene made from methanol since it is used as a stabilizer in the formaldehyde solution. On comparison to the theoretical spectra, the spectrum seems consistent with that of formaldehyde cation. However, in both the methanol precursor spectrum and the formaldehyde solution spectra, the predicted frequencies do not account for all of the peaks observed. In order to assign all of these minor peaks, more rigorous theoretical investigations were necessary.

Two types of anharmonic analysis were employed to explain the minor features in the spectra from both precursors. The first is a reduced dimensional approach that involved calculation of the anharmonic spectrum at lower levels of theory (B3LYP and MP2) and using the force constants produced to predict fermi resonances and adiabatic effects. This method is similar to that of Myshakin et al.,[58] which was previously employed in a study of CH_3O^+.[25] The

second approach is a full anharmonic treatment using second-order vibrational perturbation theory (VPT2) as implemented in CFOUR.[56] In this approach, isomer geometries are optimized at the CCSD(T)/ANO1 level and then a subsequent VPT2 analysis is performed at the MP2/ANO1 level and the anharmonic corrections obtained are applied to the harmonic frequencies obtained from the initial CCSD(T) optimization.

Comparing the two theoretical approaches, Figure 4 shows the results of the reduced dimensional approach for both *cis* and *trans*-hydroxymethylene vs the experimental methanol precursor spectrum. The theory predicts three bands for both isomers including ν_{CH} and ν_{OH} fundamentals and a combination band with single quanta in both the ν_{OH} and ν_{Ar} stretches. For the *cis* isomer, the ν_{OH} and ν_{CH} frequencies are predicted to be 2570 and 2837 cm^{-1}, respectively. For the *trans* isomer, the ν_{OH} and ν_{CH} frequencies are predicted to be 2648 and 2860 cm^{-1}, respectively. The predicted ν_{Ar} stretches for *cis* and *trans*-hydroxymethylene are 168 and 173 cm^{-1} putting the combination bands at 2738 and 2821 cm^{-1}, respectively. On comparison, the combination of both *cis* and *trans* isomers account for the majority of the peaks seen in the experimental spectrum, but the predicted bands are significantly to the red of the corresponding experimental features. The results of a similar reduced dimensional approach for formaldehyde cation vs the experimental formaldehyde precursor spectrum is shown in Figure 5. In this case, the results of the analysis are split into three parts: VPT2, fermi coupling, and adiabatic coupling. Using a combination of all three explains each of the peaks seen in the spectrum. The predicted spectrum due to fermi coupling is the result of a resonance between the symmetric C-H stretch fundamental, an overtone of the HCH bend, and a combination band between the C-O stretch with an in-plane hindered rotation. This yields three bands at 2374, 2413, and 2465 cm^{-1}. This

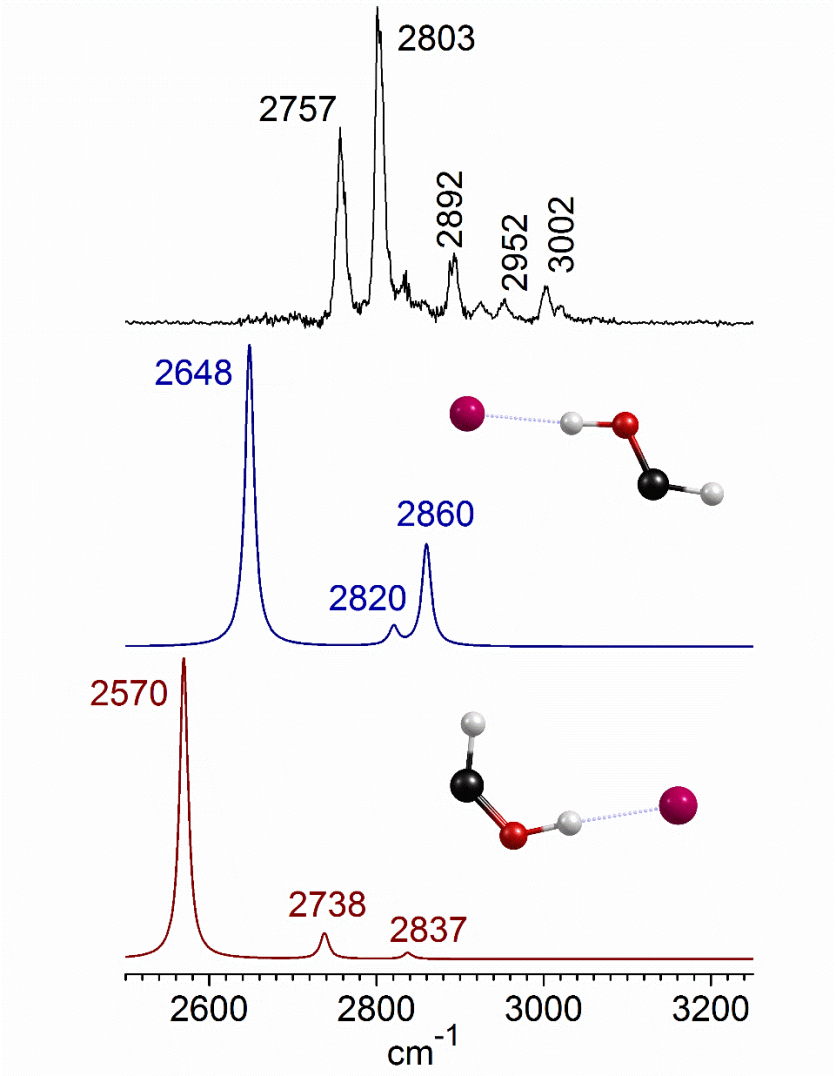

Figure 4. Experimental spectrum produced from the methanol precursor compared to that predicted by a reduced dimensional adiabatic coupling anharmonic approach for cis- and trans-hydroxymethylene using VPT2 and B3LYP/6-311G(d,p)

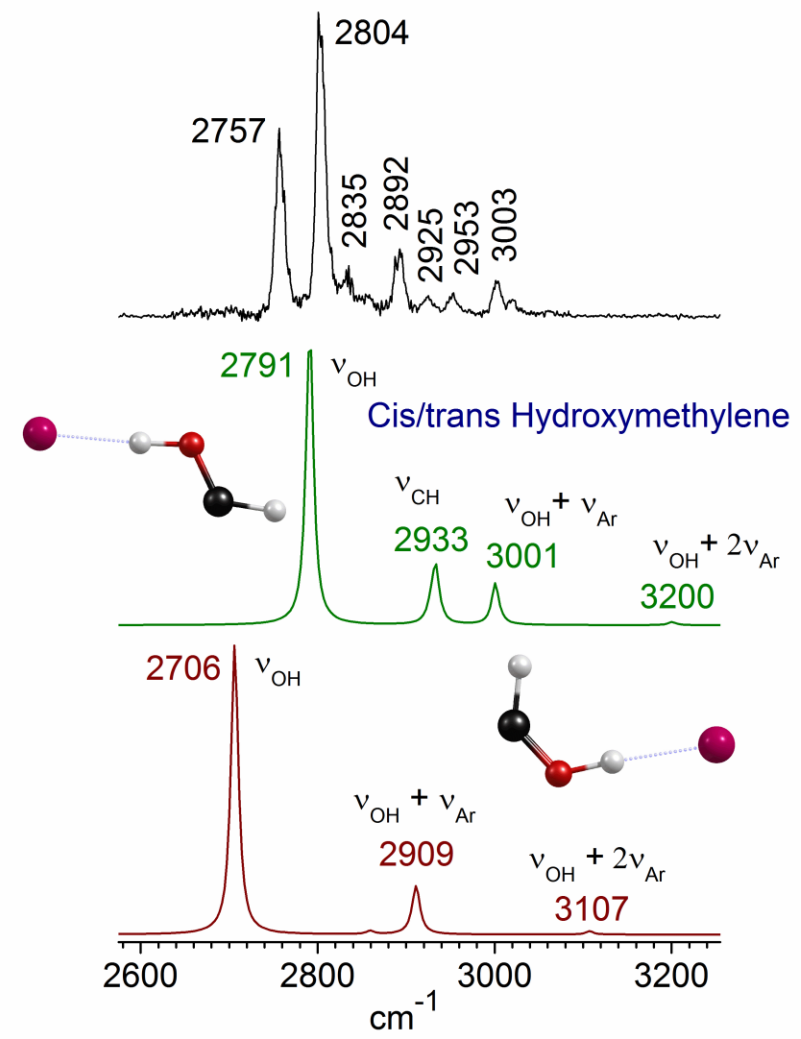

Figure 5. Experimental spectrum produced from the methanol precursor compared to that predicted by a full anharmonic approach for cis- and trans-hydroxymethylene using VPT2 and CCSD(T)/ANO1.

reproduces the first three peaks in the spectrum well and allows us to assign those peaks. The adiabatic coupling prediction shows a peak at 2510 cm^{-1} that corresponds to a combination band involving the ν_{asym} and ν_{AR} stretches. This band is seen in the experimental spectrum at 2525 cm^{-1}.

Figure 6 shows the results of the full anharmonic treatment of both *cis* and *trans*-hydroxymethylene vs the experimental methanol precursor spectrum. This approach predicts the same bands that were predicted by the reduced dimensional approach, but the band positions are more consistent with the experimental spectrum. The spectrum produced from a full anharmonic treatment of the formaldehyde cation is shown in Figure 7 along with the experimental spectrum from the formaldehyde precursor. These spectra are also compared with the original theory in the harmonic approximation. The harmonic theory seems to get the positions of the main CH stretches correct, but is less successful at predicting the proper relative intensities which are captured using the anharmonic approach. The anharmonic theory also seems to predict the correct number of peaks, but the intensities of the smaller features and their positions relative to the main peaks leave room for improvement.

Formaldehyde cation is of significant interest for interstellar chemistry. Both the neutral and its protonated counterpart have been detected in space,[8] but the CH_2O^+ cation is yet to be observed. This is surprising since it is implicated to be present based on reaction models of interstellar chemistry.[8] This work provides proof of the possibility of its production, but it is possible that other isomers are created based on which precursor is used. Unfortunately, the resolution of these spectra along with the severe frequency shifting as a result of Ar attachment

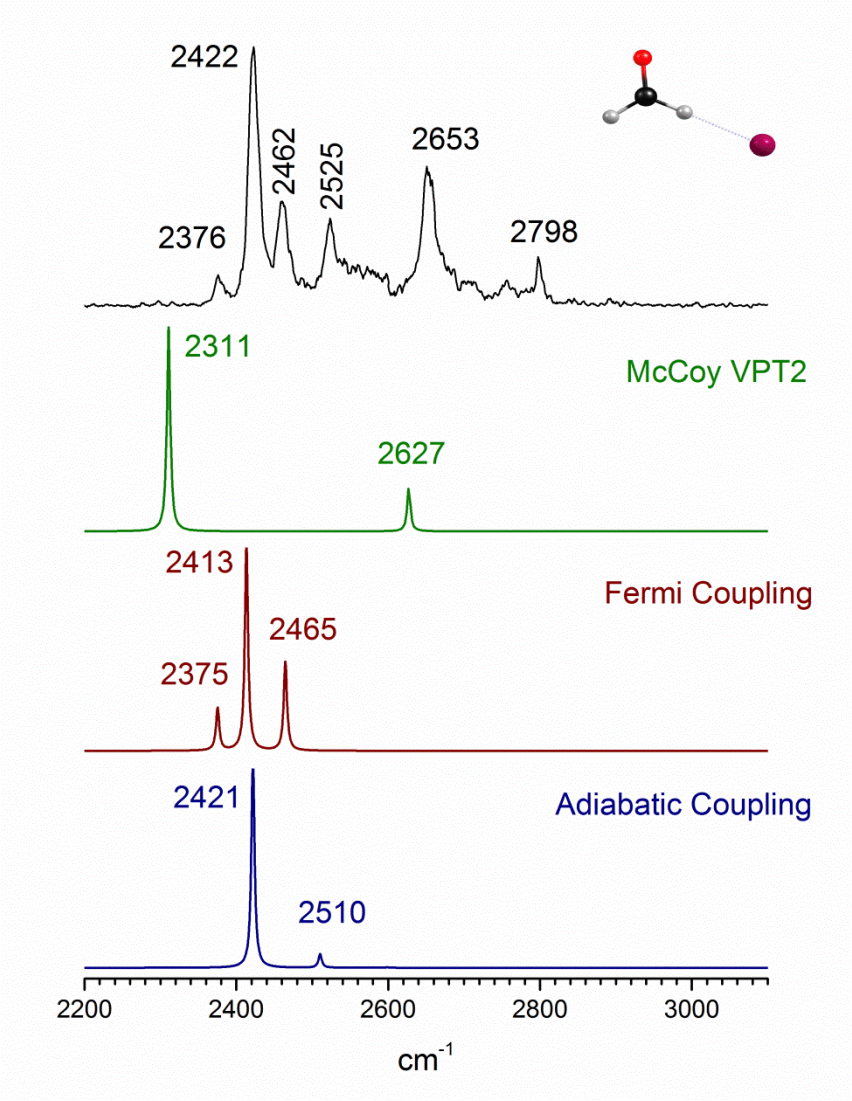

Figure 6. Experimental spectrum produced from the formaldehyde solution precursor compared to that predicted using the reduced dimensional anharmonic approaches described in the text using VPT2 and B3LYP/6-311G(d,p)

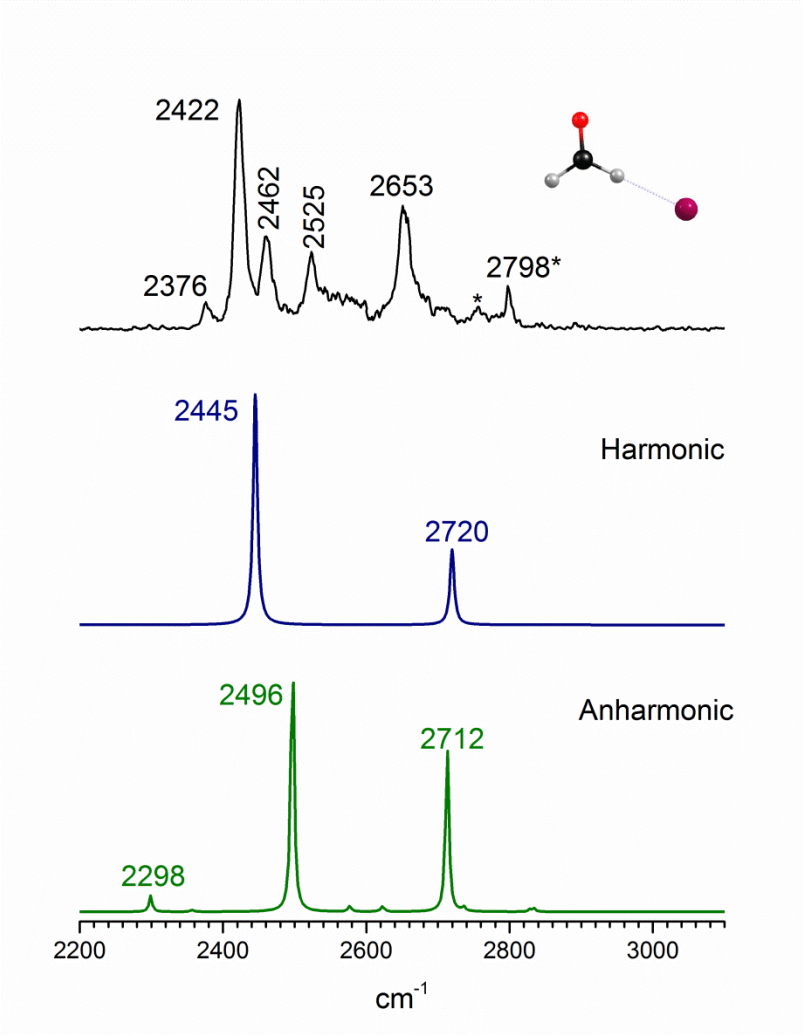

Figure 7. Experimental spectrum produced from the formaldehyde precursor compared to that predicted by harmonic theory (blue) and anharmonic theory using VPT2 (green). Both were performed using the CCSD(T)/ANO1 level of theory.

precludes their use in the search for these molecules in space. It is possible that in the future higher resolution studies of these isomers can be performed using our spectra as a guide.

Conclusion

Cations with m/z = 30 were produced with a discharge/expansion source and were investigated using mass-selected infrared photodissociation spectroscopy using the method of tagging with argon. The infrared spectrum contains sharp features between 2700 and 3100 cm^{-1} when ions are produced from methanol, and ions produced from a formaldehyde solution present exhibit peaks between 2350 and 2850 cm^{-1}. Detailed analysis of both spectra indicate that the methanol precursor produces *cis* and *trans*-hydroxymethylene isomers exclusively, whereas the spectrum obtained from the formaldehyde solution precursor indicates the production of the formaldehyde cation. Theory also indicates that the relative energy difference between these isomers is low with large barriers to rearrangement.

References

1. Bowers, M. T.; *Gas Phase Ion Chemistry*. Academic Press: New York, 1984; Vol. I-III

2. Baer, T.; Ng, C.-Y.; Powis, I., *The Structure, Energetics and Dynamics of Organic Ions*. John Wiley & Sons: Chichester, UK, 1996.

3. Holmes, J. L.; Aubrey, C.; Mayer, P. M., *Assigning Structures to Ions in Mass Spectrometry*. CRC Press: Boca Raton, FL, 2007.

4. Harquist, T. W.; Williams, D. A., *The Molecular Astrophysics of Stars and Galaxies*. Clarendon Press: Oxford, 1998.

5. Tielens, A. G. G. M., *The Physics and Chemistry of the Interstellar Medium*. Cambridge University Press: Cambridge, UK, 2005.

6. Petrie, S.; Bohme, D. K., Ions in Space. *Mass Spectrom. Rev.* **2007**, *26*, 258-280.

7. Snow, T. P.; Bierbaum, V. M., Ion Chemistry in the Interstellar Medium. *Annu. Rev. Anal. Chem.* **2008**, *1*, 229-259.

8. Klemperer, W., Astronomical chemistry. *Annu. Rev. Phys. Chem.* **2011**, 62, 173-184.

9. Carrington, A.; Thrush, B.A.; *Spectroscopy of Molecular Ions*. Royal Society: London, 1988.

10. Ebata, T.; Fujii, A.; Mikami, N. Vibrational Spectroscopy of Small-Sized Hydrogen-Bonded Clusters, Their Ions, *Int. Rev. Phys. Chem.* **1998**, *17*, 331-361.

11. Bieske, E. J.; Dopfer, O. High-Resolution Spectroscopy of Cluster Ions. *Chem. Rev.* **2000**, *100*, 3963-3998.

12. Duncan, M. A., Frontiers in Spectroscopy of Mass-Selected Molecular Ions. *Int. J. Mass Spectrom.* **2000**, *200*, 545-569.

13. Duncan, M. A., Infrared Spectroscopy to Probe Structure and Dynamics in Metal Ion-Molecule Complexes, *Int. Rev. Phys. Chem.* **2003**, *22*, 407-435.

14. Robertson W. H.; Johnson, M. A., Molecular Aspects of Halide Hydration: The Cluster Approach, *Annu. Rev. Phys. Chem.* **2003**, *54*, 173-213.

15. Rizzo, T. R.; Stearns, J. A.; Boyarkin, O. V., Spectroscopic Studies of Cold, Gas-Phase Biomolecular ions, *Int. Rev. Phys. Chem.* **2009**, *28*, 481-515.

16. Baer T.; Dunbar, R. C., Ion spectroscopy: Where Did It Come From, Where Is It Now, and Where Is It Going? *J. Am. Soc. Mass Spectrom.* **2010**, *21*, 681-693.

17. Zack L. N.; Maier, J. P. Laboratory Spectroscopy of Astrophysically Relevant Carbon Species. *Chem. Soc. Rev.* **2014**, *43*, 4602-4614.

18. Wolk, A. B.; Leavitt, C. M.; Garand E.; Johnson, M. A., Cryogenic Ion Chemistry and Spectroscopy. *Acc. Chem. Res.* **2014**, *47*, 202-210.

19. Douberly, G. E.; Ricks, A. M.; Ticknor, B. W.; McKee, W. C.; Schleyer, P. v. R.; Duncan, M. A., Infrared Photodissociation Spectroscopy of Protonated Acetylene and Its Clusters. *J. Phys. Chem. A* **2008**, *112*, 1897-1906.

20. Douberly, G. E.; Ricks, A. M.; Schleyer, P. v. R.; Duncan, M. A., Infrared Spectroscopy of Gas Phase $C_3H_5^+$: The Allyl and 2-Propenyl Cations. *J. Chem. Phys.* **2008**, *128*, 021102.

21. Douberly, G. E.; Ricks, A. M.; Schleyer, P. v. R.; Duncan, M. A., Infrared Spectroscopy of Gas Phase Benzenium Ions: Protonated Benzene and Protonated Toluene from 750 to 3400 cm^{-1}. *J. Phys. Chem. A* **2008**, *112*, 4869-4874.

22. Ricks, A. M.; Douberly, G. E.; Duncan, M. A., The Infrared Spectrum of Protonated Naphthalene and Its Relevance for the Unidentified Infrared Bands. *Astrophys. J.* **2009**, *702*, 301-306.

23. Ricks, A. M.; Douberly, G. E.; Schleyer, P. v. R.; Duncan, M. A., Infrared Spectroscopy of Gas Phase $C_3H_3^+$: The Cyclopropenyl and Propargyl Cations. *J. Chem. Phys.* **2010**, *132*, 051101.

24. Duncan, M. A., Infrared Laser Spectroscopy of Mass-Selected Carbocations, *J. Phys. Chem. A* **2012**, *116*, 11477-11491.

25. Mosley, J. D.; Cheng, T. C.; McCoy, A. B.; Duncan, M. A., Infrared Spctroscopy of the Mass 31 Cation: Protonated Formaldehdye vs Methoxy. *J. Phys. Chem. A* **2012**, *116*, 9287-9294.

26. Mosley, J. D.; Young, J. W.; Duncan, M. A., Infrared Spectroscopy of the Acetyl Cation and Its Protonated Ketene Isomer, *J. Chem. Phys.* **2014**, *141*, 024306

27. Mosley, J. D.; Young, J. W.; Huang, M.; McCoy, A. B.; Duncan, M. A. Infrared Spectroscopy of The Methanol Cation and Its Methylene-Oxonium Isomer. *J. Chem. Phys.* **2015**, *142*, 114301.

28. Crofton, M. W.; Jagod, M.-F.; Rehfuss, B. D.; Kreiner, W. A.; Oka, T., Infrared Spectroscopy of Carbo-ions III: ν3 Band of Methyl Cation CH_3^+. *J. Chem. Phys.* **1988**, *88*, 666-678.

29. Crofton, M. W.; Jagod, M.-F.; Rehfuss, B. D.; Oka, T., Infrared Spectroscopy of Carbo-ions V: Classical vs Nonclassical Structure of Protonated Acetylene $C_2H_3^+$. *J. Chem. Phys.* **1989**, *91*, 5139-5153.

30. Rosslein, M.; Gabrys, C. M.; Jagod, M.-F.; Oka, T., Detection of Infrared Spectrum of CH_2^+. *J. Mol. Spec.* **1992**, *153*, 738-740.

31. Gabrys, C. M.; Uy, D.; Jagod, M. F.; Oka T.; Amano, T., Infrared Spectroscopy of Carbo-ions VIII. Hollow-Cathode Spectroscopy of Protonated Acetylene, $C_2H_3^+$. *J. Phys. Chem.* **1995**, *99*, 15611-15623.

32. White, E. T.; Tang J.; Oka, T., CH_5^+: The Infrared Spectrum Observed. *Science* **1999**, *284*, 135-137.

33. Okumura, M.; Yeh, L. I.; Myers, J. D.; Lee, Y. T., Infrared Spectra of the Cluster Ions $H_7O^+_3 \cdot H_2$ and $H_9O^+_4 \cdot H_2$, *J. Chem. Phys.* **1986**, *85*, 2328.

34. Okumura, M.; Yeh, L. I.; Myers, J. D.; Lee, Y. T., Infrared Spectra of the Solvated Hydronium Ions: Vibrational Predissociation Spectroscopy of Mass-Selected $H_3O^+ \cdot (H_2O)_n \cdot (H_2)_m$, *J. Phys. Chem.* **1990**, *94*, 3416-3427.

35. Okumura, M.; Yeh, L. I.; Lee, Y. T. , The Vibrational Predissociation Spectroscopy of Hydrogen Cluster Ions, *J. Chem. Phys.* **1985**, *83*, 3075.

36. Yeh, L. I.; Price, J. M.; Lee, Y. T., Infrared Spectroscopy of the Pentacoordinated Carbonium ion $C_2H_7^+$. *J. Am. Chem. Soc.* **1989,** *111*, 5597-5604.

37. Boo, D. W.; Lee, Y. T., Vibrational Spectroscopy and Dynamics of Ionic Complexes of CH_5^+ and $CH_5^+(A)_x(B)_y$ (A, B = Ar, N_2, CH_4; x, y = 0-5). *Int. J. Mass. Spectrom. & Ion Process* **1996**, *159*, 209-229.

38. Nizkorodov, S. A.; Dopfer, O.; Ruchti, T.; Meuwly, M.; Maier, J. P.; Bieske, E. J., Size Effects in Cluster Infrared Spectra: The ν1 Band of Ar_n-HCO^+ (n = 1-13). *J. Phys. Chem.* **1995**, *99*, 17118-17129.

39. Nizkorodov, S. A.; Dopfer, O.; Meuwly, M.; Maier, J. P.; Bieske, E. J., Mid-Infrared Spectra of the Proton-Bound Complexes Ne_n –HCO^+ (n = 1, 2), *J. Chem. Phys.* **1996**, *105*, 1770.

40. Solcà, N.; Dopfer, O., Spectroscopic Identification of Oxonium and Carbenium Ions of Protonated Phenol in the Gas Phase: IR Spectra of Weakly Bound $C_6H_7O^+$-L Dimers (L =Ne, Ar, N_2), *J. Am. Chem. Soc.* **2004**, *126*, 1716-1725.

41. Solcà, N.; Dopfer, O., IR Spectrum and Structure of Protonated Ethanol Dimer: Implications for the Mobility of Excess Protons in Solution, *J. Am. Chem. Soc.* **2004**, *126*, 9520-9521.

42. Chakraborty, S.; Patzer, A.; Dopfer, O., IR Spectra of Protonated Benzaldehyde Clusters, $C_7H_7O^+$–L_n (L=Ar,N_2 ; $n \leq 2$) Ion-Ligand Binding Motifs of the Cis and Trans Oxonium Isomers. *J. Chem. Phys.* **2010**, *133*, 044307.

43. Dopfer, O.; Olkhov, R. V.; Mladenović, M.; Botschwina, P., Intermolecular Interaction in an Open-Shell π-Bound Cationic Complex: IR Spectrum and Coupled Cluster Calculations for $C_2H_2^+$-Ar, *J. Chem. Phys.* **2004**, *121*, 1744.

44. Chiavarino, B.; Crestoni, M. E.; Dopfer, O.; Maitre, P.; Fornarini, S., Benzylium versus Tropylium Ion Dichotomy: Vibrational Spectroscopy of Gaseous $C_8H_9^+$ Ions. *Angew. Chem. Int. Ed.* **2012**, *51*, 4947-4949.

45. Beynon, J. H.; Fontaine, A. E.; Lester, G. R., Mass Spectrometry: The Mass Spectrum of Methanol. Part I. Thermochemical Information, *Int. J. Mass Spectrom.* **1968**, *1*, 1-24.

46. Berkowitz, J., Photoionization of CH_3OH, CD_3OH, and CD_3OD: Dissociative Ionization Mechanisms and Ionic Structures, *J. Chem. Phys.* **1978**, *69*, 3044

47. Wesdemiotis, A.; McLafferty, F. W., Mass Spectral Evidence for the Hydroxymethylene Radical Cation, *Tetrahedron Lett.* **1981**, *22*, 3479-3480.

48. Burgers, P. C.; Mommers, A. A.; Holmes, J. L., Ionized Oxycarbenes: $[COH]^+$, $[CHOH]^+\bullet$, $[C(OH)_2]^+\bullet$, $[HCO_2]^+$, and $[COOH]^+$, Their Generation, Identification, Heat of Formation, and Dissociation Characteristics, *J. Am. Chem. Soc.* **1983**, *105*, 5976-5979.

49. Bouma, W. J.; Macleod, J. K.; Radom, L., An Ab Initio Molecular Orbital Study of the CH_2O^+ Isomers – Stability of the Hydroxymethylene Radical Cation, *Intl. J. Mass Spectrom. Ion Proc.* **1980**, *33*, 87-93.

50. Osamura, Y.; Goddard, J. D.; Schaefer, H. F.; Kim, K. S., Near Degenerate Rearrangement Between the Radical Cations of Formaldehyde and Hydroxymethylene, *J. Chem. Phys.* **1981**, *74*, 617

51. Wiest, O., Density Functional Theory Studies of the Methanol Radical Cation Hypersurface, *J. Mol. Struct.: THEOCHEM* **1996**, *368*, 39-48.

52. Turner, D. W.; Baker, C.; Baker, A. D. Bundle, C. R., Molecular Photoelectron Spectroscopy, (Wiley Interscience, London, 1970) pp.132.

53. Niu, B.; Shirley, D. A.; Bai, Y.; Daymo, E., High Resolution He Iα Photoelectron Spectroscopy of H_2CO and D_2CO Using Supersonic Molecular Beams. *Chem. Phys. Lett.* **1993**, *201*, 212-216.

54. Schulenburg, A. M.; Meisinger, M.; Radi, P. P.; Merkt, F., The Formaldehyde Cation: Rovibrational Energy Level Structure and Coriolis Interaction Near the Adiabatic Ionization Threshold, *J. Mol. Spectrosc.* **2008**, *250*, 44-50.

55. Mishra, S. P.; Symons, M. C., Detection of Radical H_2CO^+ by Electron Spin Resonance, *J.C.S. Chem. Comm.* **1975**, 909.

56. CFOUR, a quantum chemical program package written by J. F. Stanton, J. Gauss, M. E. Harding, and P. G. Szalay, with contributions from A. A. Auer, R. J. Bartlett, U. Benedikt, C. Berger, D. E. Bernholdt, Y. J. Bomble, L. Cheng, O. Christiansen, M. Heckert, O. Heun, C. Huber, T.-C. Jagau, D. Jonsson, J. Jusélius, K. Klein, W. J. Lauderdale, D. A. Matthews, T. Metzroth, L. A. Mück, D. P. O'Neill, D. R. Price, E.

Prochnow, C. Puzzarini, K. Ruud, F. Schiffmann, W. Schwalbach, S. Stopkowicz, A. Tajti, J. Vázquez, F. Wang, J. D. Watts; with the integral packages MOLECULE (by J. Almlöf and P. R. Taylor), PROPS (by P. R. Taylor), ABACUS (by T. Helgaker, H. J. Aa. Jensen, P. Jørgensen, and J. Olsen), and ECP routines by A. V. Mitin and C. van Wüllen, 2010.

57. Shimanouchi, T., "Molecular Vibrational Frequencies" in NIST Chemistry WebBook, NIST Standard Reference Database Number 69, Eds. P.J. Linstrom and W.G. Mallard, National Institute of Standards and Technology, Gaithersburg MD, 20899, http://webbook.nist.gov, (retrieved June 7, 2016).

58. Myshakin, E. M.; Jordan, K. D.; Sibert, E. L.; Johnson, M. A. Large anharmonic effects in the infrared spectra of the symmetrical $CH_3NO_2^-\cdot(H_2O)$ and $CH_3CO_2^-\cdot(H_2O)$ complexes. *J. Chem. Phys.* **2003**, *119*, 10138.

CHAPTER 4

SOLVATION DYNAMICS IN THE ENOL-KETO TAUTOMERIZATION OF PROTONATED ACETYLACETONE/WATER COMPLEXES

Introduction

Proton transfer is a key process in many areas of chemistry and biology including acid-base chemistry, electrochemical reactions, and photosynthesis.[1–8] It is also the basis for chemical ionization mass spectrometry,[9,10] plays a major role in hydrogen fuel cells,[11,12] and has been proposed in mechanisms implicated in atmospheric and interstellar chemistry.[13–16] In 1805, Grotthuss described the process of proton transfer in liquid water,[17–19] and evidence has been shown suggesting solvent assisted proton transfer in a number of mechanisms across chemistry and biology.[20,21] Therefore, the study of protonated systems and their solvation is an area of great interest. A number of recent studies have provided insight into the structure and solvation in hydrogen bonded systems using infrared spectroscopy of size-selected protonated water clusters in the gas-phase along with high level computational chemistry.[22–45] Moving to the gas phase allows the careful selection of specific systems with known composition. In the current work, we use these methods to obtain the infrared spectra of protonated acetylacetone (Hacac) and mixed Hacac/water clusters (n=1–3).

Proton-bound dimers, which have a shared proton in their structure, represent intermediates in proton transfer mechanisms and have been studied extensively using mass spectrometry.[9,10] A number of systems exhibiting shared protons with organic structures have

been studied previously using infrared spectroscopy.[26,46–58] Johnson showed that the frequency of the characteristic vibration arising from the motion of the shared proton is related to the difference in proton affinity of the involved neutral species.[59] This indicates a competition between the proton binding sites in different species. An interesting evolution of this idea is the possible competition between proton binding sites on a single molecule, which has been studied previously.[59,60] Amino acids have this kind of bifunctionality, so studying systems with the possibility of intramolecular shared proton motifs may provide insight into proton accommodation and solvation in proteins and peptides. One class of compounds that exhibits bifunctionality is the β-diketones.

Acetylacetone (2,4-pentanedione) is the simplest β-diketone. It exists in two tautomeric forms shown in Scheme 1: the enol that features an intramolecular hydrogen bond and resonance stabilization through a conjugated π-system, and the keto that contains two carbonyl groups with an approximate 180 degree dihedral between the two oxygens in the neutral species. The tautomers are easily distinguished using NMR.[61,62] Measurements using temperature dependent photoelectron and UV spectroscopies have shown that the enol tautomer is lower in energy by approximately 4 kcal/mol.[63,64] The equilibrium has also been shown to shift depending on the environment with the enol form dominating in gas phase measurements,[65,66] while the keto form dominates in polar solvents that are able to hydrogen bond.[67] The goal of the current investigation is to study the interaction of a possible intramolecular hydrogen bond with water, and to see the effect of solvation on the equilibrium between keto and enol tautomers of Hacac.

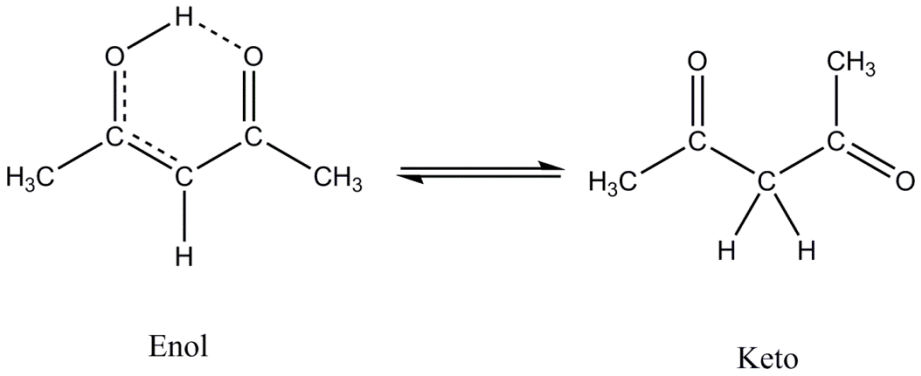

Scheme 1. Tautomers of Acetylacetone

Experimental

Protonated Hacac ions and mixed Hacac/water clusters are produced in a pulsed discharge/supersonic expansion of 10% H_2 in Ar seeded with ambient vapor pressure of both Hacac (ReagentPlus®, ≥ 99%, Sigma-Aldrich) and water at room temperature. The ions are mass selected using a reflectron time-of-flight spectrometer and interrogated using infrared laser photodissociation spectroscopy.[41,56–58] The energy absorbed in a single photon at these frequencies is not enough to break the strong covalent bonds present, so rare gas tagging is employed.[22–40, 42–45, 48,49] In this experiment, $H^+(Hacac)(H_2O)_nAr$ (n=0-3) ions are produced, mass selected, and absorption of an IR photon causes the elimination of the tag. The spectrum is recorded as the fragment ion yield versus the frequency of light absorbed. The IR laser system used is an optical parametric oscillator/amplifier system (OPO/OPA) (LaserVision) pumped by a Nd:YAG laser (Spectra Physics Pro-230) equipped with an external $AgGaSe_2$ crystal. The spectra were recorded from 1000 to 4000 cm^{-1}.

Computational studies were carried out at the DFT/B3LYP/6-311+G** level of theory using the Gaussian09 program package.[68] Vibrational spectra were scaled based on comparison of harmonic frequencies calculated for acetone at the same level to accepted values.[69]

Results and Discussion

A mass spectrum produced with the conditions mentioned above is shown in Figure 1. A large peak at mass 101 represents the protonated Hacac molecule. Starting from this peak, there are two patterns that can be seen. The first is the clustering of additional Hacac units onto the

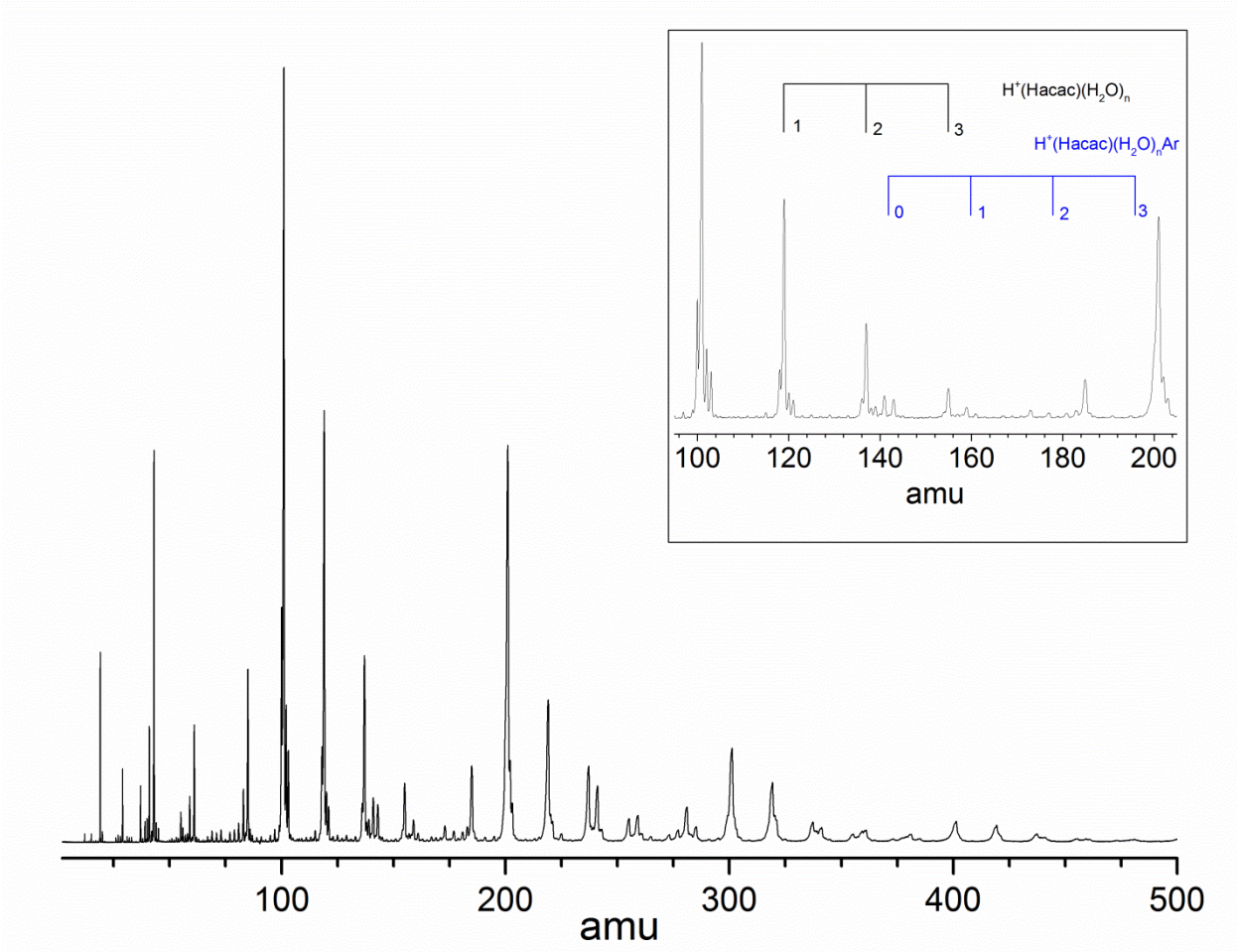

Figure 1. The full mass spectrum of acetylacetone with water produced with a needle discharge through a mixed H_2/Ar (10%/90%) expansion backed by about 7 atm pressure. Inset: An expanded view of the region between 95 and 205 amu. The progression of water attachment to protonated acetylacetone is indicated in black with the corresponding Ar-tagged species indicated in blue.

protonated molecule. These can be seen at masses 201, 301, and 401. It is possible that these extra molecules cluster around the central excess proton, but the spectra of these masses were not measured in this study. The second progression that starts at mass 101 can be seen more clearly in the inset of Figure 1. The progression of peaks at masses 119, 137, and 155 indicate the addition of 1, 2, and 3 water molecules onto the central protonated Hacac, respectively. Looking at the full mass spectrum, the clustering of water onto Hacac can also be seen in peaks to higher mass from the previously mentioned Hacac clusters. Along with water clustering, peaks corresponding to the attachment of argon onto the mixed Hacac/water clusters can be seen. These peaks were individually mass selected and their infrared spectra were collected using photodissociation of the argon tag.

Figure 2 shows a comparison of the infrared spectra obtained for the four species investigated in this investigation. The top, black trace is from H^+(Hacac)-Ar, the blue trace is from H^+(Hacac)(H_2O)-Ar, the red trace is from H^+(Hacac)(H_2O)$_2$-Ar, and the bottom, green trace is from H^+(Hacac)(H_2O)$_3$-Ar. All of the spectra from species including water exhibit broad resonances in the 2700–3500 cm^{-1} region of the spectrum indicative of hydrogen-bonding interactions. The difference in the general shape of the broad features is possibly indicative of different types of hydrogen-bonding interactions as seen in protonated water clusters.[22-45] The spectra also show different numbers of peaks in the O-H stretch region. The free O-H bonds vibrate at higher frequencies than their bound counterparts, causing multiple peaks to be seen in the spectrum. In the region below 2000 cm^{-1}, the bands seen in the n = 0-2 spectra exhibit similar features between 1650 and 1250 cm^{-1}. These are likely due to the Hacac backbone. The

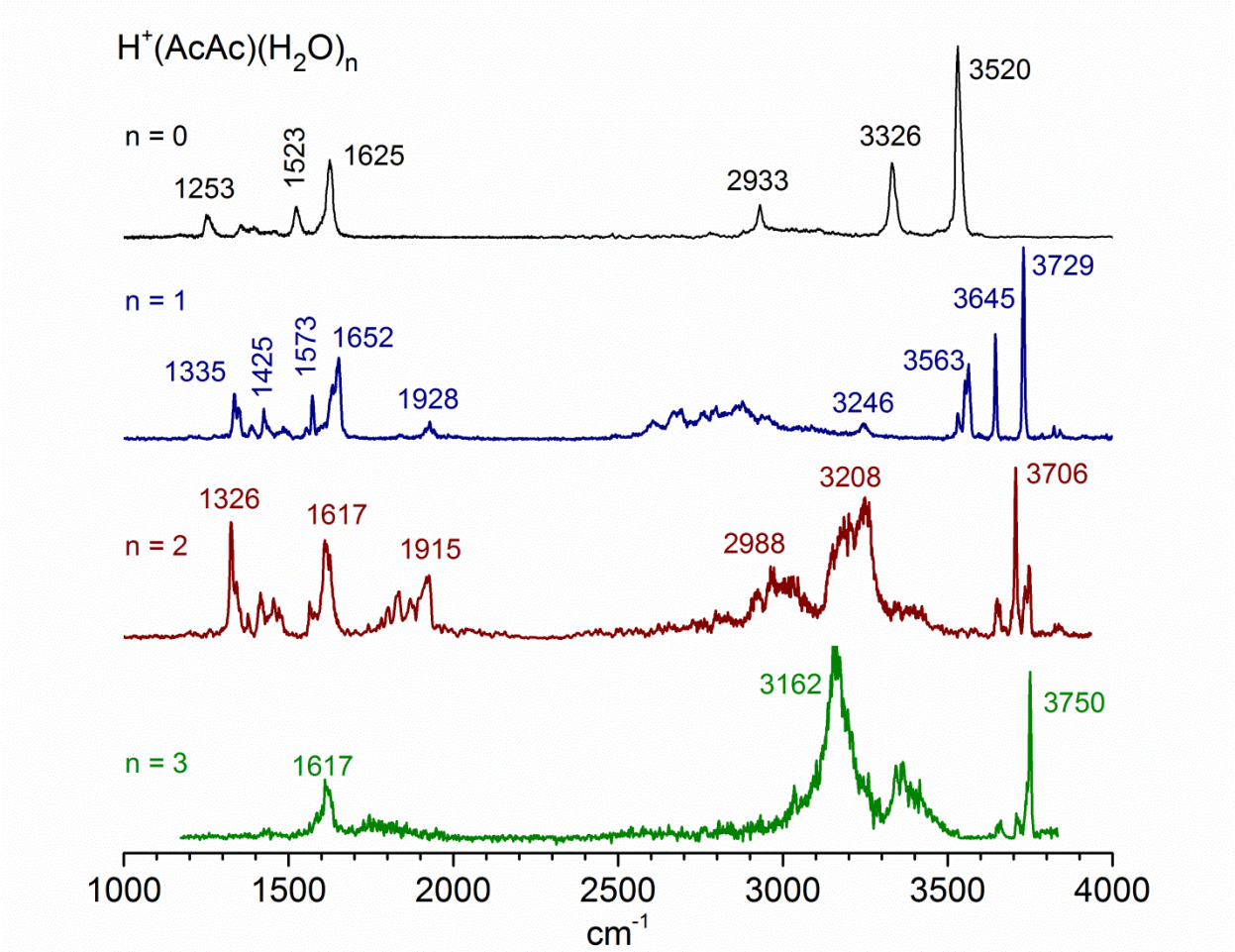

Figure 2. Comparsion of experimental spectra for $H^+(Hacac)(H_2O)_n$ (n=0-3) measured using infrared photodissociation of attached argon tag.

lack of features below 1617 cm^{-1} in the n = 3 spectrum is due to a combination of low parent ion intensity and the low laser power usually encountered in this region of the spectrum.

A. H^+(Hacac)

In order to fully investigate the spectra presented in Figure 2, computational studies were performed. Figure 3 shows the experimental spectrum obtained for protonated Hacac (black) vs theoretical spectra calculated for the two lowest enol structures (blue and green) and the lowest keto structure (red). The experimental spectrum shows strong, sharp resonances in the O-H stretching region at 3326 and 3520 cm^{-1}, along with a peak at 2933 cm^{-1} where CH stretches are typically found. The fingerprint region shows three baseline resolved peaks at 1253, 1523, and 1625 cm^{-1} and three other small, unresolved features between 1300 and 1500 cm^{-1}. Comparing with theory, there is no evidence of a carbonyl stretch in the 1900 to 2000 cm^{-1} region of the spectrum that would indicate a keto isomer as predicted by theory for all keto species. The relative intensities in both the O-H and fingerprint regions are in good agreement with the lowest energy enol isomer and all of the bands seen in the experiment can be assigned using this spectrum. Therefore we are confident in assigning the infrared spectrum for the H^+(Hacac)-Ar species to that of the lowest energy enol isomer. One important note: attachment of argon to this structure caused a red shift in the calculated O-H stretching frequencies. This effect was not seen in subsequent spectra.

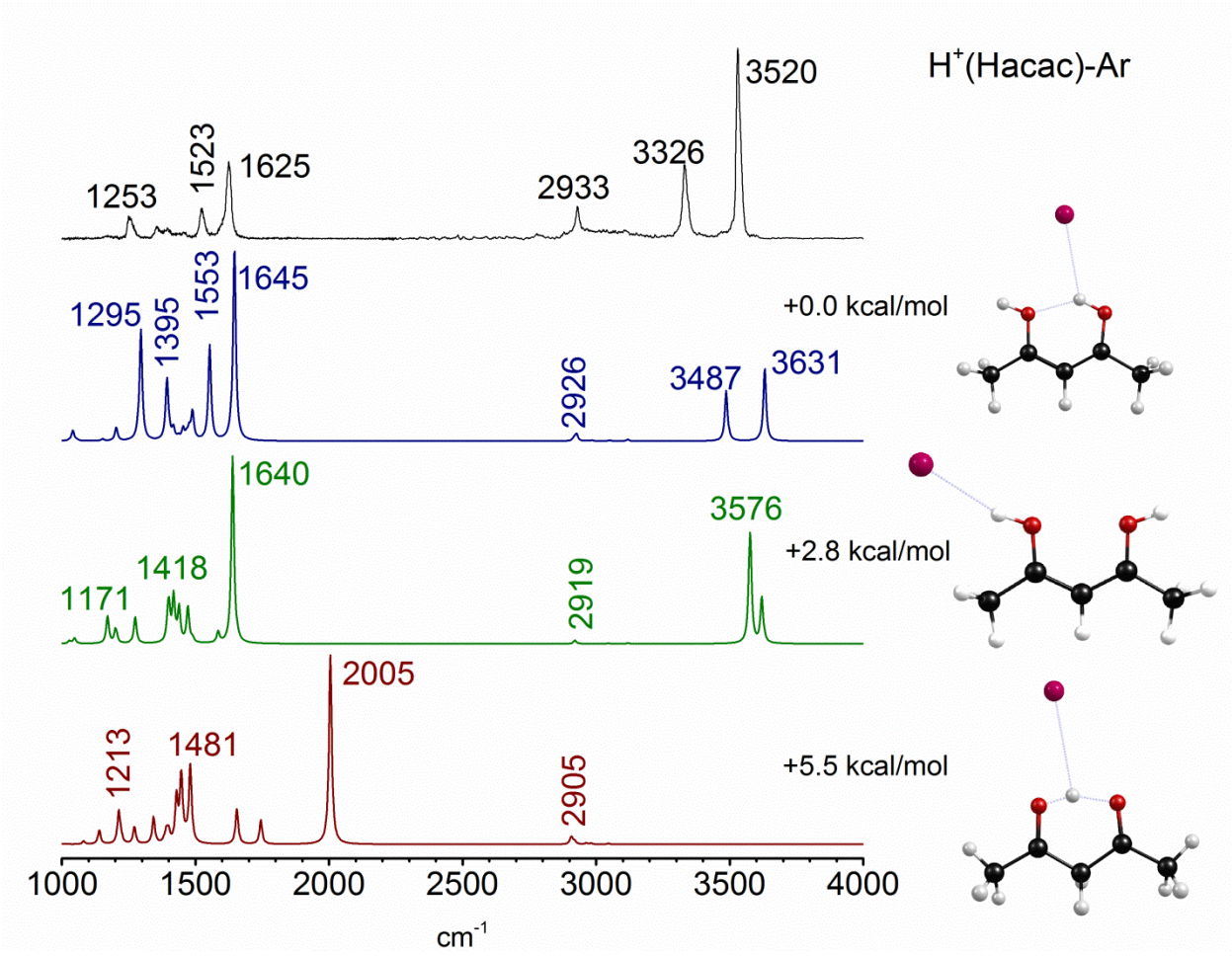

Figure 3. Infrared photodissociation spectra of H^+(Hacac)-Ar produced using the compared to predicted spectra calculated at the B3LYP/6-311+G** level of theory/basis for the two lowest enol isomers (blue, green) and the lowest keto isomer (red).

This assignment is not completely surprising. While we typically expect to produce the lowest energy isomer in our experiment, the enol form of Hacac has been shown to be the most stable tautomer in the gas phase.[63-66] The most stable structure for the enol form has an intramolecular shared proton between the two oxygen atoms, and this is seen in the assigned structure. It is likely that this structure is present initially in the vapor phase and is picked up by the carrier gas and carried into the vacuum chamber. The excess proton is then attached after the discharge. The most probable place for it to attach is on the lone pairs of one of the oxygens while conserving the shared proton motif. The second lowest energy enol isomer does not conserve the shared proton structure (Figure 3: green). An interesting note, the lowest keto isomer also has an intramolecular shared proton. This indicates that a rotation of 140 degrees along the dihedral relative to the neutral structure would be necessary in order to accommodate this structure. While it was not observed in our experiment, it would be interesting to measure the spectrum of this structure to determine if the proton is actually equally shared between the two oxygens as predicted by theory.

B. $H^+(Hacac)(H_2O)$

Figure 4 shows the experimental spectrum measured for the $H^+(Hacac)(H_2O)$ complex vs theory. The experimental spectrum exhibits three sharp peaks in the O-H stretching region at 3563, 3645, and 3729 cm^{-1} along with a small resonance at 3246 cm^{-1}, a broad feature spanning from 2500 to 3100 cm^{-1}, and small peak at 1928 cm^{-1}, and four major features in the fingerprint region at 1335, 1425, 1573, and 1652 cm^{-1}. Comparison of this spectrum with the one obtained

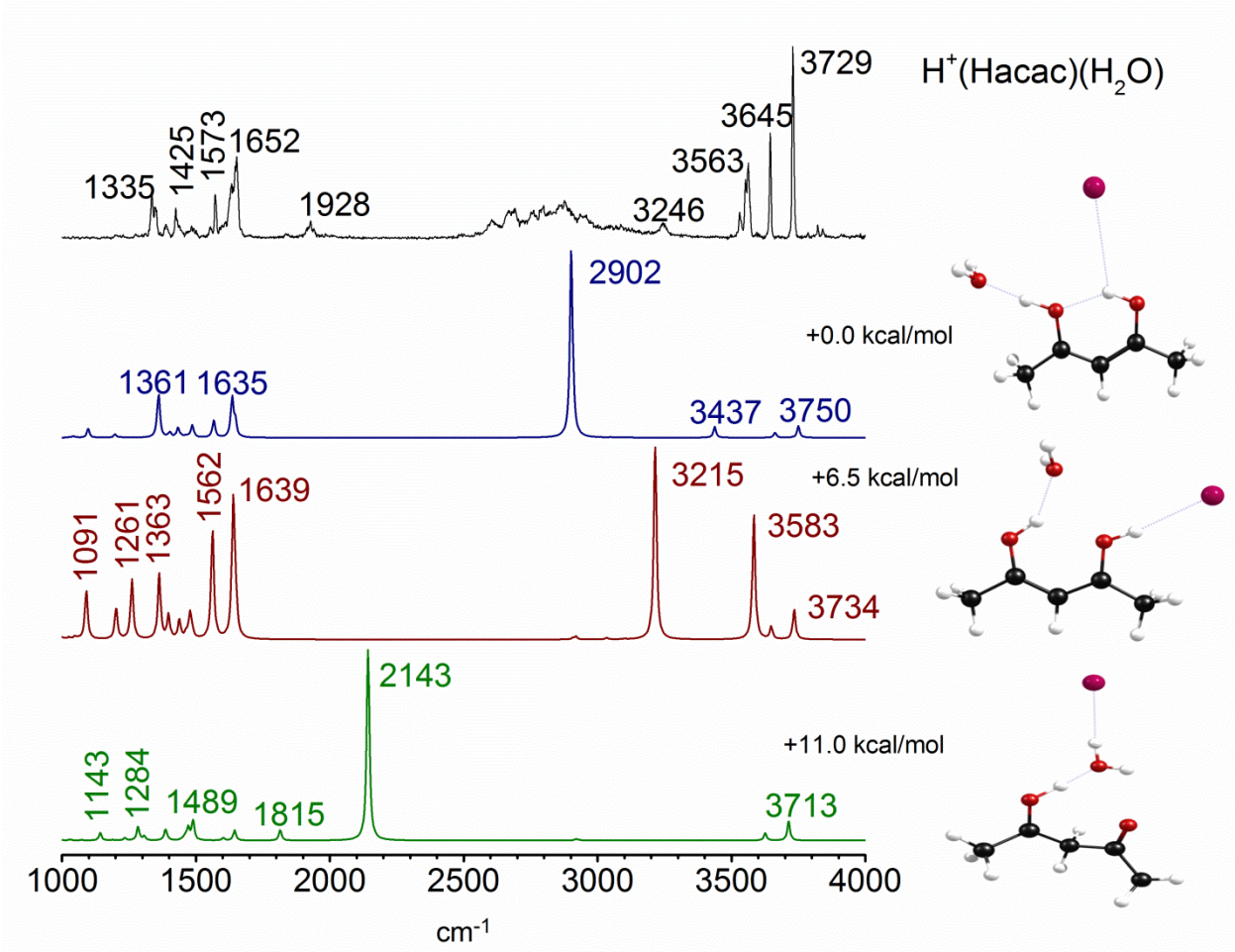

Figure 4. Infrared photodissociation spectra of $H^+(Hacac)(H_2O)$-Ar produced using the compared to predicted spectra calculated at the B3LYP/6-311+G** level of theory/basis for the two lowest enol isomers (blue, red) and the lowest keto isomer (green).

for the H^+(Hacac) complex identifies three new features. The broad feature is in an area typical of hydrogen bonding. The spectrum also features a new peak in the O-H stretching region that was not seen, likely due to O-H stretches from the attached water. The final new feature is a peak at 1928 cm^{-1} which is in a region typically attributed to C=O stretches and would likely only be seen if a keto isomer were present.

Comparing with theory, the lowest energy isomer (Figure 4: blue) corresponding to hydrogen bonding of the end O-H in Hacac with the oxygen atom in water shows good agreement with the peaks in the fingerprint region between 1300 and 1700 cm^{-1}. It also predicts a large peak at 2902 cm^{-1} that matches with the center of the broad feature. This predicted band comes from the O-H stretch of the Hacac involved in the hydrogen bond. All of the C-H stretches are also predicted to occur in this region, which are likely partially responsible for the width of the feature. Multiple O-H stretching frequencies corresponding to the intramolecular OH stretch (3437 cm^{-1}) and the symmetric and anti-symmetric O-H stretches of water (3670 and 3750 cm^{-1}) are also predicted. These also match the three large peaks in the O-H stretching region of the experiment (3563, 3645, and 3729 cm^{-1}), but the relative intensities are not quite right, and the peaks at 1928 and 3246 cm^{-1} are not reproduced. This is indicative of other isomers present.

The second lowest energy isomer (Figure 3: red, +6.5 kcal/mol), corresponds to the attachment of water to the intramolecular proton via hydrogen bond. The spectrum for this isomer also shows good agreement with experiment between 1300 and 1700 cm^{-1}. It also predicts a band at 3215 cm^{-1} which corresponds to the shared proton stretch between the water

and Hacac. This is close to the experimental band at 3246 cm^{-1} that was not previously predicted by the lowest energy isomer. The bands predicted in the O-H stretching region of the spectrum also show good agreement with the three bands seen in the experiment. A combination of the two spectra could explain the relative intensities seen in the experiment. However, neither of the lowest energy isomers has peaks in the correct region in order to assign the experimental band at 1928 cm^{-1}. The other higher energy, enol based isomers are also predicted to have no bands in this area of the spectrum.

To explain the band at 1928 cm^{-1}, other isomers were explored that had structures with diketo based Hacac motifs. The lowest energy diketo isomer (Figure 4: green, +11.0 kcal/mol) has a predicted band at 2143 cm^{-1} which could possibly account for the unexplained experimental band. This band corresponds to the shared proton stretch between the Hacac and the water molecule. Predicting shared proton frequencies has been shown by a number of different groups to be difficult,[30-39] which could explain the discrepancy between the predicted and experimental frequencies. The accepted proton affinity of Hacac is 873.5 kJ/mol,[64] but this was measured in the gas phase where the enol tautomer is significantly favored. Johnson et al. showed that frequency of the shared proton stretch is correlated to the difference in proton affinity of the two species involved.[49] For the shared proton stretch to shift to 1928 cm^{-1} for the keto structure with water, this would indicate a difference in proton affinity of approximately 100 kJ/mol. Since the proton affinity of water is 697 kJ/mol, this would indicate that the proton affinity of the keto tautomer is approximately 800 kJ/mol which is over 70 kJ/mol less than the

accepted value. This could have implications for work done in polar solvents where the keto form is favored.

C. $H^+(Hacac)(H_2O)_2$

The experimental spectrum for the tagged $H^+(Hacac)(H_2O)_2$ compared to theory is presented in Figure 5. Comparing this spectrum with that measured for the single water complex, there are now two broad, intense features in the hydrogen bonding region whereas the single water complex only exhibited one broad weak feature in this region of the spectrum. This could indicate that there are multiple hydrogen bonding environments, the shifts for which would cause multiple peaks in the spectrum corresponding to each different environment. This new spectrum also shows a significant change in intensities and spacing of the bands in the O-H stretching region, and a band at 1915 cm^{-1} that is red shifted 13 cm^{-1} from its position in the single water complex. The relative intensity of this band has also increased in this spectrum, possibly indicating a larger proportion of Hacac population undergoing tautomerization. This peak now also exhibits a number of lower intensity features directly to the red before the familiar bands between 1300 and 1650 cm^{-1} are seen. The presence of these fingerprint features is indicative of the existence of an enol type structure in one of the isomers present as seen in previous spectra.

As with the single water complex, comparison with theory also indicates that this spectrum is not consistent with any single isomer. The lowest energy structure (Figure 4: blue) is equivalent to the lowest energy structure in the single water complex (Figure 4: blue) with the second water connected to the first via a hydrogen bond. The calculated spectrum reveals the

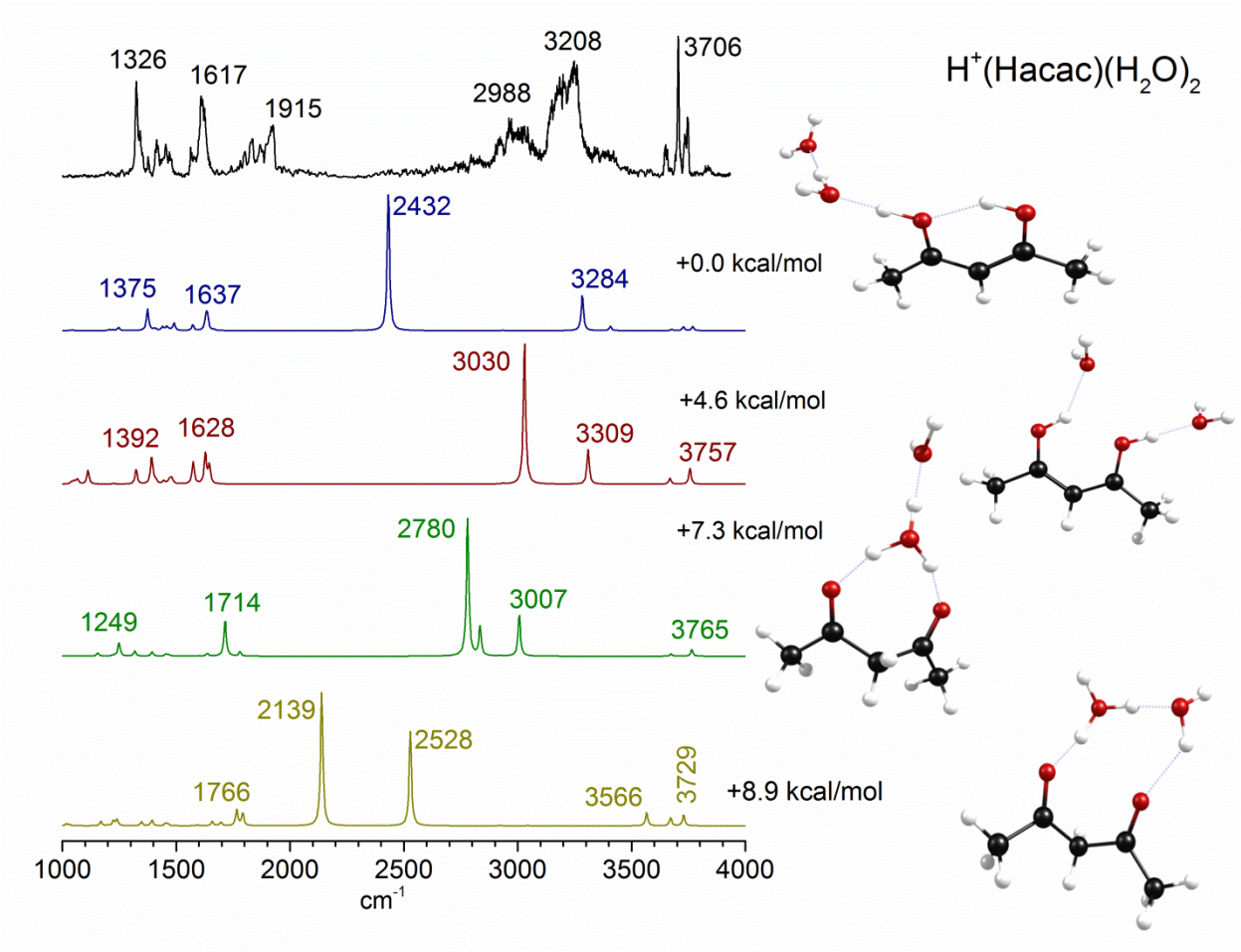

Figure 5. Infrared photodissociation spectra of $H^+(Hacac)(H_2O)_2$-Ar produced using the compared to predicted spectra calculated at the B3LYP/6-311+G** level of theory/basis for the two lowest enol isomers (blue, red) and the two lowest keto isomer (green, gold).

same pattern of peaks in the region between 1300 and 1650 cm^{-1} that is typical of enol based structures. It also has a calculated H-bond stretch at 2432 cm^{-1} coming from the shared proton between water and Hacac. This peak does not directly match the experimental spectrum, but as mentioned previously, theory can have difficulty predicting these shared proton stretches. The predicted spectrum also predicts two hydrogen bond stretches at 3284 and 3416 cm^{-1} representing the shared proton between the two water molecules and the intramolecular in the Hacac structure, respectively. The O-H stretching region of the calculated spectrum also shows three bands corresponding to the three free O-H stretches in the water chain. However, as with the single water complex, this isomer does not fully explain the experimentally obtained spectrum.

The next lowest structure energetically (Figure 5: red, +4.6 kcal/mol) corresponds to the water molecules each attaching to a separate O-H from an enol based structure. As with other enol structrures, the calculated spectrum also features the typical bands in the fingerprint region as have been seen for each of the enol structures in this paper. This spectrum also contains peaks in the H-bonding region of the spectrum corresponding to the individual shared proton stretches for the O-H positions of the enol structure to the oxygen atom of a water molecule. These two bands are calculated to occur at 3030 and 3309 cm^{-1}, respectively and their positions are in good agreement with the large features seen in the experiment. This calculated spectrum also fails to account for the peak at 1915 cm^{-1} and smaller features to the red.

A number of keto based structures were also investigated to explain these unexplained features and of these, a combination of the lowest two isomers is sufficient. These two isomers are shown in Figure 5 (green: +7.3 kcal/mol, yellow: +8.9 kcal/mol). The green spectrum shows

a peak at 1714 cm^{-1} along with large features at 2780, 2835, and 3007 cm^{-1} that likely contribute to the broad, prominent features in the experimental spectrum. The yellow spectrum shows a doublet centered at 1766 cm^{-1} along with a sharp feature at 2139 cm^{-1} that is likely responsible for the peak at 1915 cm^{-1} coming from the shared proton stretch between the hydronium motif and the carbonyl of the Hacac. It also has a peak calculated at 2528 cm^{-1} that is associated with the intermolecular H-bond between the two water molecules. This peak likely contributes to the overall intensity in the broad features in the H-bonding region of the spectrum. Combining the peaks in both calculated spectra gives assignment to the peaks in the region between 1750 and 1930 cm^{-1} of the experimental spectrum.

This spectrum of the $H^+(Hacac)(H_2O)_2$ cluster has been previously studied by Chang et al. and our spectrum between 2800 and 4000 cm^{-1} agrees with their spectrum.[71] They were previously unable to study the lower regions of the spectrum, mainly due to measurement by loss of water and because of available laser systems. Their analysis using theoretically obtained structures assigned the spectrum to a keto based structure, however the structure that they assigned to the spectrum is 11.3 kcal/mol higher in energy than the lowest energy isomer presented in this work and they did not investigate any enol based structures even though their experiment was performed in the gas phase.

D. $H^+(Hacac)(H_2O)_3$

The experimental spectrum obtained for $H^+(Hacac)(H_2O)_3$ is shown in Figure 6. Comparing to previous spectra, the features between 3000 and 3500 cm^{-1} are consistent with H-bonding features that have been seen in the two previous experimental spectra that contained

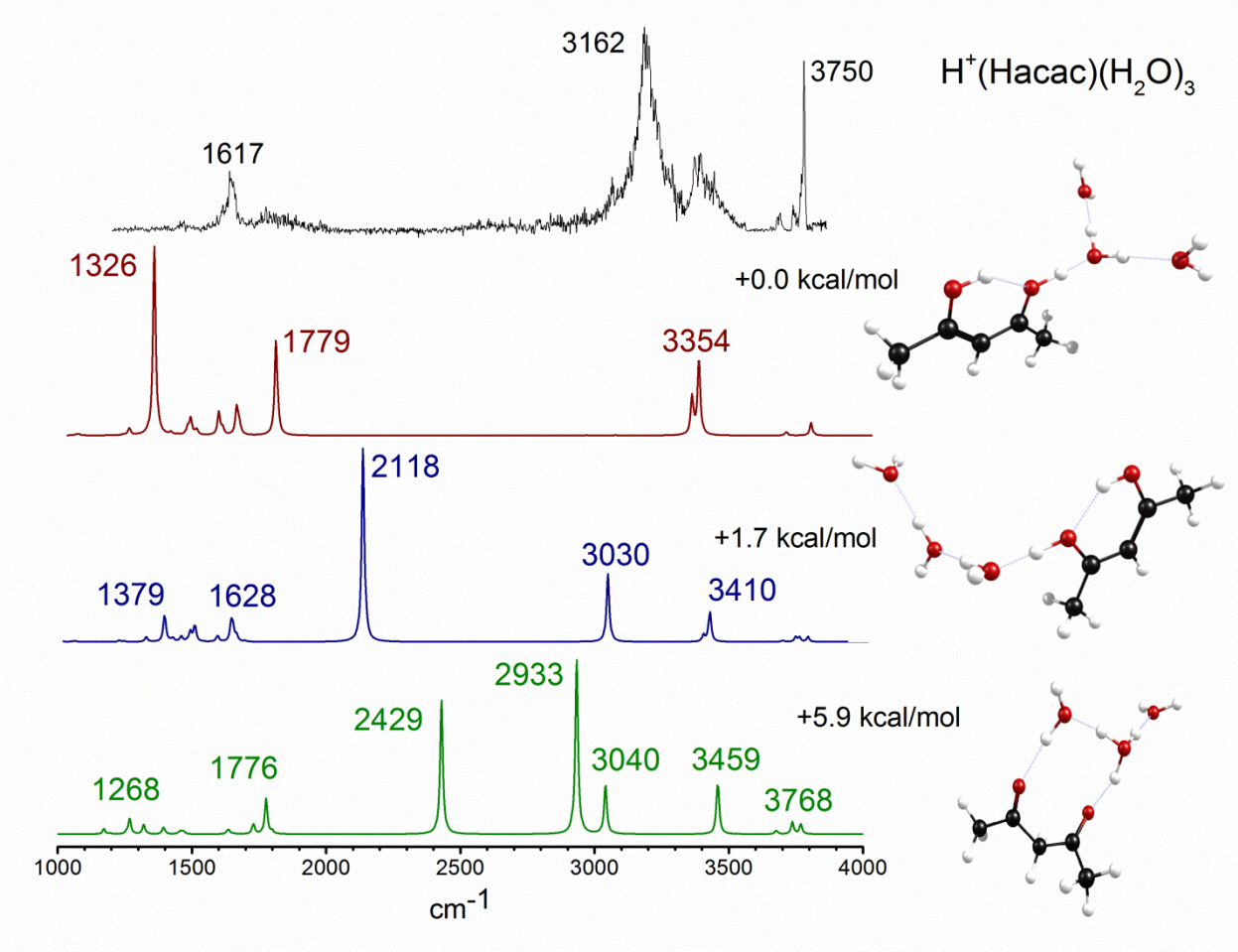

Figure 6. Infrared photodissociation spectra of $H^+(Hacac)(H_2O)_3$-Ar produced using the compared to predicted spectra calculated at the B3LYP/6-311+G** level of theory/basis for the two lowest enol isomers (blue, red) and the lowest keto isomer (green).

water, however the features in this new experimental spectrum are sharper than previous bands. Another difference between the previous experimental spectra is the change in intensity and spacing in the O-H stretching region. The spectrum now exhibits one intense band at 3750 cm^{-1} as well as two smaller features at 3658 and 3712 cm^{-1}. The lack of features to the red of the 1617 cm^{-1} band can be attributed to a combination of lack of laser power and unstable parent ion signal. Due to these issues, a complete assignment of this spectrum is difficult.

Comparison of this experimental spectrum with the two lowest enol based structures (Figure 6: red and blue) yields a reasonable agreement in the mid infrared region of the spectrum. A combination of both isomers correctly reproduces the relative intensities of the broad features in the hydrogen bonding region, as well as the correct number of features in the O-H stretching region. Looking in the far infrared, the experimental spectrum only shows a single peak that doesn't perfectly match the position predicted by either of these calculated spectra. Without more peaks in this region, we cannot definitively assign this peak to any combination of isomers. For this reason, we also cannot rule out the presence of any keto based isomers.

Based on the trend from each of the two complexes with water discussed previously, it would be likely that keto based isomers are indeed present and in larger quantities than those of previously studied complexes. Chang et al. studied this complex,[71] and as with the two water complex our experimental spectrum is consistent with their reported spectrum. They assigned the spectrum to that of the lowest keto based isomer shown in green in Figure 5. Their assignment was only based on the mid infrared region of the spectrum and comparing to the far

infrared region shown in this report, there is agreement for this isomer between the peak at 1617 cm^{-1} and the calculated peak at 1776 cm^{-1}.

Conclusion

Complexes of protonated Hacac and water were produced with a pulsed electrical discharge and their infrared spectra were obtained between 1000 and 4000 cm^{-1} using mass-selected photodissociation and argon tagging. Comparison of the experimental spectrum for H^+(Hacac) with theory showed a single enol based isomer responsible for the peaks seen which is consistent with the enol form being significantly favored in the gas phase. Upon attachment of water, a new set of features around 1920 cm^{-1} indicating the presence of keto based isomers. The amount of these keto based structures increased in concentration upon the addition of more water. In this work, we were unable to add a sufficient number of water molecules in order to fully shift the equilibrium in the tautomerization of the Hacac to the keto form. In the future, it may be possible to do so.

References

1. Bell, R. P. *The Proton in Chemistry*; Chapman & Hall: London, 1973.

2. Caldin, E.; Gold, V.; eds. *Proton Transfer Reactions*; Chapman and Hall: London, 1975.

3. Hynes, J. T.; Klinman, J. P.; Limbach, H.-H.; Schowen, R. L. eds. *Hydrogen Transfer Reactions*, Vols. 1–4; Wiley-VCH Publishers: Weinheim, 2006.

4. Bertini, I.; Gray, H. B.; Stiefel, E. I.; Valentine, J. S. *Biological Inorganic Chemistry*; University Science Books: Sausalito, CA, 2007.

5. Mohammed, O. F.; Pines, D.; Dreyer, J.; Pines, E.; Nibbering, E. T. J. Sequential Proton Transfer through Water Bridges in Acid-Base Reactions. *Science* **2005**, *310*, 83–86.

6. Wraight, C. A. Chance and Design - Proton Transfer in Water, Channels and Bioenergetic Proteins. *Biochimica et Biophysica Acta* **2006**, *1757*, 886–912.

7. Siwick, B. J.; Bakker, H. J. On the Role of Water in Intermolecular Proton-Transfer Reactions. *J. Am. Chem. Soc.* **2007**, *129*, 13412–13420.

8. Hammes-Schiffer, S.; Soudackov, A.V. Proton-Coupled Electron Transfer in Solution, Proteins, Electrochemistry. *J. Phys. Chem. B* **2008**, *112*, 14108–14123.

9. Harrison, A. G. *Chemical Ionization Mass Spectrometry*, 2nd edition; CRC Press: Boca Raton, FL, 1992.

10. Blake, R. S.; Monks, P. S.; Ellis, A. M. Proton-Transfer Reaction Mass Spectrometry, *Chem. Rev.* **2009**, *109*, 861–896.

11. Sorensen, B. *Hydrogen Fuel Cells*; Elsevier Academic Press: Burlington, MA, 2005.

12. Esswein, A. J.; Nocera, D. G. Hydrogen Production by Molecular Photocatalysis. *Chem. Rev.* **2007**, *107*, 4022–4047.

13. Ferguson, E. E.; Fehsenfield, F. C.; Albritton, D. L. "Ion Chemistry of the Earth's Atmosphere," in *Gas Phase Ion Chemistry*, edited by M. T. Bowers, Vol. 1; Academic Press: New York, 1979, p. 45.

14. Duley, W. W. Molecular Clusters in Interstellar Clouds, *Astrophys. J.* **1996**, *471*, L57–L60.

15. Tielens, A. G. G. M. *The Physics and Chemistry of the Interstellar Medium*; Cambridge University Press: Cambridge, U.K., 2005.

16. Shuman, N. S.; Hunton, D. E.; Viggiano, A. A. Ambient and Modified Atmospheric Ion Chemistry: From Top to Bottom. *Chem. Rev.* **2015**, *115*, 4542-4570.

17. de Grotthuss, C. J. T. Mémoire sur la Décomposition de l'Eau et des Corps qu'elle Tient en Dissolution à l'Aide de l'Électricité Galvanique, *Ann. Chim.* (Paris), **1805**, *LVIII*, 54-74.

18. de Grotthuss, C. J. T. Memoirs on the Decomposition of Water and of the Bodies that it Holds in Solution by Means of Galvanic Electricity (translation), *Biochimica & Biophysica Acta* **2006**, *1757*, 871-875.

19. Marx, D. Proton Transfer 200 Years After von Grotthuss: New Insights from Ab Initio Simulations, *ChemPhysChem* **2006**, *7*, 1848-1870.

20. Peters, K. S. A Theory-Experiment Conundrum for Proton Transfer, *Acct. Chem. Res.* **2009**, *42*, 89-96

21. Garczarek, F.; Gerwert, K. Functional Waters in Intraprotein Proton Transfer Monitored by FTIR Difference Spectroscopy. *Nature* **2006**, *439*, 109-112.

22. Yeh, L. I.; Okumura, M.; Myers, J. D.; Price, J. M.; Lee, Y. T. Vibrational Spectroscopy of the Hydrated Hydronium Cluster Ions $H_3O^+(H_2O)_n$ (n=1,2,3). *J. Chem. Phys.* **1989**, *91*, 7319-7330.

23. Yeh, L. I.; Lee, Y. T.; Hougen, J. T. Vibration-Rotation Spectroscopy of the Hydrated Hydronium Ions $H_5O_2^+$, $H_9O_4^+$. *J. Mol. Spec.* **1994**, *164*, 473-488.

24. Wang, Y.-S.; Jiang, J.-C.; Cheng, C.-L.; Lin, S. H.; Lee, Y. T.; Chang, H.-C. Indentifying 2-, 3-Coordinated H_2O in Protonated Ion-Water Clusters by Vibrational Pre-Dissociation Spectroscopy, Ab Initio Calculations. *J. Chem. Phys.* **1997**, *107*, 9695-9698.

25. Chang, H.-C.; Jiang, J.-C.; Hahndorf, I.; Lin, S. H.; Lee, Y. T.; Chang, H.-C. Migration of an Excess Proton upon Asymmetric Hydration: $H^+[(CH_3)_2O](H_2O)_n$ as a Model System. *J. Am. Chem. Soc.* **1999**, *121*, 4443-4450.

26. Jiang, J.-C.; Wang, Y.-S.; Chang, H.-C.; Lin, S. H.; Lee, Y. T.; Niedner-Schatteburg, G.; Chang, H.-C. Infrared Spectra of $H^+(H2O)_{5-8}$ Clusters: Evidence for Symmetric Proton Hydration. *J. Am. Chem. Soc.* **2000**, *122*, 1398-1410.

27. Asmis, K. R.; Pivonka, N. L.; Santambrogio, G.; Brummer, M.; Kaposta, C.; Neumark, D.; Wöste, L. Gas-Phase Infrared Spectrum of the Protonated Water Dimer. *Science* **2003**, *299*, 1375−1377.

28. Fridgen, T. D.; McMahon, T. B.; MacAleese, L.; Lemaire, J.; Maitre, P. Infrared Spectrum of the Protonated Water Dimer in the Gas Phase. *J. Phys. Chem. A* **2004**, *108*, 9008−9010.

29. Headrick, J. M.; Bopp, J. C.; Johnson, M. A. Predissociation Spectroscopy of the Argon-Solvated $H_5O_2^+$ "Zundel" Cation in the 1000-1900 cm^{-1}. *J. Chem. Phys.* **2004**, *121*, 11523−11526.

30. Diken, E. G.; Headrick, J. M.; Roscioli, J. R.; Bopp, J. C.; Johnson, M. A.; McCoy, A. B. Fundamental Excitations of the Shared Proton in the $H_3O_2^-$ and $H_5O_2^+$ Complexes. *J. Phys. Chem. A* **2005**, *109*, 1487−1490.

31. Hammer, N. I.; Diken, E. G.; Roscioli, J. R.; Johnson, M. A.; Myshakin, E. M.; Jordan, K. D.; McCoy, A. B.; Huang, X.; Bowman, J. M.; Carter, S. The Vibrational Predissociation Spectra of the $H_5O_2^+$ RG_n (RG = Ar, Ne) Clusters: Correlation of the Solvent Perturbations in the Free OH and Shared Proton Transitions of the Zundel Ion. *J. Chem. Phys.* **2005**, *122*, 244301/1−10.

32. Headrick, J. M.; Diken, E. G.; Walters, R. S.; Hammer, N. I.; Christie, R. A.; Cui, J.; Myshakin, E. M.; Duncan, M. A.; Johnson, M. A.; Jordan, K. D. Spectral Signatures of Hydrated Proton Vibrations in Water Clusters. *Science* **2005**, *308*, 1765−1769.

33. McCunn, L. R.; Roscioli, J. R.; Johnson, M. A.; McCoy, A. B. An H/D Isotopic Substitution Study of the $H_5O_2^+ \cdot Ar$ Vibrational Predissociation Spectra: Exploring the

Putative Role of Fermi Resonances in the Bridging Proton Fundamentals. *J. Phys. Chem. B* **2008**, *112*, 321−327.

34. McCunn, L. R.; Roscioli, J. R.; Elliott, B. M.; Johnson, M. A.; McCoy, A. B. Why Does Argon Bind to Deuterium? Isotope Effects and Structures of $Ar{\cdot}H_5O_2^+$ Complexes. *J. Phys. Chem. A* **2008**, *112*, 6074−6078.

35. Olesen, S. G.; Guasco, T. L.; Roscioli, J. R.; Johnson, M. A. Tuning the Intermolecular Proton Bond in the $H_5O_2^+$ 'Zundel Ion' Scaffold. *Chem. Phys. Lett.* **2011**, *509*, 89−95.

36. Fournier, J. A.; Johnson, C. J.; Wolke, C. T.; Weddle, G. H.; Wolk, A. B.; Johnson, M. A.; Vibrational Spectral Signature of the Proton Defect in the Three-Dimensional $H^+(H_2O)_{21}$ Cluster. *Science*, **2014**, *344*, 1009-1012.

37. Fournier, J. A.; Wolke, C. T.; Johnson, M. A.; Odbadrakh, T. T.; Jordan, K. D.; Kathmann, S. M.; Xantheas, S.; Snapshots of Proton Accommodation at a Microscopic Water Surface: Understanding the Vibrational Signatures of the Charge Defect in Cryogenically Cooled $H^+(H_2O)_{n=2-28}$ Clusters. *J. Phys. Chem. A*, **2015**, *119*, 9425-9440.

38. Fagiani, M. R.; Knorke, H.; Esser, T. K.; Heine, N.; Wolke, C. T.; Gewinner, S.; Schöllkopf, W.; Gaigeot, M-P.; Spezia, R.; Johnson, M. A.; Asmis, K. R.; Gas Phase Vibrational Spectroscopy of the Protonated Water Pentamer: The Role of Isomers and Nuclear Quantum Effects. *Phys. Chem. Chem. Phys.*, **2016**, *18*, 26743-26754.

39. Wolke, C. T.; Fournier, J. A.; Dzugan, L. C.; Fagiani, M. R.; Odbadrakh, T. T.; Knorke, H.; Jordan, K. D.; McCoy, A. B.; Asmis, K. R.; Johnson, M. A. Spectroscopic Snapshots of the Proton-Transfer Mechanism in Water. *Science*, **2016**, *354*, 1131-1135.

40. Chang, H.-C.; Wu, C.-C.; Kuo, J.-L. Recent Advances in Understanding the Structures of Medium-Sized Protonated Water Clusters. *Int. Rev. Phys. Chem.* **2005**, *24*, 553−578.

41. Douberly, G. E.; Walters, R. S.; Cai, J.; Jordan, K. D.; Duncan, M. A. Infrared Spectroscopy of Small Protonated Water Clusters, $H^+(H_2O)_n$ (n = 2−5): Isomers, Argon Tagging, and Deuteration. *J. Phys. Chem. A* **2010**, *114*, 4570−4579.

42. Mizuse, K.; Fujii, A. Infrared Photodissociation Spectroscopy of $H^+(H_2O)_6 \cdot M$ (M = Ne, Ar, Kr, Xe, H_2, N_2, and CH_4): Messenger-Dependent Balance Between H_3O^+ and $H_5O_2^+$ Core Isomers. *Phys. Chem. Chem. Phys.* **2011**, *13*, 7129-7135.

43. Mizuse, K.; Fujii, A.; Tuning the Internal Energy and Isomer Distribution in Small Protonated Water Clusters $H^+(H_2O)_{4-8}$: An Application of the Inert Gas Messenger Technique. *J. Phys. Chem. A*, **2012**, *116*, 4868-4877.

44. Shin, J.-W.; Hammer, N. I.; Diken, E. G.; Johnson, M. A.; Walters, R. S.; Jaeger, T. D.; Duncan, M. A.; Christie, R. A.; Jordan, K. D. Infrared Signature of Structures Associated with the $H^+(H_2O)_n$ (n = 6 to 27) Clusters. *Science* **2004**, *304*, 1137−1140.

45. Ebata, T.; Fujii, A.; Mikami, N. Vibrational Spectroscopy of Small-Sized Hydrogen-Bonded Clusters, Their Ions. *Int. Rev. Phys. Chem.* **1998**, *17*, 331-361.

46. Miyazaki, M.; Fuji, A.; Ebata T.; Mikami, N. Infrared Spectroscopy of Hydrated Benzene Cluster Cations, $[C_6H_6\text{-}(H_2O)_n]^+$ (n = 1-6): Structural Changes upon Photoionization and Proton Transfer Reactions. *Phys. Chem. Chem. Phys.* **2003**, *5*, 1137-1148.

47. Miyazaki, M.; Asuka, F.; Ebata, T.; Mikami, N. Infrared Spectroscopic Evidence for Protonated Water Clusters Forming Nanoscale Cages. *Science* **2004**, *304*, 1134-1137.

48. Dopfer, O.; Olkhov, R. V.; Roth, D.; Maier, J. P. Intermolecular Interaction in Proton-Bound Dimers: Infrared Photodissociation Spectra of Rg-HOCO+ (Rg=He, Ne, Ar) Complexes. *Chem. Phys. Lett.* **1998**, *296*, 585-591.

49. Verdes, D.; Linnartz, H.; Maier, J. P.; Botschwina, P.; Oswald, R.; Rosmus, P.; Knowles, P.J. Spectroscopic, Theoretical Characterization of Linear Centrosymmetric NN---H^+---NN. *J. Chem. Phys.* **1999**, *111*, 8400-8403.

50. Bieske, E. J.; Dopfer, O. High-Resolution Spectroscopy of Cluster Ions. *Chem. Rev.* **2000**, *100*, 3963-3998.

51. Solca, N.; Dopfer, O. IR Spectrum of the Benzene-Water Cation: Direct Evidence for a Hydrogen-Bonded Charge-Dipole Complex. *Chem. Phys. Lett.* **2001**, *347*, 59-64.

52. Solca, N.; Dopfer, O. Interaction of the Benzenium Ion with Inert Ligands: IR Spectra of $C_6H_7^+$-L_n Cluster Cations (L=Ar, N_2, CH_4, H_2O). *Chem. Eur.* **2003**, *9*, 3154-3163.

53. Wu, C. -C.; Chaudhuri, C.; Jiang, J. C.; Lee, Y. T.; Chang, H. -C.; Hydration-Induced Conformational Changes in Protonated 2,4-Pentanedione in the Gas Phase. *Mol. Phys.*, **2003**, *101*, 1285–1295.

54. Fridgen, T. D.; MacAleese, L.; McMahon, T. B.; Lemaire, J.; Maitre, P. Gas Phase Infrared Multiple-Photon Dissociation Spectra of Methanol, Ethanol, Propanol Proton-Bound Dimers, Protonated Propanol and the Propanol/Water Proton-Bound Dimer. *Phys. Chem. Chem. Phys.* **2006**, *8*, 955-966.

55. Roscioli, J. R.; McCunn, L. R.; Johnson, M. A. Quantum Structure of the Intermolecular Proton Bond. *Science* **2007**, *316*, 249-254.

56. Douberly, G. E.; Ricks, A. M.; Ticknor, B. W.; Duncan, M. A. Infrared Spectroscopy of Protonated Acetone and its Dimer. *Phys. Chem. Chem. Phys.*, **2008**, *10*, 77-79.

57. Douberly, G. E.; Ricks, A. M.; Ticknor, B. W.; McKee, W. C.; Schleyer, P. v. R.; Duncan, M. A. Infrared Photodissociation Spectroscopy of Protonated Acetylene and its Clusters. *J. Phys. Chem. A*, **2008**,*112*, 1897-1906.

58. Cheng, T. C.; Bandyopadhyay, B.; Mosley, J. D.; Duncan, M. A. IR Spectroscopy of Protonation in Benzene–Water Nanoclusters: Hydronium, Zundel, and Eigen at a Hydrophobic Interface. *J. Am. Chem. Soc.*, **2012**, *134*, 13046–13055.

59. DeBlase, A. F.; Bloom, S.; Lectka, T.; Jordan, K. D., McCoy, A. B.; Johnson, M. A.; Origin of the Diffuse Vibrational Signature of a Cyclic Intramolecular Proton Bond: Anharmonic Analysis of Protonated 1,8-Disubstituted Naphthalene. *J. Chem. Phys.*, **2013**, *139*, 024301.

60. Leavitt, C. M.; DeBlase, A. F.; Johnson, C. J.; van Stipdonk, M.; McCoy, A. B.; Johnson, M. A. Hiding in Plain Sight: Unmasking the Diffuse Spectral Signatures of the Protonated N-Terminus in Isolated Dipeptides Cooled in a Cryogenic Ion Trap. *J Phys. Chem. Lett.*, **2013**, *3*, 3450–3457.

61. Folkendt, M. M.; Weiss-Lopez, B. E.; Chauvel, J. P.; True, N. S. Gas-Phase 1H NMR Studies of Keto-Enol Tautomerism of Acetylacetone, Methyl Acetoacetate and Ethyl Acetoacetate. *J. Phys. Chem.* **1985**, *89*, 3347−3352.

62. Manbeck, Kimberly A.; Boaz, Nicholas C.; Bair, Nathaniel C.; Sanders, Allix M. S.; Marsh, Anderson L. Substituent Effects on Keto–Enol Equilibria Using NMR Spectroscopy. *J. Chem. Educ.* **2011**, *88*, 1444–1445.

63. Hush, N. S.; Livett, M. K.; Peel, J. B.; Willett, G. D. Variable-Temperature Ultraviolet Photoelectron Spectroscopy of the Keto-Enol Tautomers of Pentane-2,4-dione. *Aust. J. Chem.* **1987**, *40*, 599−609.

64. Nakanishi, H.; Morita, H.; Nagakura, S. Electronic Structures and Spectra of the Keto and Enol Forms of Acetylacetone. *Bull. Chem. Soc. Jpn.* **1977**, *50*, 2255−2261.

65. Howard, D. L.; Kjaergaard, H. G.; Huang, J.; Meuwly, M. Infrared and Near-Infrared Spectroscopy of Acetylacetone and Hexafluoroacetylacetone. *J. Phys. Chem. A.* **2015**, *119*, 7980–7990.

66. Yoshida, Z.; Ogoshi, H.; Tokumitsu, T. Intramolecular Hydrogen Bond in Enol Form of 3-Substituted-2,4-Pentanedione. *Tetrahedron*. **1970**, *26*, 5691–5697.

67. Reichardt, Christian . Solvents and Solvent Effects in Organic Chemistry 3rd Edition. (Wiley-VCH, Weinheim, Germany, 2003).

68. Gaussian 09, Revision D.01, Frisch, M. J.; Trucks, G. W.; Schlegel, H. B.; Scuseria, G. E.; Robb, M. A.; Cheeseman, J. R.; Scalmani, G.; Barone, V.; Mennucci, B.; Petersson, G. A.; Nakatsuji, H.; Caricato, M.; Li, X.; Hratchian, H. P.; Izmaylov, A. F.; Bloino, J.; Zheng, G.; Sonnenberg, J. L.; Hada, M.; Ehara, M.; Toyota, K.; Fukuda, R.; Hasegawa, J.; Ishida, M.; Nakajima, T.; Honda, Y.; Kitao, O.; Nakai, H.; Vreven, T.; Montgomery,

J. A., Jr.; Peralta, J. E.; Ogliaro, F.; Bearpark, M.; Heyd, J. J.; Brothers, E.; Kudin, K. N.; Staroverov, V. N.; Kobayashi, R.; Normand, J.; Raghavachari, K.; Rendell, A.; Burant, J. C.; Iyengar, S. S.; Tomasi, J.; Cossi, M.; Rega, N.; Millam, J. M.; Klene, M.; Knox, J. E.; Cross, J. B.; Bakken, V.; Adamo, C.; Jaramillo, J.; Gomperts, R.; Stratmann, R. E.; Yazyev, O.; Austin, A. J.; Cammi, R.; Pomelli, C.; Ochterski, J. W.; Martin, R. L.; Morokuma, K.; Zakrzewski, V. G.; Voth, G. A.; Salvador, P.; Dannenberg, J. J.; Dapprich, S.; Daniels, A. D.; Farkas, Ö.; Foresman, J. B.; Ortiz, J. V.; Cioslowski, J.; Fox, D. J. Gaussian, Inc., Wallingford CT, 2009.

69. Shimanouchi, T., Tables of Molecular Vibrational Frequencies Consolidated Volume I, National Bureau of Standards, 1972, 1-160.

70. Hunter, E.P.; Lias, S.G. Evaluated Gas Phase Basicities and Proton Affinities of Molecules: An Update. *J. Phys. Chem. Ref. Data* **1998**, *27*, 413-656.

71. Wu, C. -C.; Chaudhuri, C.; Jiang, J. C.; Lee, Y. T.; Chang, H. -C. Hydration-Induced Conformational Changes in Protonated 2,4-Pentanedione in the Gas Phase. *Mol. Phys.*, **2003**, *101*, 1285-1295.

CHAPTER 5

COMPUTATIONAL PREDICTIONS OF ELECTRONICALLY EXCITED STATES FOR CARBOCATIONS OF POSSIBLE ASTROPHYSICAL INTEREST: A TDDFT STUDY

Introduction

When light passes through material in space, it causes absorption by hundreds of possible atomic and molecular species. Many of these bands in the microwave and visible regions of the spectrum correspond to known molecules. The bands seen in the near-infrared to the ultraviolet regions are not rotationally resolved and are collectively known as the diffuse interstellar bands (DIBs) which were first seen in 1922.[1] The identity of the carriers responsible for these bands has remained a mystery,[2-7] and a large amount of work in the astronomical community has been undertaken to solve this riddle. The presence of bands in this region of the spectrum suggests molecular electronic transitions, and the shapes and widths of the DIBs are consistent with gas phase molecular systems. Because of the abundance of carbon in space, and the even higher abundance of hydrogen, small hydrocarbon molecules are believed to be ubiquitous in nearly all astro-environments, including circumstellar matter, interstellar dense and diffuse clouds, planetary nebulae, star-forming regions, etc.[2-4,8-10] For this reason, most of the predictions for the structures of molecular carriers of the DIBs have been carbon based, particularly carbon chains and polycyclic aromatics.[5,6] Most of the work done to this point focuses on neutral species, particularly radicals, but there are a number of stable cationic species that are likely to be in space and whose electronic absorption spectra have yet to be seen.[11-13] A significant

amount of work has been done on these systems. The groups of Maier[14-19] and Bieske[20-24] have used a combination of laser photodissociation and matrix isolation techniques to measure the electronic spectra of a number of different species. However, to this point, there has been very little conclusive evidence for attribution of DIBs to these structures.[19]

Theoretical calculations have been used extensively for over 30 years to solve problems in astrochemistry, mainly for the identification of molecules in the interstellar medium seen in microwave spectra.[25-27] Unfortunately, the level of accuracy that is seen in these calculations[28,29] cannot be obtained for electronically excited states.[30] This difficulty can be attributed to the greater sensitivity of electronic transition energies to the accuracy of the quantum mechanical model applied, as well as the coupling of electronic transitions to vibrational modes.[28,29] Efforts by a number of groups are ongoing to create more accurate models to properly describe the transitions of large numbers of proposed DIB carriers.[31] This work focuses on time dependent density functional theory (TDDFT). TDDFT is widely used in many areas of chemistry and biology to calculate electronic properties of a number of systems due to its low computational cost when scaled up to large systems, and for its reasonable accuracy for electronically excited states with errors typically in the 0.2-0.6 eV range.[28,29] In particular, the studies described herein are concerned with five specific molecules: allyl cation and its isomer 1-propenyl, cyclopentadiene, 1,3-dimethylcyclopentene, and [10]annulene. These molecules were chosen because they fall in the range of molecular sizes which are likely to be seen in space, their ground state structures are well known, and their electronic spectra have yet to be measured.

Computational Details

Equilibrium geometries and ground state harmonic frequencies were calculated using the Gaussian09 suite of electronic structure programs.[32] Density functional theory (DFT) was used with the B3LYP functional[33,34] and Dunning's correlation consistent aug-cc-pVDZ basis set.[35] Vertical electronic transition energies and oscillator strengths were calculated for the lowest 20 excited states using TDDFT with the B3LYP functional, the first three of which can be found in Table 1. Afterwards, equilibrium geometries and harmonic frequencies were calculated for select excited states using the TDB3LYP functional. The calculated equilibrium geometries and normal mode frequencies from the DFT calculations were then used as input into a multidimensional FC simulation, using the PGOPHER program suite.[36]

The method used in this study was used to calculate the vertical excitation energies of some small molecules to known electronic spectra. The results can be seen in the appendix. The groups of Bieske and Maier have used this method with varying basis sets extensively to predict excited state spectra to compare with experimentally obtained spectra and the results show good agreement between the calculated and experimental transition energies.[14-24]

Results and Discussion

$C_3H_5^+$: Allyl and 2-Propenyl

We start with the allyl cation, which is one of the two main isomers with the formula, $C_3H_5^+$. It, along with 2-propenyl, has been studied extensively in the past and is predicted to be the lowest energy isomers.[37-42] 2-Propenyl is predicted to be 8 kcal/mol higher in energy and

Table 1. The first three predicted excited states of selected carbocations calculated at the TDB3LYP/aug-cc-pVDZ level of theory.

Name	Number	State	Vertical (eV)	Adiabatic (eV)	Intensity
Allyl	1	$^1B_1$	5.43		0.001
	2	$^1B_2$	5.63	2.75	0.326
	3	$^1B_1$	7.06		0.002
2-Propenyl	1	$^1A''$	3.35	2.66	0.001
	2	$^1A'$	7.25		0.006
	3	$^1A''$	7.56		0.003
Cyclopentadiene	1	$^3A_1'$	3.66		0.022
	2	$^3E_1''$	3.66	3.21	0.022
	3	$^3E_1'$	4.74		0.000
1,3-Dimethylcypentene	1	$^1B_2$	5.08		0.427
	2	$^1B_1$	5.45		0.007
	3	$^1B_1$	6.04		0.001
[10]Annulene	1	^1A	2.04	1.13	0.054
	2	^1A	3.30		0.027
	3	^1A	4.02		0.288

separated by an 18 kcal/mol barrier from allyl.[37] The presence of such a large barrier suggests that it may be possible for both allyl and 2-propenyl to exist in the interstellar medium.

The predicted structures for the ground states of both allyl and 2-propenyl calculated at the B3LYP/aug-cc-pVDZ level of theory are shown in Figure 1a. The ground state of allyl cation is C_{2v} symmetric with C-C bond lengths of 1.39 Å and C-C-C angle of 118.7 degrees. The symmetry of the electronic ground state is $^1A_1$ which is consistent with previous theory. The 2-propenyl cation is C_s symmetric with C=C bond length of 1.28 Å, C-C bond length of 1.41 Å, and a C-C-C bond angle of 178.0 degrees. These structures have been confirmed with infrared spectroscopy.[43] The electronic ground states of allyl and 2-propenyl are predicted to be $^1A_1$ and $^1A'$, respectively. From these ground state geometries, vertical excitation energies were calculated and the results for the first three excited states can be found in Table 1.

The first excited state predicted for the allyl cation is the $^1B_1$ state which occurs at 5.43 eV. This state is predicted to be extremely weak and is unlikely to be seen. The second excited state, $^1B_2$, is predicted at 5.63 eV with a large intensity. The orbitals for the ground and excited states involved in this transition can be seen in Figure 1b. Because of the large calculated intensity, this state was chosen for optimization. An excited state symmetry of $^1B_2$ indicates a breaking of the C_{2v} symmetry upon excitation and that is exactly what is predicted. Upon excitation, the symmetry of the excited state switches to C_s as one of the CH_2 groups rotates 90 degrees relative to the C-C-C plane. Recalculation of the excited state after optimization of the excited state yields a new adiabatic excitation energy of 2.75 eV.

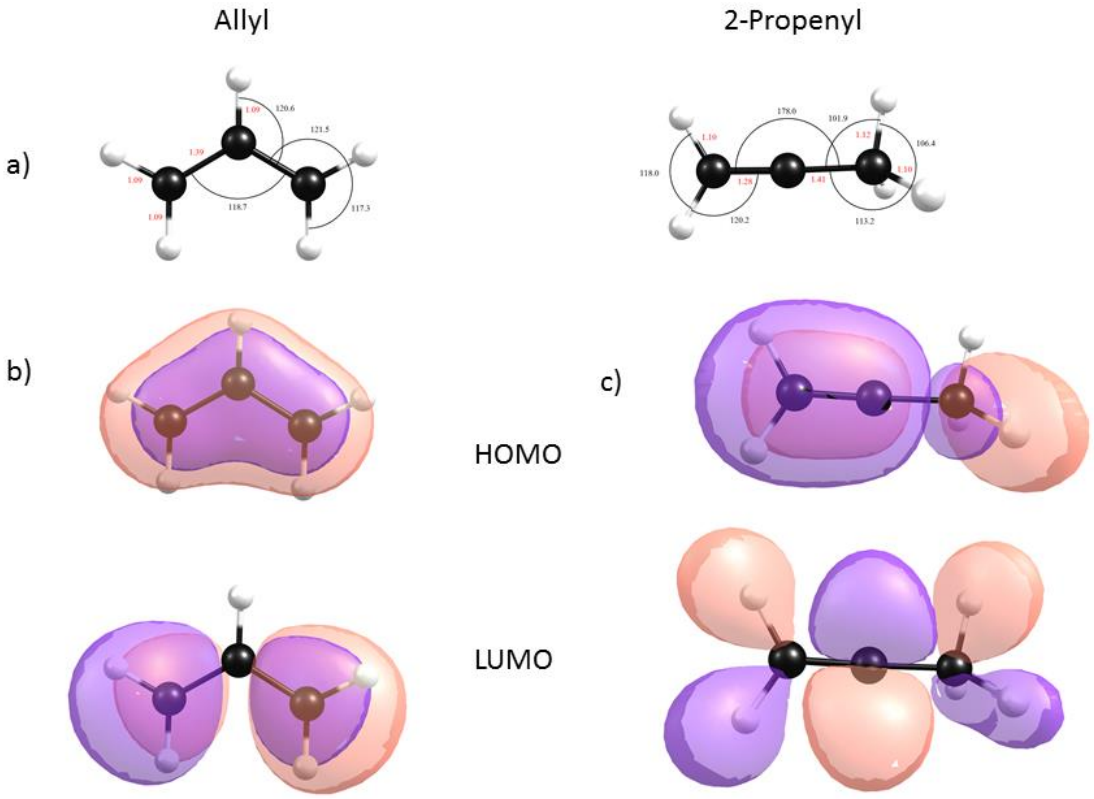

Figure 1. a) ground state structures of the allyl and 2-propenyl cations calculated at the B3LYP/aug-cc-pVDZ levl of theory. Bond lengths (red) are in Å and bond angles (black) are in degrees. b) Highest occupied molecular orbital (HOMO) and lowest unoccupied molecular orbital (LUMO) for the $X\ ^1A_1 \rightarrow 2\ ^1B_2$ transition of the allyl cation. c) Highest occupied molecular orbital (HOMO) and lowest unoccupied molecular orbital (LUMO) for the X ^{1}A' → 1 ^{1}A" transition of the 2-propenyl cation.

The large change in excitation energy after optimization of the excited state has been seen previously in calculations of the excited states of the allyl cation at the EOM-CCSD(T) level of theory.[44] The vertical and adiabatic excitation energies calculated in that work, 5.55 and 2.67 eV, are within the previously stated errors usually associated with TDDFT calculations.[28,29] The large geometry and excitation energy change upon excitation indicates that the excited state spectrum of the allyl cation will likely have a long progression along the vibrational mode associated with the torsion of the CH_2. This type of behavior is contrary to the features seen in the DIBs which show single resonances with little correlation between peaks. This indicates that the carriers of the DIBs likely have a very small geometry change upon excitation. For this reason, it is unlikely that the allyl cation is a DIB carrier, but it is still possible that its spectrum could be seen in some other environment.

Of the excited states calculated for the 2-propenyl cation, only the first one at 3.35 eV is possibly in the range to be considered for a DIB. The other calculated excited states are above 7 eV which are much too high to be considered. The first predicted excited state, ^{1}A", after optimization exhibits a C-C-C bond angle of 141.9 degrees, a 36.1 degree change from the ground state. The C=C bond also lengthens by 0.1 Å. The adiabatic excitation energy upon excitation drops by 0.69 eV to 2.66 eV, which is close to a number of DIBS. The closest DIB to the calculated value is that at 4662 Å which is less than 1 Å from the calculated value.[45] The calculated lineshape of the first excited state of 2-propenyl is shown in Figure 2. The simulation was created using a rotational temperature of 30 K and a Lorentzian linewidth of 1 Å to best match the width of the DIB. The simulation shows a progression spaced by approximately 62

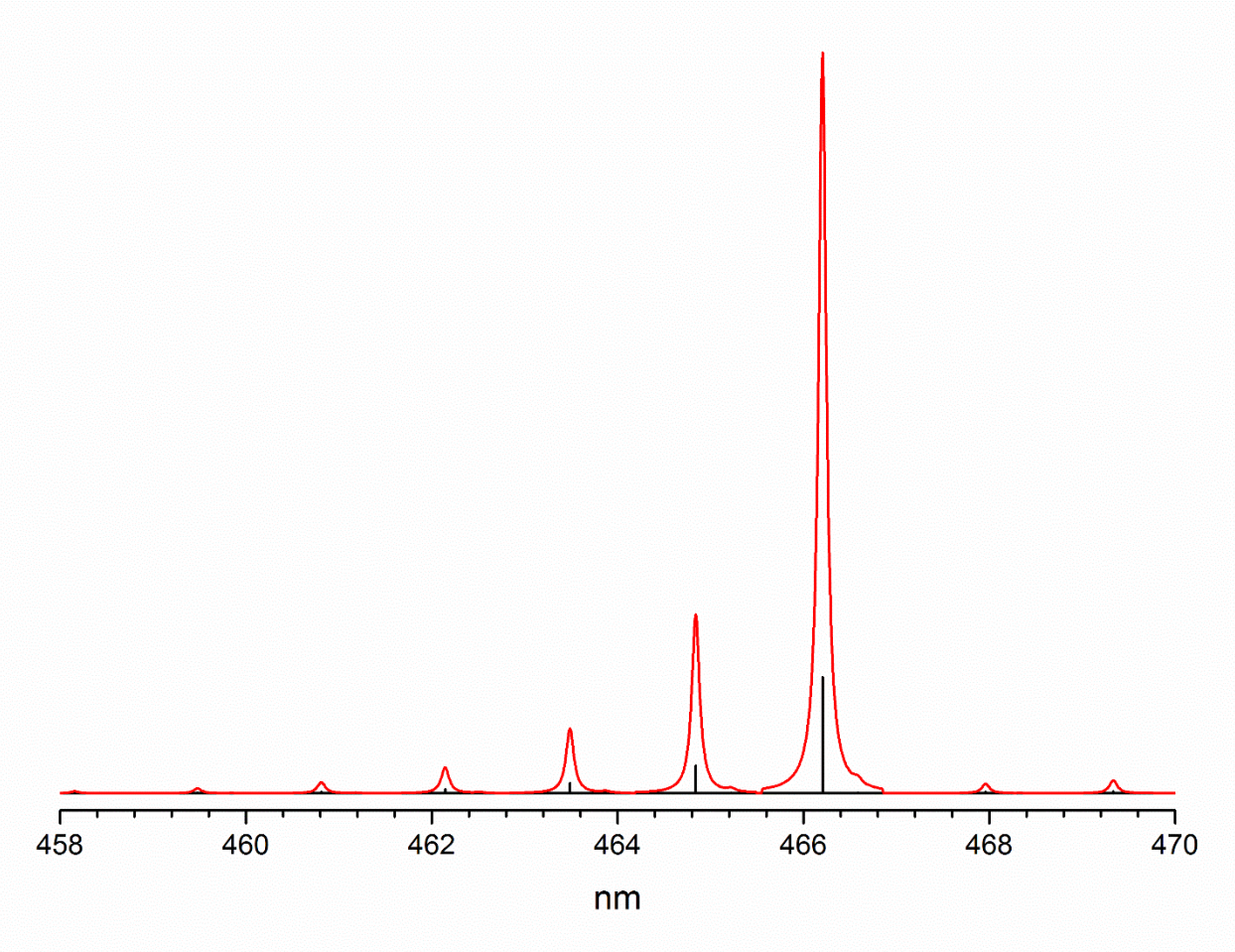

Figure 2. Predicted electronic spectrum for the X ^{1}A' → 1 ^{1}A" transition of the 2-propenyl cation. The simulation was carried out using PGOPHER with rotational temperature of 30 K and lorentzian linewidth of 0.1 nm.

cm^{-1}. This progression is not seen in the DIB spectra and we can therefore rule out 2-propenyl from consideration. Another reason for exclusion of 2-propenyl is the predicted intensity of the electronic transition. The predicted transition is extremely weak, making it more unlikely for 2-propenyl to be attributed to the 4662 Å DIB.

$C_5H_5^+$: Cyclopentadienyl

The cyclopentadienyl cation has been of great interest over the past 40 years. It is anti-aromatic based on Huckel's Rule,[46] having only 4 π electrons. It has been the subject of numerous theoretical investigations,[47-52] but its spectra in non-perturbative environments have yet to be seen. In both combustion and astrochemistry, it is predicted as an intermediate whose formation is proposed to be a product of the reaction of cyclopropenyl and acetylene.[53] Based on this reaction, low level calculations predict a number of isomers, with the cyclic triplet structure predicted to be the global minimum.[53] For this reason, the cyclic triplet structure is the focus here, but based on conditions of formation, any of the other possible isomers are possible. Their excited states were also calculated at the TDB3LYP/aug-cc-pVDZ level of theory, but all of the calculated transitions for those other molecules lie well into the UV, making them unlikely as DIB carriers and as such, will not be discussed here. The first five calculated transitions and intensities for these structures can be found in the appendix.

The structure with bond lengths and angles for the $^3A_1'$ ground state can be seen in Figure 3a. The ground state exhibits D_{5h} symmetry with C-C bond lengths of 1.43 Å and C-H bond lengths of 1.09 Å. The first three vertical excited states predicted for this cation are reported in

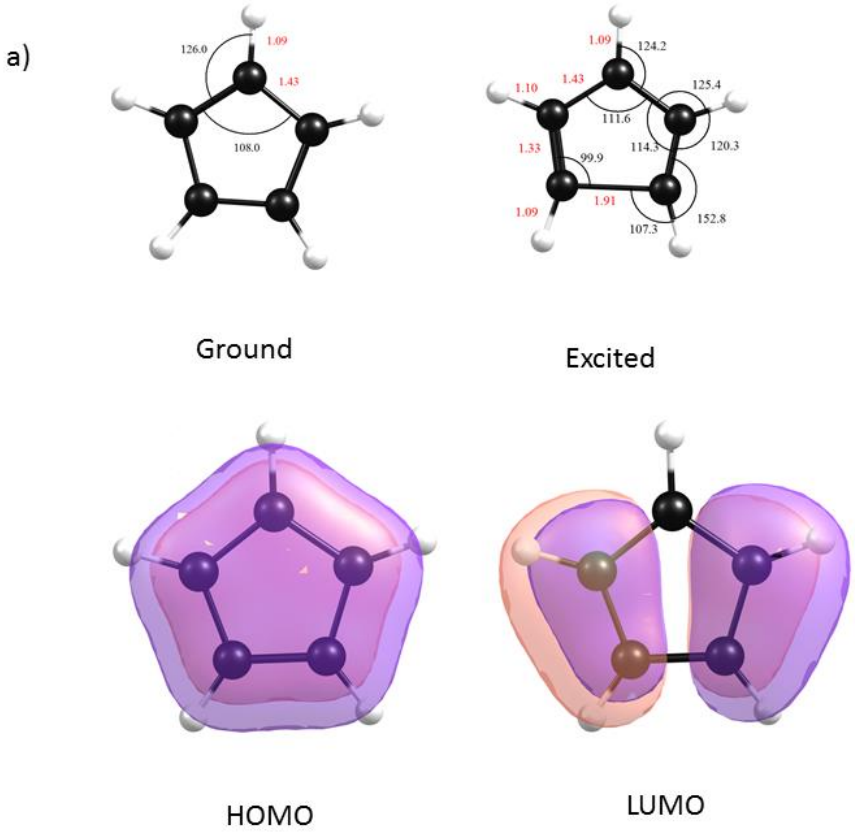

Figure 3. a) ground state structures of the cyclopentadienyl ($C_5H_5^+$) cation calculated at the B3LYP/aug-cc-pVDZ levl of theory. Bond lengths (red) are in Å and bond angles (black) are in degrees. b) Highest occupied molecular orbital (HOMO) and lowest unoccupied molecular orbital (LUMO) for the $X\ ^3A_1' \rightarrow 2\ ^1E_1''$ transition of the cyclopentadienyl cation.

Table 1. The first and second excited states are degenerate, having the same excitation energy, 3.66 eV, and transition intensity. Both of these transitions correspond to the promotion of an electron from the highest fully occupied orbital to one of the singly occupied orbitals. The orbitals involved in the excitation to each of these excited states can be seen in Figure 3b. Upon excitation, the molecule breaks from D_{5h} and moves to C_{2v} symmetry which can clearly be seen in the orbitals. Of these two states, the 2 $^3E_1$" state was chosen for optimization. The optimized geometry for this state is shown in Figure 3a. Two of the C-C bonds shorten to 1.33 Å, while the C-C bond at the bottom of the molecule as shown in Figure 3a elongates to 1.91 Å. The vertical excitation energy for this is predicted to be 3.66 eV. Upon relaxation of the excited state, the transition energy lowers by 0.45 eV to 3.21 eV. It is likely that the electronic spectrum for this cation will be either broad or complicated due to these two overlapping states. For this reason, it is unlikely that this molecule is a DIB carrier, but without a laboratory spectrum it is not possible to know for sure.

1,3-Dimethylcyclopentene ($DMCP^+$)

$DMCP^+$ is the lowest energy structure on the $C_7H_{11}^+$ potential energy surface. Its structure has a five-membered ring allyl type resonance with methyl groups optimally placed at either end of the conjugation, both of which provide stabilization. It has been shown that rearrangements of bicyclic ions proceed towards related compounds with five-membered rings.[54] Only recently has its unperturbed infrared spectrum been obtained,[55] but its electronic spectrum has yet to be measured and little theory has been done on its electronic structure.

The C_{2v} ground state structure with bond lengths and angles can be seen in Figure 4a. The structure exhibits eclipsed methyl groups, C-C bond lengths between 1.40 and 1.54 Å, and C-H bond lengths of 1.10 Å. Of the three lowest excited states, only the first excited state has a reasonable calculated intensity. The orbitals involved in this excitation are shown in Figure 4b. The LUMO exhibits one more nodal plane than that of the HOMO, indicating a breaking of the symmetry along the allyl substructure. The electronic symmetry also changes from $^1A_1$ to $^1B_2$. This behavior is similar to that seen in the allyl cation discussed earlier (Figure 1b). This would also mean that the excited state would likely undergo a significant geometry change upon excitation to break the C_2v symmetry. Unfortunately, the optimization of this state using the B3LYP/auc-cc-pVDZ method was unsuccessful, resulting in a geometry change that is unphysical. It is currently unknown whether this is an effect of the functional/basis set used, but further analysis is needed. Considering similarities between this system and allyl, it is likely that subsequent to relaxation the energy of the excited state will also be lower for $DMCP^+$. This would bring the excitation energy down into the range of the DIBs.

[10]Annulene

A leading theory on the identity of the DIB carriers is that they are carbon based, particularly carbon chains, fullerenes, and polycyclic aromatic hydrocarbons. However after decades of study on carbon chains and polycyclic aromatics, no conclusive evidence has been found to attribute these to the DIB features.[14] Recently, two near-infrared DIB bands, first predicted to be due to C_{60}^+,[56] have been confirmed using gas phase photodissociation.[19] Of the molecular motifs that are possible, one that has not received much attention is the annulene

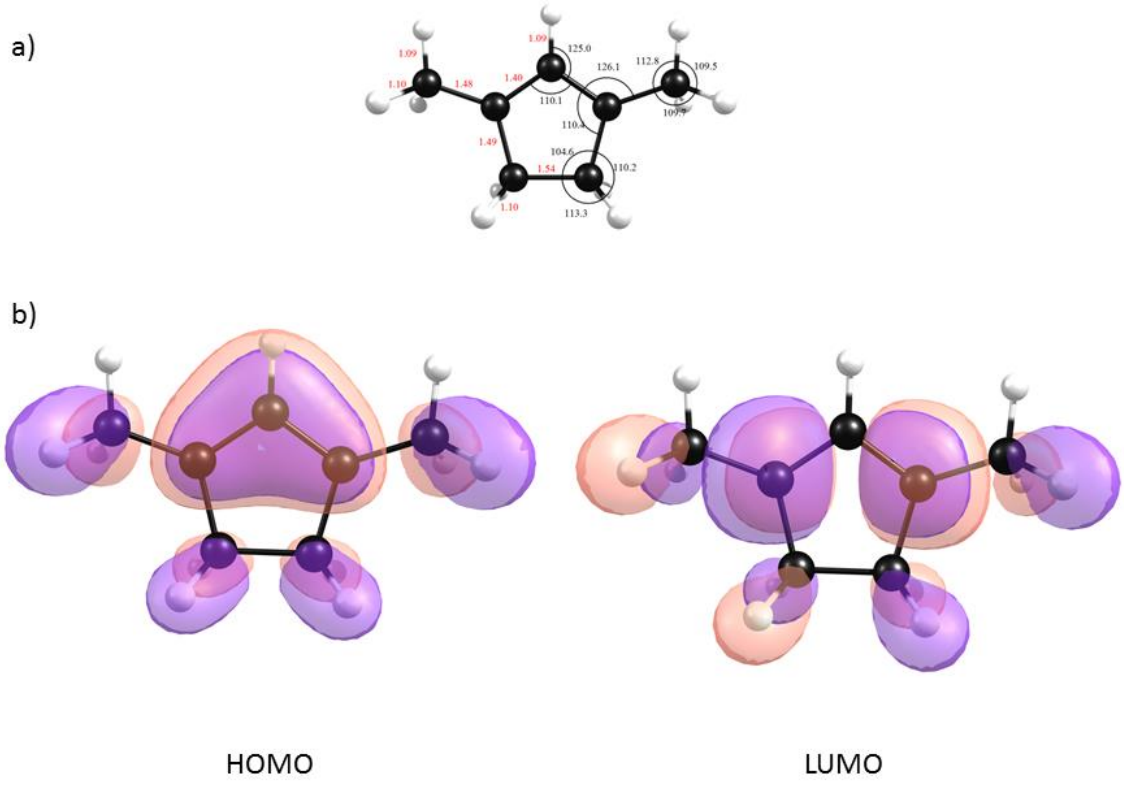

Figure 4. a) The ground state structure 1,3-dimethylcyclopentadienyl (DMCP) cation calculated at the B3LYP/aug-cc-pVDZ level of theory. Bond lengths (red) are in Å and bond angles (black) are in degrees. b) The highest occupied molecular orbital (HOMO) and lowest unoccupied molecular orbital (LUMO) for the $X\ ^1A_1 \rightarrow 1\ ^1B_2$ transition of the DMCP cation.

class of molecules. These structures, with benzene and cyclobutadiene being the simplest members, are fully conjugated carbon chains that form a cyclic structure. These structures tend to resemble their polycyclic counterparts. One such molecule that could possibly provide bands in the visible region is [10]annulene. [10]Annulene is a close relative to naphthalene, where the C-C bridging bond is replaced with two hydrogens. This substitution causes a significant amount of ring strain and the resulting annulene molecule is twisted to accommodate the steric strain of the added hydrogen atoms. The cation of this molecule is unstable and quickly breaks the ring structure, but the protonated form is stable and this is the focus here.

The excess proton can be added anywhere along the cycle, and the difference in relative energies between the various protonation sites is negligible. From this ground state structure, the first 20 excited states were calculated, the lowest three of which are reported in Table 1. All three of these states have reasonable intensity, with the first falling at the red end of the visible region. Upon optimization of the first excited state, there is very little change in the molecular structure. This is not surprising because of the relative rigidity of the structure. The adiabatic excitation energy for the first transition red shifts upon optimization by almost an eV. This shifts the transition out of the visible and into the infrared. If a similar shift is seen for the second excited state, this state would move into a region of the visible where a number of DIBs are seen. With little change in the geometry of the molecule upon excitation, the expected spectrum for this molecule is likely to have little vibrational excitation and would therefore have a single peak. This behavior is consistent with the DIBs and laboratory measurement of its spectrum could yield a possible match to one or more DIB features. In the future, more work could also be done to calculate and measure the spectra of more annulene structures for consideration in the hunt for DIB carriers.

Conclusion

In this work, the excited states of some possible cationic carriers of DIBs were calculated. In all the molecules, significant shifts in excitation energy were seen upon relaxation of the excited states. In two cases, allyl and 2-propenyl, this relaxation was accompanied by a significant change in the molecular geometry. This change is predicted to give rise to vibrational progressions in the excited state spectrum of the species. Each of the cases is predicted to have at least one feature in the range of the DIBs, but the accuracy of the method used to predict these states precludes their definitive assignment. However, these predictions could be used by future researchers to measure the laboratory spectra of the species for direct comparison to the DIB features.

References

1. Heger, M. L. Further study of the sodium lines in class B stars. *Lick Observatory Bulletin* **1922**, *10*, 337.
2. Tielens, A. G. G. M. The Physics and Chemistry of the Interstellar Medium, Cambridge University Press, Cambridge, U.K., 2005.
3. Hartquist, T. W.; Williams, D. A. The Molecular Astrophysics of Stars and Galaxies, Clarendon Press, Oxford, 1998.
4. Osterbrock, D. E.; Ferland, G. J. Astrophysics of Gaseous Nebulae and Active Galactic Nuclei, 2nd edition, University Science Books, Sausalito, CA, 2006.
5. ÅHerbig, G. H. The Diffuse Interstellar Bands. *Annu. Rev. Astrophys.*, **1995**, *33*, 19-74.
6. Ehrenfreund, P., The Diffuse Interstellar Bands as evidence for polyatomic molecules in the diffuse interstellar medium. *Bull. Amer. Astronom. Soc.* **1999**, *31*, 880.
7. Sarre, P. J. The Diffuse Interstellar bands: A Major Problem in Astronomical Chemistry. *J. Mol. Spectrosc.*, **2006**, *238*, 1-10.
8. Ehrenfreund, P.; Charnley, S. B. Organic Molecules in the Interstellar Medium, Comets and Meteorites: A Voyage from Dark Clouds to the Early Earth. *Annu. Rev. Astron. Astrophys.*, **2000**, *38*, 427-483.
9. Snow, T. P.; McCall, B. J. Diffuse Atomic and Molecular Clouds. *Annu. Rev. Astron. Astrophys.* **2006**, *44*, 367-414.
10. Herbst, E.; van Dishoeck, E. F. Complex Organic Interstellar Molecules. *Annu. Rev. Astron. Astrophys.* **2009**, *47*, 427-480.
11. Smith, D. The Ion Chemistry of Interstellar Clouds. *Chem. Rev.* **1992**, *92*, 1473-1485.
12. Petrie, S.; Bohme, D. K. Ions in Space. *Mass Spectrom. Rev.* **2007**, *26*, 258-280.

13. Snow, T. P.; Bierbaum, V. M. Ion Chemistry in the Interstellar Medium. *Annu. Rev. Anal. Chem.* **2008**, *1*, 229-259.

14. Maier, J. P.;Walker, G. A. H.; Bohlender, D. A. On the Possible Role of Carbon Chains as Carriers of Diffuse Interstellar Bands. Astrophys. J. 2004, 602, 286-290.

15. Jochnowitz, E. B.; Maier, J. P. Electronic Spectrocopy of Carbon Chains. *Ann. Rev. Phys. Chem.* **2008**, *59*, 519-544.

16. Nagarajan, R; Maier, J. P. Electronic spectra of carbon chains and derivatives. *Int. Rev. Phys. Chem.* **2010**, *29*, 521–554.

17. Nagy, A.; Fulara, J.; Garkusha, I; Maier, J. P. On the Benzylium/Tropylium Ion Dichotomy: Electronic Absorption Spectra in Neon Matrices. *Angew. Chem. Int. Ed.* **2011**, *50*, 3022–3025.

18. Rice, C.A.; Maier, J. P. Electronic Spectroscopy of Carbon Chains and Rings of Astrophysical Interest. *J. Phys. Chem. A* **2013**, *117*, 5559-5566.

19. Campbell, E. K.; Holz, M.; Gerlich, D.; Maier, J. P., Laboratory Confirmation of C_{60}^+ as the Carrier of Two Diffuse Interstellar Bands. *Nature* **2015**, *523*, 322-323.

20. Dryza, V.; Chalyavi, N.; Sanelli, J. A.; Bieske, E. J. Electronic absorptions of the benzylium cation. *J. Chem. Phys.* **2012**, *137*, 204304.

21. Chalyavi, N.; Dryza, V.; Sanelli, J. A.; Bieske, E. J. Gas-phase electronic spectroscopy of the indene cation ($C_9H_8^+$). *J. Chem. Phys.* **2013**, *138*, 224307.

22. Chalyavi, N.; Sanelli, J. A.; Dryza, V.; Bieske, E. J. Electronic Spectroscopy of the 1,3-Cyclopentadiene Cation ($C_5H_6^+$). *J. Phys. Chem. A* **2013**, *117*, 11276−11281.

23. Chalyavi, N.; Catani, K. J.; Sanelli, J. A.; Dryza, V.; Bieske, E. J. Gas-phase electronic spectrum of the indole radical cation. *Mol. Phys*. **2015**, *113*, 2086-2094.

24. Catani, K. J.; Muller, G.; da Silva, G.; Bieske, E. J. Electronic spectrum and photodissociation chemistry of the linear methyl propargyl cation $H_2C_4H_3^+$. *J. Chem. Phys.* **2017**, *146*, 044307.

25. Green, S.; Montgomery, J. A.; Thaddeus, P. Tentative Identification of U93.174 as the Molecular Ion N_2H^+, *Astrophys. J.*, **1974**, *193*, L89-L91.

26. Guelin, M.; Thaddeus, P. Tentative Detection of the C_3N Radical. *Astrophys. J.*, **1977**, *212*, L81-L85.

27. Wilson, S.; Green, S. Theoretical Study of the Butadienyl and Cyanoethynyl Radicals – Support for the Identification of C_3N in IRC +10216. *Astrophys. J.*, **1977**, *212*, L87-L90.

28. Lee, T. J.; Scuseria, G. E., In Quantum Mechanical Electronic Structure Calculations with Chemical Accuracy (ed S. R. Langhoff), Kluwer Academic Publishers, Dordrecht, The Netherlands, **1995**, 47-108.

29. Helgaker, T.; Ruden, T.A.; Jorgensen, P.; Olsen, J.; Klopper, W., A Priori Calculation of Molecular Properties to Chemical Accuracy. *J. Phys. Org. Chem.* **2004**, *17*, 913-933.

30. Yarkony, D. R., Conical Intersections: Diabolical and Often Misunderstood. *Acc. Chem. Res.* **1998**, *31*, 511-518.

31. Fortenberry, R. C.; King, R. A.; Stanton, J. F.; Crawford, T. D. A Benchmark Study of the Vertical Electronic Spectra of the Linear Chain Radicals C_2H and C_4H. *J. Chem. Phys.*, **2010**, *132*, 144-303.

32. Gaussian 09, Revision D.01, Frisch, M. J.; Trucks, G. W.; Schlegel, H. B.; Scuseria, G. E.; Robb, M. A.; Cheeseman, J. R.; Scalmani, G.; Barone, V.; Mennucci, B.; Petersson, G. A.; Nakatsuji, H.; Caricato, M.; Li, X.; Hratchian, H. P.; Izmaylov, A. F.; Bloino, J.;

Zheng, G.; Sonnenberg, J. L.; Hada, M.; Ehara, M.; Toyota, K.; Fukuda, R.; Hasegawa, J.; Ishida, M.; Nakajima, T.; Honda, Y.; Kitao, O.; Nakai, H.; Vreven, T.; Montgomery, J. A., Jr.; Peralta, J. E.; Ogliaro, F.; Bearpark, M.; Heyd, J. J.; Brothers, E.; Kudin, K. N.; Staroverov, V. N.; Kobayashi, R.; Normand, J.; Raghavachari, K.; Rendell, A.; Burant, J. C.; Iyengar, S. S.; Tomasi, J.; Cossi, M.; Rega, N.; Millam, J. M.; Klene, M.; Knox, J. E.; Cross, J. B.; Bakken, V.; Adamo, C.; Jaramillo, J.; Gomperts, R.; Stratmann, R. E.; Yazyev, O.; Austin, A. J.; Cammi, R.; Pomelli, C.; Ochterski, J. W.; Martin, R. L.; Morokuma, K.; Zakrzewski, V. G.; Voth, G. A.; Salvador, P.; Dannenberg, J. J.; Dapprich, S.; Daniels, A. D.; Farkas, Ö.; Foresman, J. B.; Ortiz, J. V.; Cioslowski, J.; Fox, D. J. Gaussian, Inc., Wallingford CT, 2009.Beck 1993

33. Lee, C.; Yang, W.; Parr, R. G., Development of the Colle-Salvetti Correlation-Energy Formula Into a Functional of the Electron Density, *Phys. Rev. B.* **1988**, *37*, 785-789.

34. Becke, A. D. Density-Functional Thermochemistry. III. The Role of Exact Echange. *J. Chem. Phys.*, **1993**, *98*, 5648.

35. Dunning Jr., T. H., Gaussian Basis Sets for Use in Correlated Molecular Calculations. I. The Atoms Boron Through Neon and Hydrogen. *J. Chem. Phys.* **1989**, *90*, 1007.

36. Western, C. M. 2010, PGOPHER, a Program for Simulating Rotational Structure, Version 7.1.108, University of Bristol, http://pgopher.chm.bris.ac.uk

37. Fairley, D. A.; Milligan, D. B.; Wheadon, L. M.; Feeman, C. G.; Maclagan, R. G. A. R.; McEwan, M. J. Flow Tube and Theoretical Study of Proton Transfer of $C_3H_5^+$ Ions. *Int. J. Mass. Spectrom.* **1999**, *185*, 253-261.

38. Radom, L.; Hariharan, P. C.; Pople, J. A.; Schleyer, P. v. R. Molecular Orbital Theory of the electronic Structure of Organic Compounds. XIX. Geometries and Energies of C_3H_5

Cations. Energy Relations Among Allyl, Vinyl, and Cyclopropyl Cations. *J. Am. Chem. Soc.* **1973**, *95*, 6531-6544.

39. Gobbi, A.; Frenking, G. Resonance Stabilization in Allyl Cation, Radical, and Anion. *J. Am. Chem. Soc.* **1994**, *116*, 9275-9286.

40. Mo, Y.; Lin, Z.; Wu, W.; Zhang, Q. Delocalization in Allyl Cation, Radical, and Anion. *J. Phys. Chem.* **1996**, *100*, 6469-6474

41. Wiberg, K. B.; Schleyer, P. v. R.; Streitwieser, A. The Role of Hydrogens in Stabilizing Organic Ions. *Can. J. Chem.* **1996**, *74*, 892-900.

42. Reindl, B.; Clark, T.; Schleyer, P. v. R. Empirical Force Field and Ab Initio Calculations on Allyl Cations. *J. Comput. Chem.* **1997**, *18*, 533-551.

43. Douberly, G. E.; Ricks, A. M.; Schleyer, P. v. R.; Duncan, M. A. Infrared spectroscopy of gas phase $C_3H_5^+$: The allyl and 2-propenyl cations. *J. Chem. Phys.* **2008**, *128*, 021102.

44. Fortenberry, R.C.; Crawford, T. D. Electronically Excited States in Interstellar Chemistry. *Annu. Rep. Comp. Chem.* **2011,** *7*, 195-212.

45. Hobbs, L. M.; York, D. G.; Snow, T. P.; Oka, T.; Thorburn, J. A.; Bishof, M.; Friedman, S. D.; McCall, B. J.; Rachford, B.; Sonnentrucker, V; Welty, D. E. A Catalog of Diffuse Interstellar Bands in the Spectrum of HD 204827. *Astrophys. J.* **2008**, *680*, 1256.

46. Morrison, R. T.; Boyd, R. N., Organic Chemistry. 3 ed.; Allyn and Bacon: Boston, 1973.

47. Applegate, B. E.; Miller, T. A.; Barckholtz, T. A., The Jahn-Teller and Related Effects in the Cyclopentadienyl Radical. I. Ab Initio Calculation of Spectroscopically Observable Parameters. *J. Chem. Phys.* **2001**, *114*, 4855-4868.

48. Applegate, B. E.; Bezant, A. J.; Miller, T. A., The Jahn-Teller and Related Effects in the Cyclopentadienyl Radical. II. Vibrational Analysis of the $\tilde{A}\ ^2A_2''$-$X\ ^2E_1''$ Electronic

Transition Related Effects in the Cyclopentadienyl Radical. II. Vibrational Analysis of the $\tilde{A}\ ^2A_2''$-$X\ ^2E_1''$ Electronic Transition. *J. Chem. Phys.* **2001**, *114*, 4869-4882.

49. Zilberg, S.; Hass, Y. A., Valence Bond Analysis of Electronic Degeneracies in Jahn-Teller Systems: Low-Lying States of the Cyclopentadienyl Radical and Cation. *J. Am. Chem. Soc.* **2002**, *124*, 10683-10691.

50. Wörner, H. J.; Merkt, F., Diradicals, Antiaromaticity, and the Pseudo-Jahn-Teller Effect: Electronic and Rovibronic Structures of the Cyclopentadienyl Cation. *J. Chem. Phys.* **2007**, *127* ,034303.

51. Glukhovtsev, M. N.; Reindl, B.; Schleyer, P. v. R., What is the Preferred Structure of the Singlet Cyclopentadienyl Cation. *Mendeleev Commun.* **1993**, *3*, 100-102.

52. Lee, E. P. F.; Wright, T. G., A Study of the Lowest-Lying Triplet and Singlet States of the Cyclopentadienyl Cation ($c\text{-}C_5H_5^+$). *Phys. Chem. Chem. Phys.* **1999**, *1*, 219-225.

53. Feng, J. K.; Leszczynski, J.; Weiner, B.; Zerner, M. C., TheReaction $C_3H_3^+ + C_2H_2$ and the Structural Isomers of $C_5H_5^+$. *J. Am. Chem. Soc.* **1989**, *111*, 4648-4655.

54. Deno, N. C.; Houser, J. J. Carbonium Ions. XIV. The Opening of Bicyclic Alcohols to Cyclohexenyl Cations and the Further Conversion of Cyclopentenyl Cations. *J. Am. Chem. Soc.* **1964**, *86*, 1741 – 1743.

55. Mosley, J. D; Young, J. W.; Agarwal, J.; Schaefer, H. F.; Schleyer, P. v. R.; Duncan, M. A. Structural Isomerization of the Gas-Phase 2-Norbornyl Cation Revealed with Infrared Spectroscopy and Computational Chemistry, *Angew. Chem. Int. Ed.* **2014**, *53*, 5888-5891.

56. Foing, B. H.; Ehrenfreund, P. New Evidences for Interstellar C_{60}^+.Astron. Astrophys. **1997**, *319*, L59-L62.

APPENDIX TO CHAPTER 5

Structure	Number	Vertical (eV)	Intensity
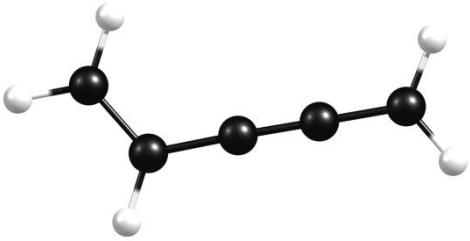	1	2.3490	0.0000
	2	4.3329	0.5012
	3	5.4635	0.0001
	4	5.6640	0.0268
	5	5.9606	0.0000
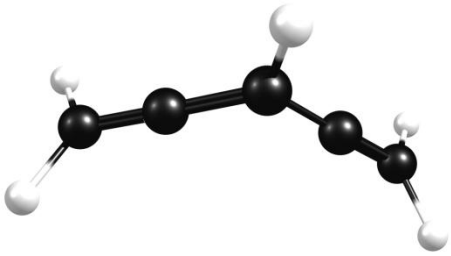	1	3.2349	0.0000
	2	3.4918	0.0000
	3	5.5369	0.4796
	4	6.9582	0.0002
	5	7.0139	0.3779

Name	Number	Vertical (eV)	Intensity
$CH_2OH_2^+$	1	4.7872	0.0008
CH_2NH^+	1	3.3699	0.0003
	2	5.5325	0.0002
CHOOH	1	1.3053	0.0000
	2	3.2243	0.0005
	3	5.1446	0.0006
$C_4H_4O^+$	1	2.1467	0.0130
	2	4.5844	0.0000
	3	4.8738	0.0298
CH_3OH	1	2.2943	0.0014
	2	5.0238	0.1011
H_2O^+	1	2.1689	0.0006
$C_2H_6CO^+$	1	2.8958	0.0000
	2	3.5437	0.0005
	3	3.8519	0.0110
	4	4.0043	0.0011

Name	Number	Vertical (eV)	Intensity
Styrene^{+}	1	1.1842	0.0003
	2	2.4501	0.0672
	3	3.2818	0.0000
	4	3.6406	0.0001
	5	3.8836	0.0987
	6	4.0537	0.1133
	7	4.1787	0.1567
COT^{+}	1	1.2448	0.0000
	2	2.8722	0.0339
	3	3.2114	0.0004
	4	4.0603	0.0029
	5	4.6217	0.0234
Allylbenzene	1	1.0439	0.0002
	2	1.7036	0.1190
	3	3.1865	0.0002
	4	3.2416	0.0023
	5	3.5589	0.0076